LESION SIZE ESTIMATOR FOR CARDIAC RADIOFREQUENCY ABLATION

by

YU-CHI LAI

UNIVERSITY OF WISCONSIN-MADISON

DEPT. OF ELECTRICAL AND COMPUTER ENGINEERING

Committee Members:

J. G. WEBSTER, DEPT. OF BIOMEDICAL ENGINEERING

D. J. BEEBE, DEPT. OF BIOMEDICAL ENGINEERING

Y.-H. HU, DEPT. OF ELECTRICAL AND COMPUTER ENGINEERING

H.-L. PLOEG, DEPT. OF MECHANICAL ENGINEERING

W. J. TOMPKINS, DEPT. OF BIOMEDICAL ENGINEERING

J. A. WILL, DEPT. OF ANIMAL HEALTH AND BIOMEDICAL SCIENCES

FINAL ORAL DEFENSE

3:45PM — 5:45PM, FEB 26, 2007

ROOM 4610 ENGINEERING HALL

LESION SIZE ESTIMATOR FOR CARDIAC RADIO-FREQUENCY

ABLATION

by

Yu-Chi Lai

A dissertation submitted in partial fulfillment of

the requirement of the degree of

Doctor of Philosophy

(Electrical and Computer Engineering)

at the

UNIVERSITY of WISCONSIN-MADISON

2008

ACKNOWLEGEMENT

TABLE OF CONTENTS

ABSTRACT

This work outlines a process for finite element (FE) modeling implementations of temperature-controlled radiofrequency (RF) ablation (TCRFA) with an automated temperature controller to investigate effects of changes in control temperature and contact conditions on the formation of lesions. The conditions investigated include ablation location, dimension of the myocardium, blood–electrode and blood–myocardium convection coefficients, penetration depth, and insertion angle.

In different *in-vitro* experiments, experimenters may choose arbitrary myocardial tissue sizes. We investigated the effects of the changes in myocardial tissue sizes on the formation of lesions. The results showed that it is proper to choose a myocardial tissue size of $30 \times 30 \times 10$ mm for the experimental comparison. Blood flow is an important parameter for lesion formation. We investigated the effects of changes in convective coefficients on lesion formation. We found that the electrode–blood convective coefficient has a significant effect on the formation of the lesion for two flow states.

A preliminary architecture of the lesion size estimator was created by considering applied locations, material properties, and target tip temperatures. It could be used as a first-step predictor to estimate possible lesion formations in different settings. Additionally, we performed *in-vitro* ablation on bovine myocardium by setting up a flow system to simulate different flow rates at different applied sites inside the heart chamber. It allowed us to compare the theoretical and experimental results for the preliminary lesion size estimator.

Penetration depth and penetration angle affect electrode–blood and electrode–myocardium contact areas, which influence the efficiency of RF energy transfer and the cooling effect on the thermistor. We found that the largest lesion is formed at a penetration depth of about 2.0 mm to

3.0 mm. And the lesion becomes larger as the insertion angle increases. However, when applying a high insertion angle, we take the risk of overheating the myocardium because the cooling effect becomes so large that the power supply induces too much energy, causing the popping effect.

We found that target tip temperature, cooling effect, and energy delivery efficiency have significant effects on the formation of lesions.

CHAPTER 1

INTRODUCTION

I. GOAL

The goal of this work is to establish a lesion size estimator, which can take into account different application conditions during radiofrequency (RF) cardiac ablation. These conditions include applied locations, total applied durations, target tip temperatures, material properties and catheter–myocardium contact conditions such as penetration depth and insertion angle.

II. BACKGROUND

A. *Anatomical terms and pathology*

Cardiac ablation is applied to the heart. Basic anatomy of the heart and several pathological terms related to the cardiac ablation follow. Fig. 1(a) shows that the heart has four chambers. The upper chambers consist of the left and right atria, and the lower chambers consist of the left and right ventricles. A wall of muscle called the septum separates the left and right atria and the left and right ventricles. The left ventricle is the strongest chamber in the heart. The chamber walls of the left ventricle are only about 13 mm thick, but they have enough force to push blood through the aortic valve and into the body. The heart pumps the blood to all tissues inside the body. The main pumping function is supplied by the ventricles, and the atria are merely antechambers to store blood during the time the ventricles are pumping. Four types of valves regulate blood flow through the heart:

- The tricuspid valve controls blood flow from the right atrium to the right ventricle.
- The pulmonary valve controls blood flow from the right ventricle to the pulmonary arteries, which carry blood to the lungs to pick up oxygen.

- The mitral valve lets oxygen-rich blood from your lungs pass from the left atrium into the left ventricle.

- The aortic valve opens the way for oxygen-rich blood to pass from the left ventricle into the aorta, the body's largest artery, where it is delivered to the rest of the body.

The smooth, rhythmic contraction of the atria and ventricles has an underlying electrical precursor in the form of a well-coordinated series of electrical events that take place within the heart. Fig. 1(b) shows electrical signal conducting paths inside the heart chamber. Electrical impulses to the heart muscle (the myocardium) cause the contraction of the heart. This electrical signal begins in the sinoatrial (SA) node, located at the top of the right atrium. The SA node is sometimes called the heart's "natural pacemaker." An electrical impulse from this natural pacemaker travels through the muscle fibers of the atria and ventricles, causing them to contract. The SA node sends electrical impulses at a rate, which may change depending on physical demands, stress, or hormonal factors.

Cardiac arrhythmia is a group of conditions in which the muscle contraction of the heart are irregular or are faster or slower than normal. Cardiac dysrhythmia might be a more correct phrase to describe the condition, as arrhythmia would imply that there is "no rhythm," but this term is not used frequently. Some arrhythmias are life-threatening medical emergencies that can cause cardiac arrest and sudden death. Others cause aggravating symptoms, such as an awareness of a different heart beat, or palpitation, which can be annoying. Some are quite benign and normal.

A serious variety of arrhythmia is known as fibrillation. The muscle cells of the heart normally function together, creating a single contraction when stimulated. Fibrillation occurs when the heart muscle begins a quivering motion due to a disunity in contractile cell function.

Fibrillation can affect the atrium (atrial fibrillation) or the ventricle (ventricular fibrillation); ventricular fibrillation is imminently life-threatening.

A heart rate faster than 100 beats/min is considered tachycardia. This number varies with age, as the heartbeat of a younger person is naturally faster than that of an older person. With exercise the sinus node increases its rate of electrical activity to accelerate the heart rate. The normal fast rate that develops is called sinus tachycardia. Arrhythmias that are due to fast, abnormal electrical activity can cause tachycardias that are dangerous. If the ventricles of the heart experience one of these tachycardias for a long period of time, there can be deleterious effects. Individuals may sense a tachycardia as a pounding sensation of the heart, known as palpitations. If the tachycardia is too fast, the pump function of the heart is impeded, which may lead to a sudden death.

B.   *Cardiac arrhythmia and RF ablation*

In the United States, cardiac arrhythmia affects more than 2 million people. Arrhythmia is caused by abnormalities in the formation and/or the conduction of the cardiac electrical impulse through the myocardium. These abnormalities disturb the normal rhythm of the heart and reduce the blood-pumping efficiency. There exist several different therapeutic methods including open-chest surgical procedures, drug therapy, defibrillator implantation, and radiofrequency (RF) cardiac ablation. The surgical procedure is to dissect the foci or to create a maze in the endocardium to block abnormal cardiac signal conduction pathways. The rate of success is high and the recurrence rate is low. However, these methods induce a long and painful recovery period. In addition, because of the invasiveness, reapplying the surgery soon is almost impossible. Drug therapy could ease symptoms of cardiac arrhythmia. It is also the least invasive method. However it is very expensive and not very effective in the long-term. The most serious problem is that it may cause serious side effects. Defibrillator implantation is effective to prevent

sudden death. However, pain caused by frequently induced electric shocks is very uncomfortable. Moreover, the effectiveness of the implanted device decays with implant time due to biological effects on the implanted catheter tip. The lifetime of the device battery also limits its prevalence.

RF ablation applies electric energy to eliminate discrete foci or to create a maze-like lesion to cure the arrhythmia. Because of efficacy, controllability, and minimal invasiveness, RF cardiac ablation has proven an effective method to treat some cardiac arrhythmias, such as atrioventricular node re-entry, atrial tachycardia, atrial flutter, and fascicular ventricular tachycardias [1]–[3]. Several research groups also suggest that it may be a good method for palliative suppression of ventricular tachycardias [3]–[5].

To be therapeutically effective, the formation of the lesion must cover the targeted region and it must also be as small as possible. However, it is hard to create a criterion for perfect lesion ablation since the optimal lesion geometries depend on the kinds of arrhythmia. For example, long thin lesions may be desired for curing atrial fibrillation, whereas deep and wide lesions are more effective for curing monomorphic ventricular tachycardia. In addition, the formation of a lesion is also affected by many parameters such as thermal and geometrical properties at the applied location, the applied duration, and the target tip temperature. Therefore, it would be useful to have an estimator to predict the dimensions of lesions before applying cardiac ablation.

C.   *Heat transfer during cardiac ablation*

RF cardiac ablation utilizes an RF generator and a catheter-tip-based delivery system. RF power, typically between 5 and 50 W, is delivered to heat the tissue to temperatures above 50 °C to create a lesion but below 95 °C to prevent tissue charring and blood coagulation. Fig. 2 shows a simple system for the energies involved during RF ablation. RF ablation applies an electric

current between the catheter electrode inserted into the myocardium and the dispersive electrode attached to the back of the patient. At the electrode–myocardium interface, the electric power is transformed to Joule heating, which increases the temperature of the tissue around the electrode as a result of the impedance of the surrounding cardiac tissue to the electric current flow. Thermal conduction causes increasing temperature deeper in the myocardium by conducting heat away from the Joule heating region. The thermistor embedded at the tip of the catheter is used to adjust the applied power by detecting the temperature of the myocardium in contact with the thermistor. It provides feedback control to the RF generator. However, blood convection in the cardiac chamber cools the blood-contacting surface of the electrode and the myocardium. Due to these temperature gradients caused by blood convection, the thermistor carried by the catheter usually does not measure precisely the highest temperature inside the tissue. We desire a mechanism that can precisely predict the temperature distribution inside the cardiac tissue to achieve an effective and safe treatment.

D.   *Bioheat equation*

The formation of the RF ablation lesion depends on the temperature distribution inside the tissue. The temperature changes during ablation inside the myocardium are governed by the bioheat equation

$$\rho \cdot c \frac{\partial T}{\partial t} = \nabla \cdot k \nabla T + J \cdot E - Q_h \tag{1}$$

with the following initial and boundary conditions:

$T = 37$ °C when $t = 0$ at Ω and

$T = 37$ °C when $t \geq 0$ at ∂B_0

where

Ω	the entire domain of the model
T	the temperature distribution in Ω
ρ	density (kg/m^3)
C	specific heat (J/kg·K)
K	thermal conductivity (W/m·K)
J	current density vector (A/m^2)
E	electric field intensity (V/m)
Q_h	heat loss due to blood perfusion in the myocardium, and is neglected inside the tissue since it is small [14]
∂B_0	the outermost boundary of the model

We can normally neglect Q_h inside the cardiac tissue because it is small during the normal cardiac ablation duration [12]. However, at the blood–catheter and the blood–tissue interfaces, heat exchange due to convection to the blood exists. We can calculate the heat fluxes by

$$k\frac{\partial T}{\partial n} = h_b(T - T_{bl}) \tag{2}$$

where

h_b the convective heat transfer coefficient due to the blood velocity

in $W/m^2 \cdot K$

T_{b1} the blood temperature in °C, normally body temperature

We solve Eq. (1) by two steps. First, since there is no RF energy source within the tissue, we can solve the Laplace equation to find the potential distribution V in the tissue.

$$\nabla \cdot \sigma \nabla V = 0 \tag{3}$$

with the following boundary conditions:

$V = 0$ at ∂B_0 , and

$V = V_0$ at ∂B_1

where

σ the electric conductivity (S/m)

V_0 the applied RF voltage at the electrode

∂B_1 the surface of the ablation electrode

Second, we can compute the electric field intensity and the current density from the

potential distribution V by

$$E = -\nabla V \tag{4}$$

$$J = \sigma E \tag{5}$$

Then, Eq. (1) yields the temperature distribution T. By using the critical temperature 50 °C, we

can determine the size of the lesion. Because it is not practical to solve the coupled problem

analytically, we use the finite element (FE) method to solve it numerically.

E.   *Finite element (FE) method*

The FE method is a very useful numerical tool, which has been used to solve partial differential

equations in many different fields such as structural analysis, fluid dynamics, heat transfer, and

electromagnetics. The FE algorithm transforms the calculus problem into an algebraic problem

by discretizing the solution domain into a finite number of small elements. Then various

numerical techniques are used to solve the resulting linear equations. The solution of the linear

equations provides the piecewise approximation to the unknown values within the domain. For

the analyses of cardiac ablation, we solve the bioheat equation for the change in potential and

temperature distributions. We create a FE model by dividing the solution domain into a finite

number of elements. The process of discretization converts the continuous problem into a

problem with a finite number of unknowns within each element. Within each element, these

unknowns express the unknown field variables (voltages and temperatures) in terms of certain

interpolation functions. The interpolation functions are defined at nodes of the element in terms

of the values of the field variables. Therefore, the nodal values of the field variables become new unknowns and the values of the field variables inside the elements are determined from the nodal values by the interpolation functions. Recursively repeating this process, the unknowns converge to a consistent solution. Burnette et al. [14] prove that the solution of the FE model converges to the true solution as the element size decreases to zero.

FE simulation can predict the process of ablation based on application conditions such as power delivered, duration, geometry, material characteristics and myocardial properties, such as resistivity, thermal conductivity, specific heat, etc., which vary with temperature. It functions as a tool to reduce the cost incurred when conducting many experimental studies. In this study, we investigated many different sets of cardiac RF ablation conditions. It is laborious and time-consuming to conduct all those settings in *in-vitro* and *in-vivo* experiments. The idea here is to use FE modeling to simulate possible settings and then to pick several representative conditions to verify the FE simulations in *in-vitro* and *in-vivo* experiments. This also minimizes the number of required *in-vivo* experiments and the use of live animals.

F.   *Temperature-controlled and power-controlled mode*

The technique of RF cardiac ablation delivers through the catheter RF power, typically between 5 and 50 W, to heat the tissue to a temperature above 50 °C. Moreover, to avoid charring and tissue micro-explosions, it is very important to control the tissue temperature below 95 °C. The entire process is commonly operated in two modes, power-controlled or temperature-controlled mode. During power-controlled ablation, the RF generator adjusts the delivered current to maintain a constant power delivered to the contact region even though the impedance may change during ablation. In temperature-controlled mode, an insulated thermistor is embedded at the tip of the catheter and reads the temperature at the point of contact with the endocardium. At

the beginning of ablation, the generator first applies an incremental voltage to raise the temperature at the catheter tip. Once the catheter tip temperature reaches the preset target temperature, the ablation generator adjusts the voltage level to keep the catheter tip temperature at the preset target temperature. To ensure safety, there are limits of the allowed maximum power and the allowed maximum catheter tip temperature to avoid charring of the endocardium and blood coagulation. Since catheter ablation is a heating process, the temperature-controlled mode ablation provides better control of lesion size than the power-controlled mode ablation [8] [9]. Clinical electrophysiologists empirically set different target temperatures, generally >55 $^{\circ}$C. In isolated tissue preparation models, a higher preset target temperature results in a larger lesion [8] [11].

G.   *Automatic control of FE simulation*

Large numerical models can be solved in acceptable time, but we must change parameters at each step because resistivity, etc. change with temperature. Solution time also increases with more precise simulations requiring more elements and nodes in each model and from increments in geometrical complexity in newly developed probes for more effective therapy. It is very laborious, time-consuming, and inaccurate to adjust the input of the FE simulation manually at each time step. Cao et al. [7] and Haemmerich et al. [10] implement two different types of controllers to automatically adjust the delivered power (i.e. the voltage applied to the catheter electrode) based on the current temperature at the catheter and certain criteria. It is especially efficient to automatically control similar repeating simulations with different parameter settings.

During RF ablation, the input of the entire system is the voltage applied to the electrode surface, and the output is the temperature measured at the thermistor. We obtained the relationship between the applied voltage and the rising temperature in myocardium from

Bhavaraju [13]. There are different ways of controlling the tip temperature such as proportional-integral-derivative (PID) control, adaptive control, neural network prediction control and fuzzy logic control. We chose to implement a relatively simple proportional-integral (PI) controller for our control system. Fig. 3 shows the complete closed-loop control system. T_{set} is the desired tip temperature and $T_{thermistor}$ is the current tip temperature. The control error to the PI controller is e = $T_{set} - T_{thermistor}$. The output of the PI controller corresponding to the applied voltage is used to modify the input script file of ABAQUS.

The PI controller is described in the time-domain by

$$u = K_P e + K_i \cdot \int e(\tau(\tau)) \tag{7}$$

To implement this controller in software, we use the discrete time-domain version of

$$u_n = K_p e_n + K_i \sum_{m=1}^{n} \frac{e_m + e_{m-1}}{2} \Delta t \tag{8}$$

The second term represents the approximation of the integral term in Eq. 7 by trapezoidal numerical integration. The behavior of the PI controller is determined by the two parameters K_p and K_i. Therefore, we analyzed the dynamic transfer function of the cardiac system [13] using the control simulation software ANA 2.52 (Freeware, Dept. of Control Engineering, Tech. Univ. Vienna/Austria). Once we identified an approximation of the dynamic system (FE model), we designed a feedback PI control system. Using the analysis developed by Haemmerich et al. [10], we set the PI control coefficient to be $K_p = 0.5$ and $K_i = 0.3$ to minimize overshoot of the controlled temperature.

H.   The properties of the myocardium

In previous research, the parameters of myocardial properties used in FE modeling for RF ablation vary significantly [11], [14], [15]. Thus, Tungjitkusolmun et al. [6] used the FE method

to quantify the effects of these properties on the formation of lesions in the power- and temperature-modes. The entire quantification can be explained using the bioheat equation.

In the ablation process, the heat source is from the Joule heating effect between the catheter electrode and the Joule heat region. Eq. 5 shows that the current density depends on the magnitude of the electric field injected by the generator, and the electric conductivity of the tissue. The effect of electric conductivity on lesion formation is totally different in power- and temperature-controlled modes. Since we focus on temperature-controlled operation, we present the effect in the temperature-controlled mode only. For temperature-controlled mode, the tip temperature is maintained at a constant level. The power delivered into the cardiac tissue is inversely proportional to the electric conductivity $P = J^2/\sigma$.

In Eq. 1, the thermal conductivity also affects the temperature distribution inside the cardiac tissue by the term $\nabla \cdot k\nabla T$. The effect of changes in myocardial thermal conductivity is as follows: In the temperature-controlled mode, constant tip temperature is maintained. Thus the easier the heat can be conducted away, the more tissue around is heated to 50 $^{\circ}$C and in return, yields a larger lesion size.

Eq. 1 shows that temperature-varying rate is inversely proportional to the specific heat. We could easily heat up tissue with a low specific heat. This would yield a larger lesion size at lower specific heat capacity in the temperature-controlled mode.

Fig. 4 shows the variation of cardiac impedance, heat conductivity, and specific heat at different temperatures measured by Tsai et al. [17]

I.   *Blood flow*

The blood inside the heart chamber keeps flowing during ablation. Furthermore, the blood remains at 37 $^{\circ}$C during ablation. According to the bioheat equation, the temperature difference

between the ablated myocardium and blood flow in the heart chamber causes heat transfer from the endocardium to the blood by heat convection. There is a similar heat transfer between the interface of the electrode surface and blood flow in the heart chamber. The cooling effect on the myocardium and on the electrode causes the embedded thermistor to report the deficiency in controlled temperature to the generator, and the controller of the generator increases power into the electrode to maintain the target temperature. This increase in power has several effects on lesion formation.

1. It increases the current density and the Joule heat generation inside the myocardium. As a result, the Joule heated rim rises to a higher temperature and becomes larger. It conducts more heat to the surrounding tissue to a larger boundary due to the higher temperature gradient. Thus, it raises the myocardial temperature in other regions and causes a larger lesion.

2. The higher the delivered power is, the faster the myocardial temperature rises, especially in the directly heated rim. It has more time to conduct heat into the surrounding myocardium and reaches a larger boundary. This also increases the lesion dimensions.

Thus, the entire effect is to make the lesion size larger.

Tangwongsan et al. [16] show that the heat transfer rate increases with blood flow. The higher the flow rate, the more heat is carried away by convection. As heat is carried away from these surfaces, the temperature at the endocardial surface is lower than the temperature inside the myocardium. Consequently, the lesion diameter on the surface is smaller than the maximum lesion diameter inside the myocardium. Fig. 5. shows the different convective coefficients inside the heart chamber adapted from Tangwongsan et al. [16]. In our simulation, we chose two representative convective coefficients to present the two common ablation blood flow groups.

III. SUMMARY

Chapter 2 presents a study investigating the effects of changes in myocardial tissue sizes on lesion formation by using a set of 2D axisymmetric FE models. The results of the study offer guidance in choosing the proper myocardial tissue size in future *in-vitro* experiments. We also investigated the effects of changes in blood convective coefficients on lesion formation by setting up several sets of convective coefficients for blood–myocardium interfaces and blood–electrode interfaces.

Chapter 3 presents a process of FE modeling a system including blood, myocardium, and an ablation catheter with a thermistor embedded at the tip. The simulation uses a simple proportional-integral (PI) controller to control the entire process operated in temperature-controlled mode. The result represents the time response of RF ablation at different locations by using different target temperatures.

Chapter 4 presents an *in-vitro* experiment on the effects of blood flow rates, target temperatures, and applied durations on lesion formation during RF cardiac catheter ablation. We performed *in-vitro* ablation on bovine myocardium by setting up a flow system to simulate the different flow rates at different applied sites inside the heart chamber. We also present comparison between the numerical simulation and experiment results.

Chapter 5 presents a study investigating the effects of changes in penetration depths. During cardiac ablation, the catheter must penetrate the cardiac tissue. If the penetration depth is small, most energy may dissipate to the blood and the lesion is small. If the penetration is deep, the blood convection may be small; consequently, only a small amount of energy is applied by the power generator in the temperature-controlled mode. The lesion cannot increase further. We present an ideal penetration depth that results in the maximum lesion size

Chapter 6 presents an investigation of the relationship between the insertion angle and the lesion size. The cardiac ablation process is applied by an experienced clinical electrophysiologist who cannot really see the catheter. Different insertion angles may result in different sizes of the contact area. In this study, we investigate the relationship between the insertion angle and the lesion formation.

Chapter 7 is the conclusion of the entire dissertation

REFERENCES

[1] S. K. S. Huang and D. J. Wilber, Eds., *Radiofrequency Catheter Ablation of Cardiac Arrhythmias: Basic Concepts and Clinical Applications*, 2nd ed., Armonk, NY: Futura, 2000.

[2] D. P. Zipes and M. Haïssaguerre, *Catheter Ablation of Arrhythmias*. 2nd ed. Armonk, NY: Futura, 2002.

[3] F. Morady, "Drug therapy: radio-frequency ablation as treatment for cardiac arrhythmias," *N. Engl. J. Med.*, vol. 340, pp. 534-544, 1999.

[4] D. Panescu, "Intraventricular electrogram mapping and radiofrequency cardiac ablation for ventricular tachycardia," *Physiol. Meas.*, vol. 18, pp. 1-38, 1997.

[5] H. Nakagawa, K. J. Beckman, and J. H. McClelland, "Radiofrequency catheter ablation of idiopathic left ventricular tachycardia guided by a Purkinje potential," *Circulation*, vol. 85, pp. 1666-1674, 1992.

[6] Tungjitkusolmun, S., Woo, E. J., Cao, H., Tsai, J.-Z., Vorperian, V. R., and Webster, J. G., "Thermal-electrical finite element modeling for radio-frequency cardiac ablation: effects of changes in myocardial properties," *Med. Biol. Eng. Comput.*, vol. 38, pp. 562-568, 2000.

[7] H. Cao, *Measuring Contact Area and Temperature during Radio-Frequency Cardiac Catheter Ablation*, Ph. D. Dissertation, Univ. of Wisconsin, Madison, May 2001

[8] D. E. Haines, "The biophysics of radiofrequency catheter ablation in the heart: The importance of temperature monitoring," *PACE*, vol. 16, pp. 596-591, Mar. 1993.

[9] D. E. Haines, and D. D. Watson, "Tissue heating during radiofrequency catheter ablation: A thermodynamic model and observation in isolated perfused and superfused canine right ventricular free wall," *PACE*, vol. 12, pp. 962-976, June 1989.

[10] D. Haemmerich, J. G. Webster, "Automatic control of finite element models for temperature-controlled radiofrequency ablation", Biomed. Eng. Online, 4(1):42, 2005.

[11] D. Panescu, J. G. Whayne, S. D. Fleischman, M. S. Mirotznik, D. K. Swanson and J. G. Webster, "Three-dimensional finite element analysis of current density and temperature distributions during radio-frequency ablation," *IEEE Trans. Biomed. Eng*. vol. 42, pp. 879-890, 1995.

[12] H. H. Peterson, X. Chen, A. Pietersen, J. H. Svendsen, S. Hauns, "Lesion dimensions during temperature-controlled radiofrequency catheter ablation of left ventricular porcine myocardium: impact of ablation size, electrode size and convective cooling," *Circulation*, vol. 99, pp. 319-325, 1999.

[13] N. C. Bhavaraju, *Heat Transfer Modeling During Radiofrequency Cardiac Ablation in Swine Myocardium*, Ph. D. Dissertation, Univ. Texas, Austin, Mar. 2000.

[14] Shahidi, A. V. and Savard, P. "A finite element model for radio-frequency ablation of the myocardium". *IEEE Trans. Biomed. Eng.*41: 963–968, 1994.

[15] Tsai, J.-Z., J. A. Will, S. Hubbard-Van Stelle, H. Cao, S. Tungjitkusolmun, Y. B. Choy, D. Haemmerich, V. R. Vorperian, and J. G. Webster, "*In vivo* measurement of swine myocardial resistivity", *IEEE Trans. Biomed. Eng*., 49, 472-483, May 2002b.

[16] C. Tangwongsan, J. A. Will, J. G. Webster, K. L. Meredith Jr., D. M. Mahvi, "*In vivo* measurement of swine endocardial convective heat transfer coefficient", *IEEE Trans. Biomed. Eng.*, 51, 1478-1486, 2004

[17] Tsai, J.-Z., "Personal Communication", 2002

FIG. AND TABLE CAPTIONS

Fig. 1. (a) Simple anatomy of the heart shows the four chambers and four valves. (b). The electrical signal initiates at the SA node regularly, passes through AV node, and reaches the bottom of the heart.

Fig. 2. Electric power through the electrode heats the myocardium. Blood velocity cools it. The black arrows represent the Joule heat generated close to the electrode. The white arrows represent the heat conduction from the hotter Joule heat region to the cooler myocardium.

Fig. 3. Closed loop system incorporating a PI controller and the dynamic system (FE model).

Fig. 4. The myocardial temperature-dependent properties (a) The thermal conductivity (b) The impedance (c) The specific heat (adapted from [18])

Fig. 5. The median values of *h* from *in-vivo* measurements in 15 pigs in 22 locations mapping on a heart diagram. (adapted from [16])
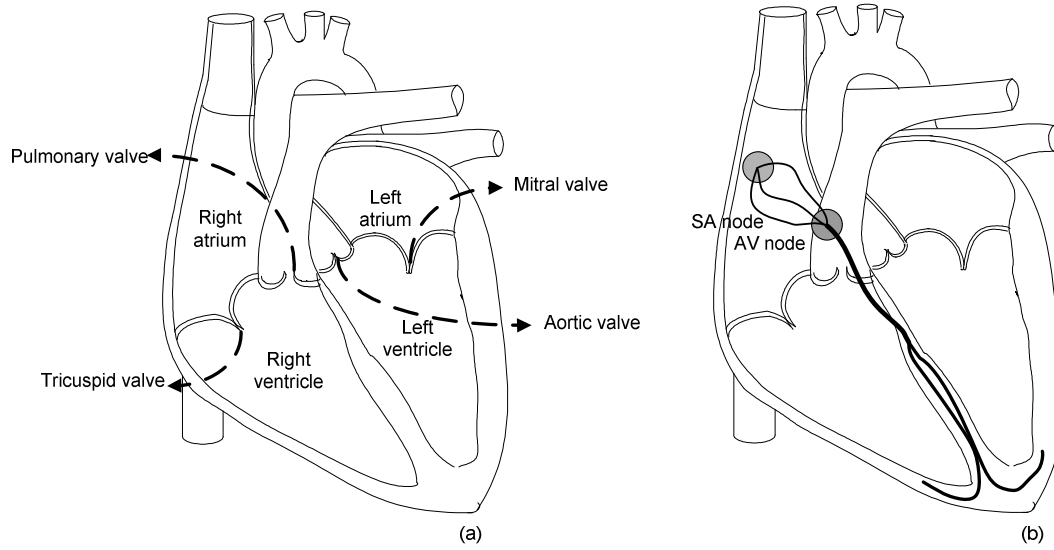
Fig. 1 (a) Simple anatomy of the heart shows the four chambers and four valves. (b). The electrical signal initiates at the SA node regularly, passes through AV node, and reaches the bottom of the heart.
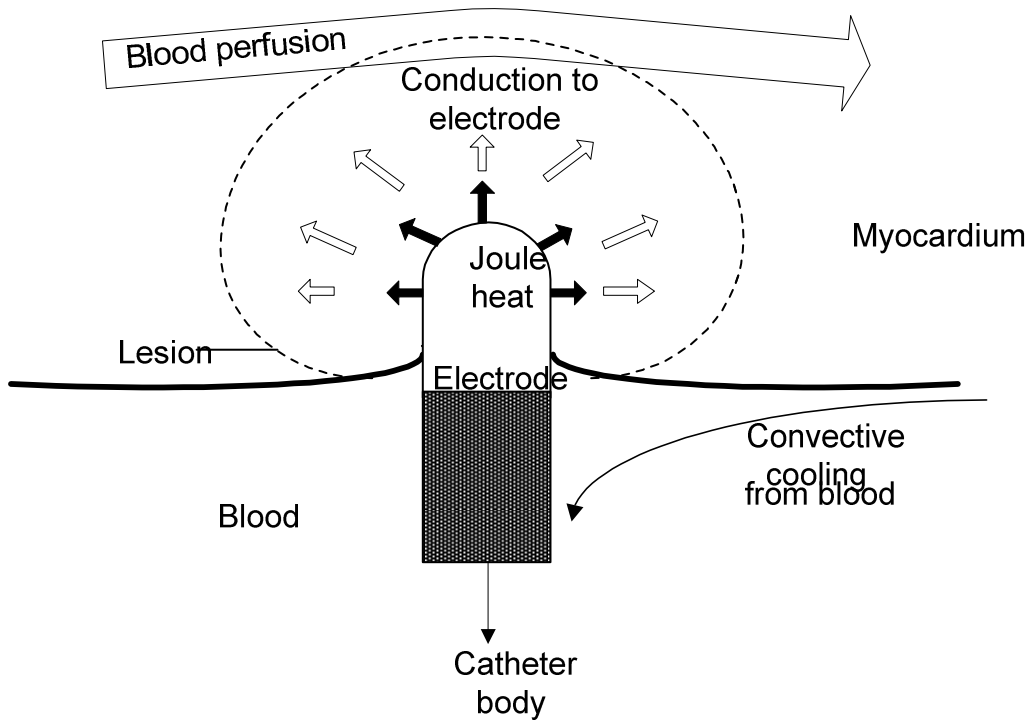
Fig. 2 Electric power through the electrode heats the myocardium. Blood velocity cools it. The black arrows represent the Joule heat generated close to the electrode. The white arrows represent the heat conduction from the hotter Joule heat region to the cooler myocardium.
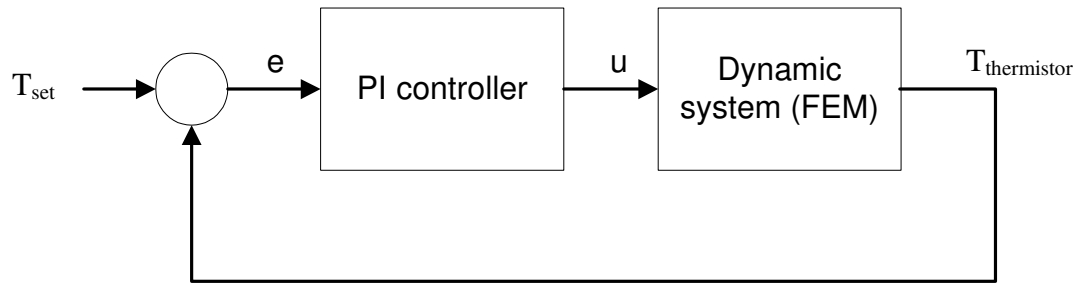

Fig. 3 Closed loop system incorporating a PI controller and the dynamic system (FE model).

(a)

Electrical Conductivity

(b)
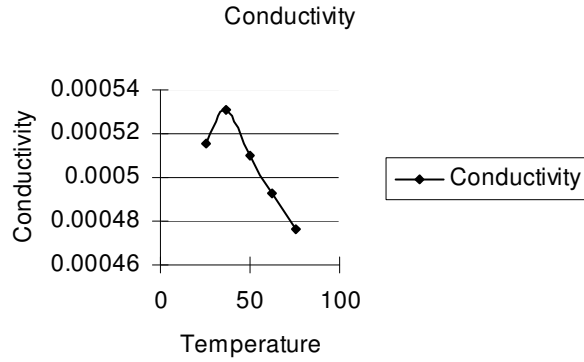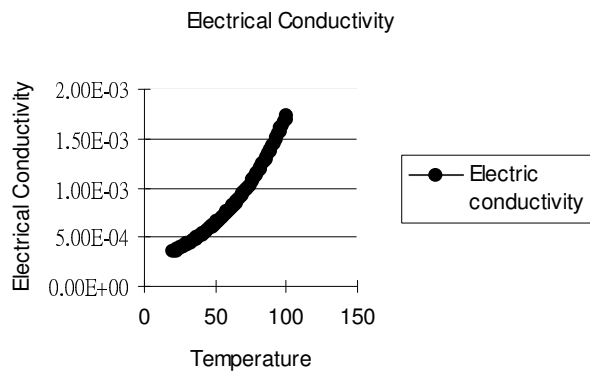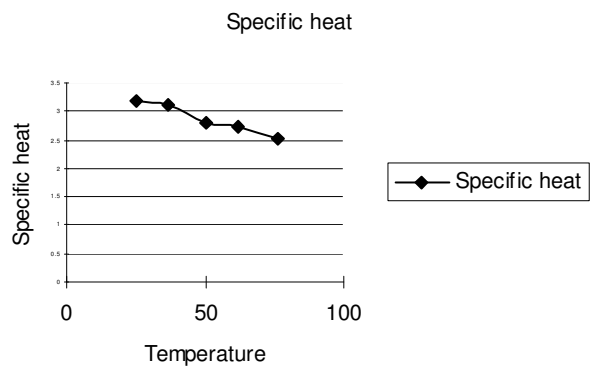
Specific heat

(c)

Fig. 4 The myocardial temperature-dependent properties (a) The thermal conductivity in W/m·K

(b) The impedance in $m^2 \cdot kg/s^2 \cdot A^2$ (c) The specific heat in J/kg·K (adapted from [18])

Fig. 5 The median values of *h* in W/m^2·K from *in-vivo* measurements in 15 pigs in 22 locations mapping on a heart diagram. (adapted from [16])

CHAPTER 2

THE MYOCARDIAL TISSUE SIZE AND CONVECTIVE COEFFICIENT IN CARDIAC ABLATION

Abstract—In different *in-vitro* experiments, the experimenters have chosen arbitrary myocardial tissue sizes such as $30 \times 30 \times 15$ mm. However, they did not verify whether this choice affected the formation of lesions. We investigated the effects of the changes in myocardial tissue sizes on the formation of the lesion by using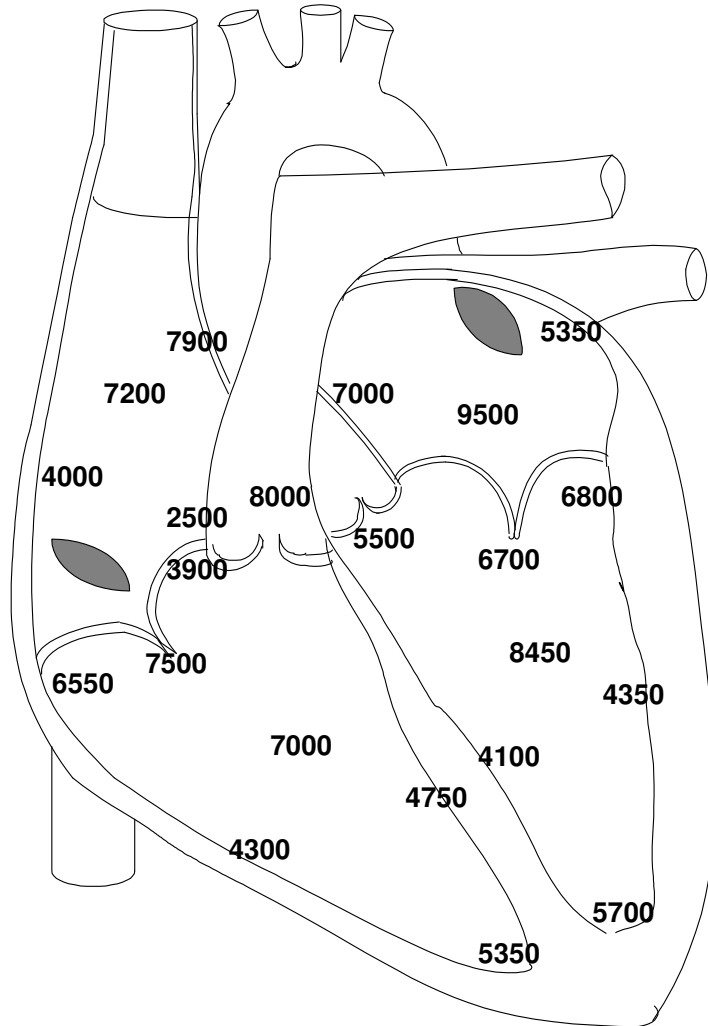 finite element (FE) method. The thickness and width of the myocardial tissue were considered in the study. Although the blood heat transfer convective coefficient has a large impact on the lesion size, the values of the blood–myocardium interfaces measured under different blood flow conditions by different research groups were very different. Additionally, the values of the blood–electrode interfaces under different blood flow conditions were calculated theoretically in previous simulations. We examined the effects of changes in the blood–myocardium and blood–electrode convective coefficients on the formation of lesions. The impact of the convective coefficients on the size of the lesion was qualified. The results show that the cardiac tissue size of $30 \times 30 \times 10$ mm is proper for the *in-vitro* comparison experiment for the preliminary framework of the lesion size estimator and the blood–electrode convective coefficients have more significant effects on the formation of lesions.

I. *INTRODUCTION*

Because of the efficacy, controllability, and minimal invasiveness, radiofrequency (RF) catheter ablation has proven an effective method to treat some cardiac arrhythmias, such as atrioventricular node re-entry, atrial tachycardia, atrial flutter, and fascicular ventricular tachycardias [1] – [3]. Several research groups also suggest that it may be a good method for palliative suppression of ventricular tachycardias [3] – [5].

Previous *in-vitro* experiments always stated that they used an appropriate cardiac tissue size such as $30 \times 30 \times 10$ mm. However, no one ever verified that this choice of size did not affect the formation of lesions in *in-vitro* experiments. Cao et al. [9] noted that the electric

current density in the myocardium and blood decrease rapidly with distance from the catheter electrode. It is similar to the case of a metal sphere immersed in the myocardium where the current density decreases as $1/r^2$; where r is the distance away from the electrode. Thus, the electric power delivered decreases as $1/r^4$. Thus, the temperature increment due to electric power is limited to a small rim of tissue next to the electrode as shown in Fig. 1. In addition, the heat conduction region depends on the temperature gradients and material properties and is also limited to a finite region next to the electric heating region. We conducted a sequence of simulations to verify that the selection of this myocardial tissue size only introduces an insignificant error in measurement.

In addition, the extent of the tissue heating and the volume of myocardial lesion formation depend heavily on the blood flow during cardiac ablation. The blood flow carries heat away from the myocardium and from the electrode by convection. It has a cooling effect on the thermistor and has a large impact on the final lesion size [7], [12], [13]. The blood velocities are significantly different at different locations inside the heart. So the cooling effect due to the blood convection differs at different ablation locations. Even though the tip temperature is set at the same temperature, different lesion sizes result at different locations. However, the measurements of convective coefficients are different among different groups [12], [14]. Thus, we investigated the effects of the blood–myocardium convective coefficient on the lesion size. In addition, the convective coefficient of the blood–electrode interface in previous FE studies was deduced from theoretical calculation [6]. We also examined the relationship between the blood–electrode convective coefficient and the lesion formation.

In order to investigate all the effects, we solved the bioheat equation for the cardiac ablation system. The commercial software (ABAQUS), a common FE bioheat equation solver, was used to determine the temperature distribution in the myocardium. FE modeling takes into

account the myocardial properties (electrical conductivity, thermal conductivity, density, and specific heat capacity) and the convection of the blood flow. Thus it has been demonstrated that it is a useful tool in the qualitative assessment of lesion dimensions created by RF ablation [6], [7], [8].

Thus, we had two objectives in this study: first, we verified that the choice of the myocardial tissue size *in-vitro* experiments did not introduce significant deviation into the lesion formation. Second, we quantified the effects of changing the convective coefficients between the blood–electrode interface and between the blood–myocardium interface for high blood flow and low blood flow on the lesion formation.

For achieving the first objective, several FE models with different myocardial tissue widths and thicknesses were constructed and an automatic control algorithm was used to control the entire process in constant temperature-mode at three different target temperatures, 50, 60, and 70 °C and at two flow rates.

In order to achieve the second objective, we set up the FE model having fixed width and thickness with different sets of convective coefficients for blood–electrode and blood–myocardium interfaces. The same control program was used to control the entire process at three different target temperatures, 50, 60, and 70 °C.

II. SIMULATION PROCESS

Fig. 2. shows the entire simulation procedure. The initial conditions including application time, period of each simulation step, data exported period, applied target tip temperature, input model file having the data of all thermal and electrical properties were fed into the simulation controller to generate the ABAQUS script file for the FE solver. Then the program sent the script file to the FE solver. The FE solver found the solution numerically for each time step and output a data file

containing temperature and potential distribution. The data collection analyzed the data file to extract temperature at the thermistor for the controlling algorithm to set up the applied voltage in the next-step script file. The data collection also saved the data file for fixed times for the creation of the database for the lesion size estimator. The next-script file was fed to the FE solver again. This process continued until the simulation time reached the preset applied time.

We implemented the simulation controller in a C++ program by using a proportional-integral (PI) algorithm. The controller determined the applied voltage at each uniform step time (0.5 s) by comparing the set temperature and the temperature at the thermistor. The thermistor temperature was read from the resulting file created by ABAQUS when it finished the simulation of each time step.

For all of the simulations, the ablation electrode was of standard size used in clinical practice (4 mm long, and 2.6 mm diameter). A temperature-sensing thermistor was embedded at the electrode tip. Similar to Tungjikusolmun et al. [6], we modeled the system by an axisymmetric model. The blood pool extended 40 mm beyond the myocardium. It was used to model the body fluid beyond the myocardium. We assumed that they were totally still and thus the convection due to fluid flow was negligible. The only heat transfer in this region was thermal conduction. We set the temperature of the blood on the boundary of the model to 37 °C, the blood temperature in the cardiac chamber. Using the Dirichlet boundary conditions, we assumed that the voltages on the outer surfaces of the model were 0 V. The electrical and thermal properties of all the materials used in the electrode were taken from [14]. The electrical conductivity of the myocardium varies with the temperature. Tsai et al. [15] measured it using the four-terminal method at 500 kHz every degree from 20 to 100 °C. We used the temperature-dependent thermal conductivity and the specific heat of the myocardium from Foster and Schwan [16] and Bhavaraju and Valvano [15]. Fig. 1 shows the simplified diagram of the

geometry of the ablation electrode model and the tissue at different penetration depths. The detailed values of the electrode refers to Ch. 3. Table 1 lists the total number of nodes and elements in each model.

III.   RESULTS AND DISCUSSION

A. *Data collection and lesion size measurement*

Fig. 3 shows a simplified diagram of our 2D model. For investigating the lesion formation results from different myocardial widths, we created 2D axisymmetric models with respective widths (*W*) of 20, 30, 40, and 80 mm and a constant thickness of 10 mm. For examining the effect of different myocardial thicknesses, we created models with respective thicknesses (*T*) of 8, 14, 18, and 20 mm and a constant width of 80 mm. Tables 1 and 2 list the total number of nodes and elements used for each model.

To investigate the effects of the changes in the blood–myocardium convective coefficients and in the blood–electrode convective coefficients, we used a 2D axisymmetric model with a constant width of 80 mm and with a constant thickness of 10 mm. The model contains 3273 nodes and 11216 elements. For the study of the changes in the blood–myocardium convective coefficients, there were 5 designed sets. These sets were established by varying the value of the blood–myocardium convective coefficient by the increments of 50%, 25%, 0%, –25%, –50 % of the measured values obtained from [12] and by using the theoretically calculated values for the blood–electrode convective coefficients. Table 3 lists the values for the high and low blood flow regions.

For investigating the effects of the changes in the blood–electrode convective coefficients on the lesion formation, there are five designed sets. These sets are established by varying the value of the blood-myocardium convective coefficient with an increments of 50%, 25%, 0%,

–25%, –50% of its theoretical value obtained from [6] and by fixing the blood–electrode convective coefficients to the measured values [12] for the high and low blood flow regions listed in Table 4.

The automatic control algorithm l controlled the simulation at a constant target temperature. These target temperatures were 50, 60, and 70 °C for different blood flow states. Data were collected at 10, 20, 40, and 90 s after start of the ablation simulation for each set temperature.

Nath [13] observed that when the tissue temperature reached 50 °C, irreversible myocardial injury occurred during RF cardiac ablation. The cells lost electrical excitability and the re-entrant pathways were interrupted. Thus 50 °C is usually considered as the threshold for lesion formation. We implemented a C++ program to search the temperature distribution in the system to find those points exceeding the critical temperature of 50 °C. Fig. 4 shows a typical shape of the lesion formed by RF ablation. We define W as the maximum width of the lesion, and D as the maximum depth of the lesion.

Figs. 5 to 16 show the results at 90 s.

B. Comparison in different widths of myocardium

The width of the myocardium affects where the boundary is in the X direction. The convection between the blood–myocardium interface is almost fixed because that convection is due to the change in width, which is far away from the electrode and therefore does not cause cooling of the thermistor. In addition, the Joule heating region only exists a few millimeters around the electrode tip. Thus, the heat conduction is the most important factor for lesion formation. In equilibrium, the temperature gradient in the X and Y directions affects the lesion width and depth. The smaller the width is, the larger the temperature gradient is in the X

direction. Thus, it affects the formation of the lesion. However, it is only observable when the width is comparatively small like 20 mm. We can get a larger lesion width and a smaller lesion depth with the width of 20 mm but the change is negligible. We cannot observe any difference in the lesion formation with widths of 30, 40, and 80 mm.

C. Comparison in different depths of myocardium

Similarly, the myocardial tissue thickness affects the temperature gradient in the *Y* direction. However, the range of the values, which is from 8 to 20 mm, is relatively smaller than the range of the values from 20 to 80 mm. Thus, we found that the effect of changes in the thickness was more observable than that in the width. There are two effects here. Instead of the effect discussed in the previous section, the heat that reaches the other end of the myocardial tissue is conducted away by the body fluid. This affects the temperature of the thermistor and lets it introduce more energy to maintain the tip temperature. The smaller the thickness is, the more energy is introduced. Thus, we observed an increment in the lesion depth with a thickness of 8 mm. This became more obvious when the target temperature became higher.

When the thickness of the myocardium increases, this can cause reduction of the lesion width or addition to the lesion width. In the low blood flow locations, the decreasing of the induced energy is more important. We observed that the lesion width decreased as the thickness increased. However, the result was different in the high blood flow regions. When the thickness was small, the effect of the reduction in induced energy resulted in the lesion width decreasing as the thickness increased. However, the temperature-gradient factor became more and more important as the thickness increased. Thus, we observed an increment in the lesion width as the thickness of myocardium increased over the value of 14 mm. The minimum of the lesion width appeared at the thickness of 14 mm.

We observed that the variations in the lesion dimension among these different thicknesses were insignificant compared to other factors such as the blood flow rate. Thus we believe that it is safe to choose the myocardial tissue size of $30 \times 30 \times 10$ mm. We also conclude that the lesion formation may be very different at the atrium and the ventricle during RF ablation because of the thickness of the myocardium.

D. Comparison of different blood–electrode and blood–myocardium coefficients

The blood flow contacts the electrode and the myocardium. The thermal conductivity of the metal part of the electrode is much higher than that in the cardiac tissue. Thus the heat is more easily carried away from the thermistor by following the heat transport path of the conduction through the metal and the convection between the blood–electrode interface than that of the conduction through the cardiac tissue and the convection between the blood–myocardium interface. Thus, we observed that the change in the value of the blood–electrode convective coefficient has larger effects on the lesion formation than the value of the blood–myocardium convective coefficient. We observed a steady increase pattern between the blood–electrode convective coefficient and the lesion size. The higher the blood–electrode convective coefficient is, the larger the lesion that is formed in both blood flow states.

Since in the high blood flow region the major portion of the heat was carried away through the blood–electrode interface, the variation of the blood–myocardium convection was negligible. However, in the low blood flow region, the relative portion of heat carried away through the blood–myocardium interface was larger relative to the heat through the blood–electrode interface. Thus, the larger the blood–myocardium convection was, the larger the lesion was; but the effect is relatively trivial.

IV.   CONCLUSION

From the results, we know that the width of the cardiac tissue had insignificant effects on the lesion formation. The thickness had more observable effects on the lesion size. However, these effects were insignificant. Thus, for *in-vitro* experiments, it is proper to choose a myocardial tissue size of $30 \times 30 \times 10$ mm. However, tissue dimensions become important when applying cardiac ablation to the atrium whose thickness is about 3 to 5 mm.

The electrode–blood convective coefficient had more significant effect on the formation of the lesion in both flow states. The blood–myocardium convective coefficient only had observable effect on lesion in low flow regions. Thus, in order to get a more accurate simulation for cardiac ablation, the measurement of electrode convective coefficient plays a more important role in getting a more accurate simulation for cardiac ablation.

REFERENCES

[1] S. K. S. Huang and D. J. Wilber, Eds., *Radiofrequency Catheter Ablation of Cardiac Arrhythmias: Basic Concepts and Clinical Applications*, 2nd ed., Armonk, NY: Futura, 2000.

[2] D. P. Zipes and M. Haïssaguerre, *Catheter Ablation of Arrhythmias*. 2nd ed. Armonk, NY: Futura, 2002.

[3] F. Morady, "Drug therapy: radio-frequency ablation as treatment for cardiac arrhythmias," *N. Engl. J. Med*., vol. 340, pp. 534-544, 1999.

[4] D. Panescu, "Intraventricular electrogram mapping and radiofrequency cardiac ablation for ventricular tachycardia," *Physiol. Meas*., vol. 18, pp. 1-38, 1997.

[5] H. Nakagawa, K. J. Beckman, and J. H. McClelland, "Radiofrequency catheter ablation of idiopathic left ventricular tachycardia guided by a Purkinje potential," *Circulation*, vol. 85, pp. 1666-1674, 1992.

[6] S. Tungjitkusolmun, E. J. Woo, H. Cao, J.-Z. Tsai, V. R. Vorperian, and J. G. Webster, "Thermal-electrical finite element modeling for radio-frequency cardiac ablation: effects of changes in myocardial properties," *Med. Biol. Eng. Comput.*, vol. 38, pp. 562-568, 2000.

[7] H. Cao, V. R. Vorperian, S. Tungjikusolmun, J.-Z. Tsai, D. Haemmerich, Y. B. Choy, and J. G. Webster, "Flow effect on lesion formation in RF cardiac catheter ablation, *IEEE Trans. Biomed. Eng.*, vol. 48, pp. 425-433, 2001.

[8] H. Cao, *Measuring Contact Area and Temperature during Radio-Frequency Cardiac Catheter Ablation*, Ph. D. Dissertation , Univ. of Wisconsin, Madison, May 2001.

[9] H. Cao, S. Tungjitkusolmun, Y. B. Choy, J.-Z. Tsai, V. R. Vorperian, and J. G. Webster, Using electrical impedance to predict catheter–endocardial contact during RF cardiac ablation, *IEEE Trans. Biomed. Eng.*, 49, 247-253, 2002.

[10] D. Haemmerich, J. G. Webster, "Automatic control of finite element models for temperature-controlled radiofrequency ablation", Biomed. Eng. Online, 4(1):42, 2005.

[11] D. Panescu, J. G. Whayne, S. D. Fleischman, M. S. Mirotznik, D. K. Swanson and J. G. Webster, "Three-dimensional finite element analysis of current density and temperature distributions during radio-frequency ablation," *IEEE Trans. Biomed. Eng.*, vol. 42, pp. 879-890, 1995.

[12] C. Tangwongsan, J. A. Will, J. G. Webster, K. L. Meredith Jr., D. M. Mahvi, "*In vivo* measurement of swine endocardial convective heat transfer coefficient", *IEEE Trans. Biomed. Eng.*, 51, 1478-1486.

[13] S. Nath, C. Lynch, J. G. Whayne, D. E. Haines, "Cellular electrophysiological effects of hyperthermia on isolated guinea pig papillary muscle implication for catheter ablation," *Circulation*, vol. 88, part 1, pp. 1826–1831, 1993.

[14] S. D. Edwards and R. A. Stern, *Electrode and Associated Systems Using Thermally Insulated Temperature Sensing Elements*, U. S. Patent 5 688 266, 1997.

[15]. J.-Z. Tsai, *Measurement of in vivo and in vitro swine myocardial resistivity*, PhD Dissertation, Univ. of Wisconsin-Madison, May 2001.

[16] K. R. Foster, and H. P. Schwan, "Dielectric properties of tissues and biological materials: a critical review," *CRC Crit. Rev. Biomed. Eng.*, vol. 17, pp. 25-104, 1989.

[17] N. C. Bhavaraju and J. W. Valvano, "Thermophysical properties of swine myocardium," *Int. J. Thermophys.*, vol. 20, pp. 665-676, 1999.

Fig. and Table Captions:

Fig. 1. Simplified diagram of the catheter ablation. The catheter is normal to the myocardium. There is an electric current applied between the catheter electrode and the dispersive electrode. The myocardium adjacent to electrode is mainly heated by the Joule effect. The myocardium is mainly heated by heat conduction. The blood flow removes the heat from the myocardium and catheter by convection.

Fig. 2. The FE simulation collects data for the creation of the lesion size estimator database .

Fig. 3. The simplified 2D model diagram for all the variable settings.

Fig. 4. Lesion volume is calculated from depth *D* and width *W*.

Fig. 5. Results at 90 s in different myocardial widths and thickness at high blood flow at 50 ^{o}C target temperature. The numbers in the labels (W, T) represent the width and thickness of the cardiac tissue in mm.

Fig. 6. Results at 90 s in different myocardial widths and thickness at low flow at 50 ^{o}C target temperature. The numbers in the labels (W, T) represent the width and thickness of the cardiac tissue in mm.
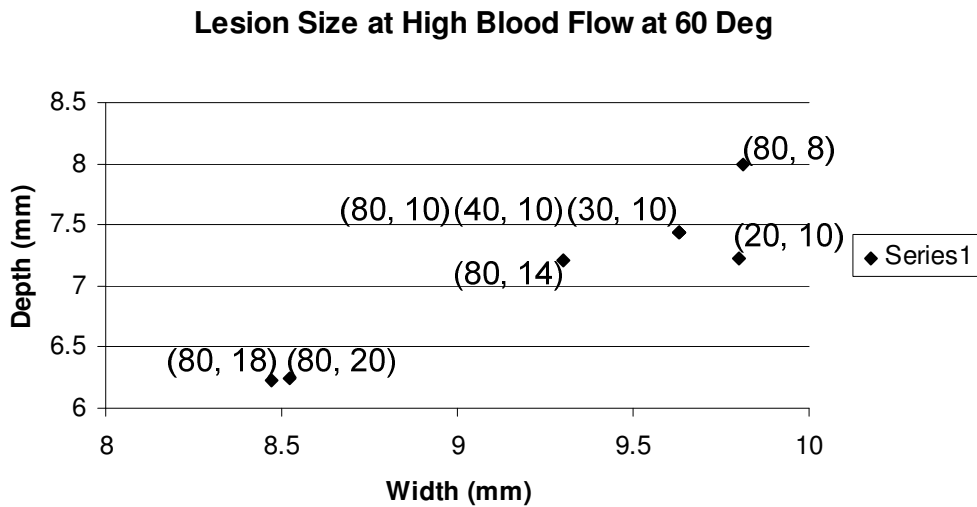
Fig. 7. Results at 90 s in different myocardial widths and thickness at high blood flow at 60 ^{o}C target temperature. The numbers in the labels (W, T) represent the width and thickness of the cardiac tissue in mm.

Fig. 8. Results at 90 s in different myocardial widths and thickness at low flow at 60 ^{o}C target temperature. The numbers in the labels (W, T) represent the width and thickness of the cardiac tissue in mm.

Fig. 9. Results at 90 s in different myocardial widths and thickness at high blood flow at 70 ^{o}C target temperature. The numbers in the labels (W, T) represent the width and thickness of the cardiac tissue in mm.

Fig. 10. Results at 90 s in different myocardial widths and thickness at low flow at 70 $^{\circ}$C target temperature. The numbers in the labels (W, T) represent the width and thickness of the cardiac tissue in mm.

Fig 11. Results at 90 s in different blood–electrode and blood–myocardium convective coefficients in high blood flow at 50 $^{\circ}$C target temperature. The numbers in the labels, (BM, BE), represent increment percentages of the blood–myocardium and blood–electrode to their respective base values.

Fig 12. Results at 90 s in different blood–electrode and blood–myocardium convective coefficients in low blood flow at 50 $^{\circ}$C target temperature. The numbers in the labels, (BM, BE), represent increment percentages of the blood–myocardium and blood–electrode to their respective base values.

Fig 13. Results at 90 s in different blood–electrode and blood–myocardium convective coefficients in high blood flow at 60 $^{\circ}$C target temperature. The numbers in the labels, (BM, BE), represent increment percentages of the blood–myocardium and blood–electrode to their respective base values.
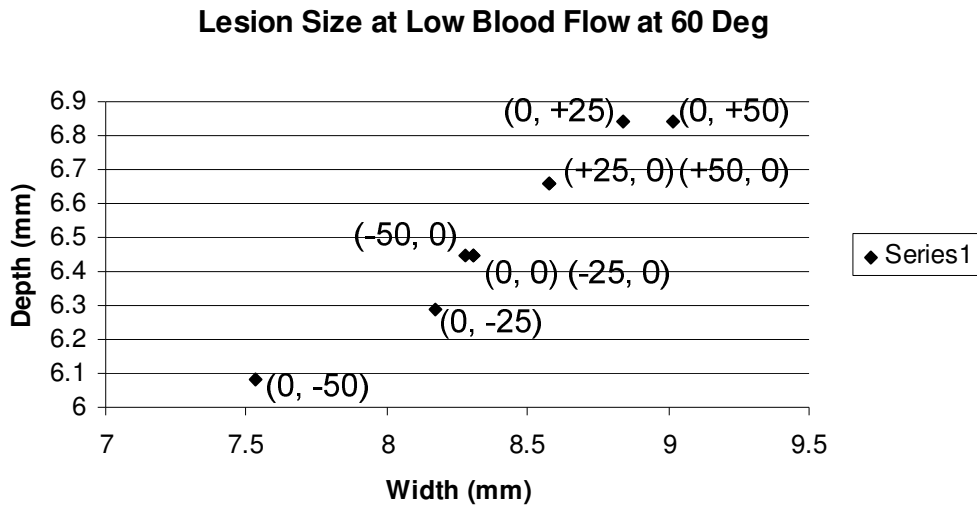
Fig 14. Results at 90 s in different blood–electrode and blood–myocardium convective coefficients in low blood flow at 60 $^{\circ}$C target temperature. The numbers in the labels, (BM, BE), represent increment percentages of the blood–myocardium and blood–electrode to their respective base values.

Fig 15. Results at 90 s in different blood–electrode and blood–myocardium convective coefficients in high blood flow at 70 $^{\circ}$C target temperature. The numbers in the labels, (BM, BE), represent increment percentages of the blood–myocardium and blood–electrode to their respective base values.

Fig 16. Results at 90 s in different blood–electrode and blood–myocardium convective coefficients in low blood flow at 70 $^{\circ}$C target temperature. The numbers in the labels, (BM, BE), represent increment percentages of the blood–myocardium and blood–electrode to their respective base values.

Table 1. The number of nodes and elements contained in each model with different widths in mm.

Table 2. The number of nodes and elements contained in each model with different thicknesses in mm.

Table 3. The convective coefficient sets were constructed by fixing the convective coefficient at the blood–electrode interface when changing the convective coefficient at the blood–myocardium interface with increments of 50%, 25%, 0, –25%, –50%.

Table 4. The convective coefficient sets were constructed by fixing the convective coefficient at the blood–myocardium interface when changing the convective coefficient at the blood–electrode interface with increments of 50%, 25%, 0, –25%, –50%.
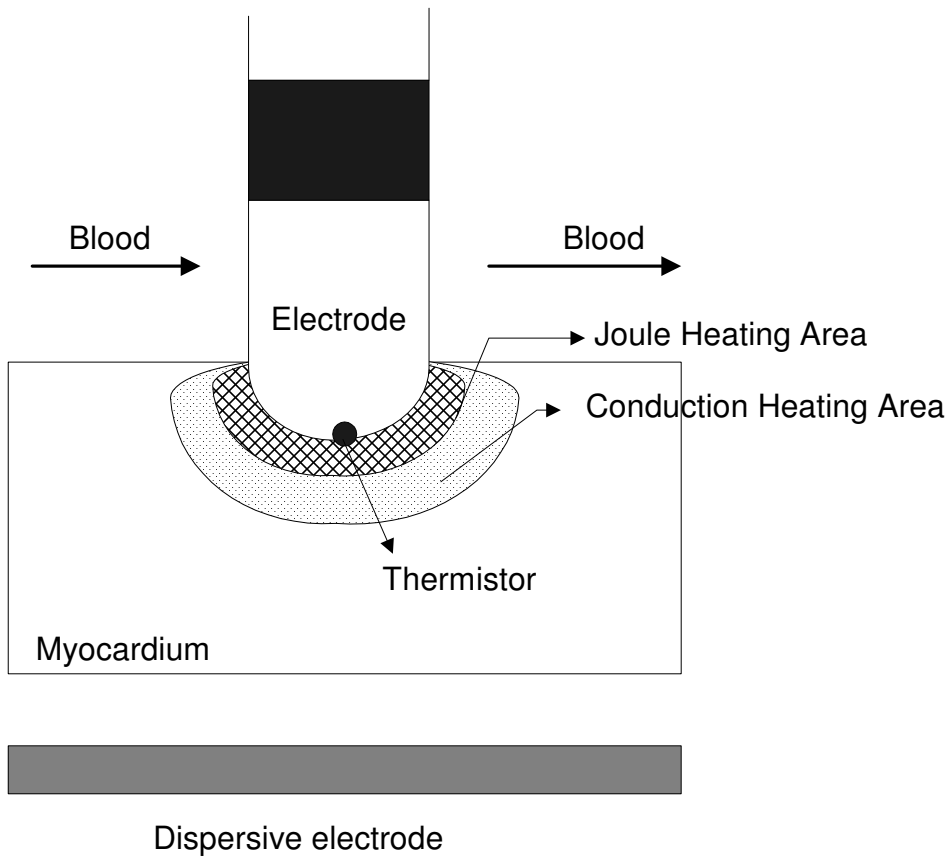
Fig. 1. Simplified diagram of the catheter ablation. The catheter is normal to the myocardium. There is an electric current applied between the catheter electrode and the dispersive electrode. The myocardium adjacent to electrode is mainly heated by the Joule effect. The myocardium is mainly heated by heat conduction. The blood flow removes the heat from the myocardium and catheter by convection.
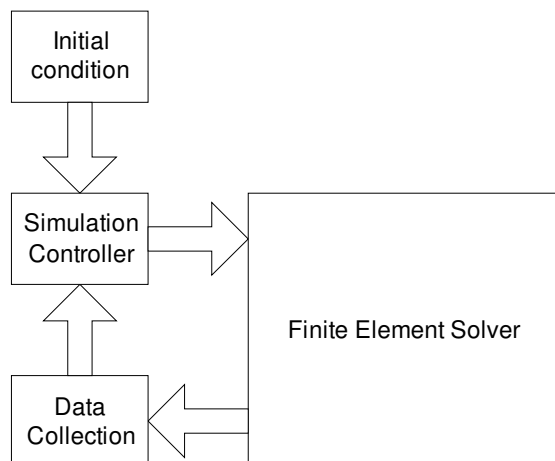
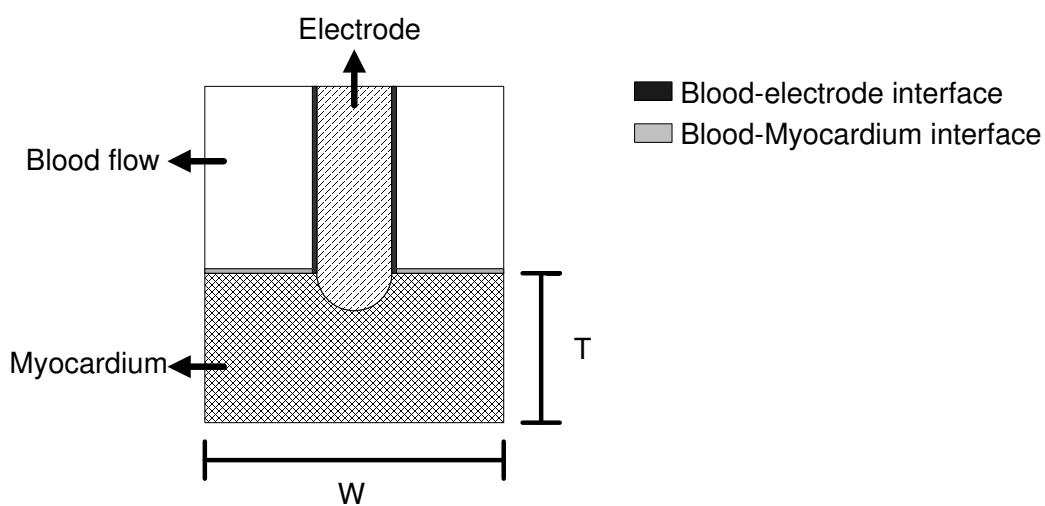**Fig. 2.** The FE simulation collects data for the creation of the lesion size estimator database.

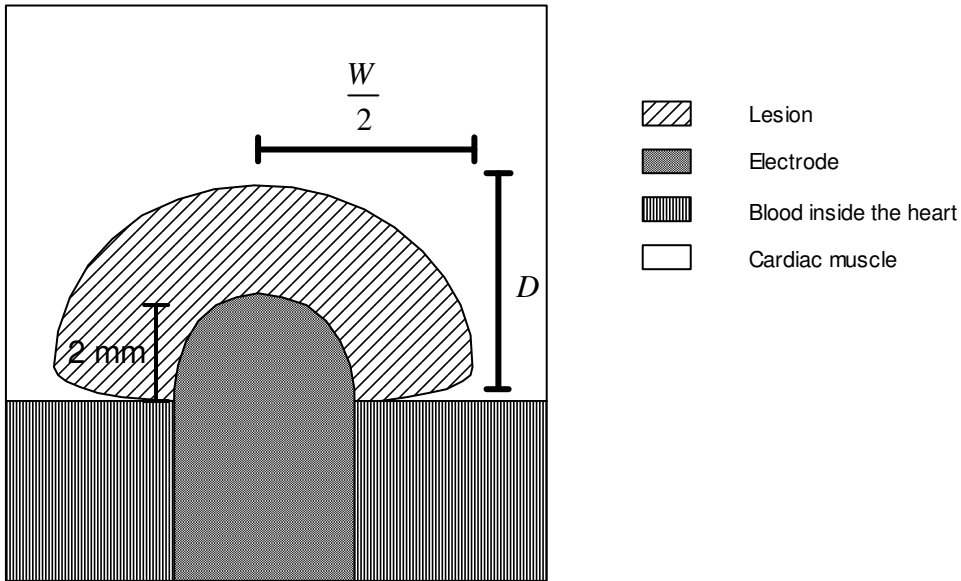**Fig. 3.** The simplified 2D model diagram for all the variable settings.

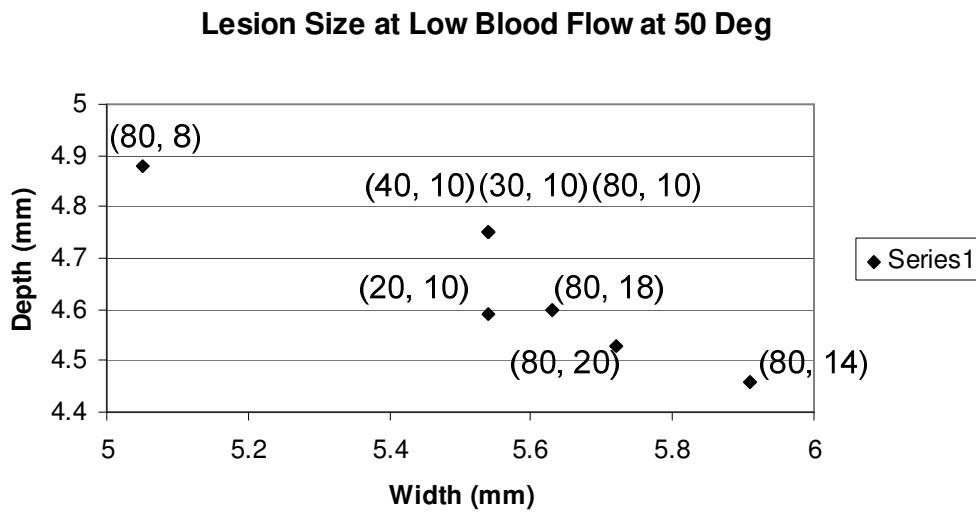**Fig. 4** Lesion volume is calculated from depth *D* and width *W*.

Fig. 5 Results at 90 s in different myocardial widths and thickness at high blood flow at 50 $^{\circ}$C target temperature. The numbers in the labels (W, T) represent the width and thickness of the cardiac tissue in mm.

Lesion Size in Low Blood Flow at 50 Deg

Fig. 6. Results at 90 s in different myocardial widths and thickness at low flow at 50 ^{o}C target temperature. The numbers in the labels (W, T) represent the width and thickness of the cardiac tissue in mm.

Lesion Size at High Blood Flow at 60 Deg

Fig. 7 Results at 90 s in different myocardial widths and thickness at high blood flow at 60 ^{o}C target temperature. The numbers in the labels (W, T) represent the width and thickness of the cardiac tissue in mm.
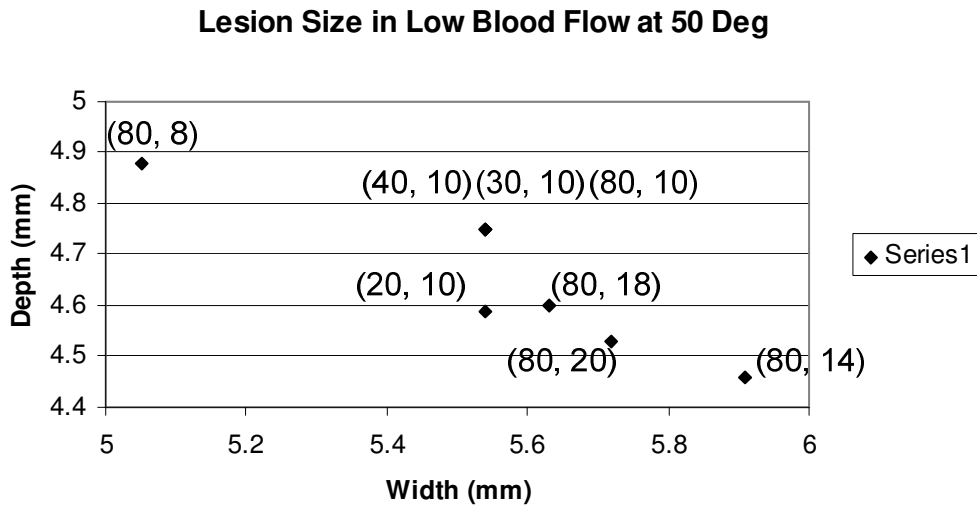
Lesion Size at Low Blood Flow at 60 Deg

(80, 10)(40, 10)(30, 10)

(80, 8)

(80, 18)   (80, 20)

Depth (mm)

(20, 10)

(80, 14)

◆ Series1

Width (mm)

Fig. 8. Results at 90 s in different myocardial widths and thickness at low flow at 60 ^{o}C target temperature. The numbers in the labels (W, T) represent the width and thickness of the cardiac tissue in mm.

Lesion Size at High Blood Flow at 70 Deg

(80, 10)(40, 10)(30, 10)

(20, 10)

(80, 14)   (80, 18)   (80, 20)

Depth (mm)

(80, 8)

◆ Series1

Width (mm)

Fig. 9. Results at 90 s in different myocardial widths and thickness at high blood flow at 70 ^{o}C target temperature. The numbers in the labels (W, T) represent the width and thickness of the cardiac tissue in mm.
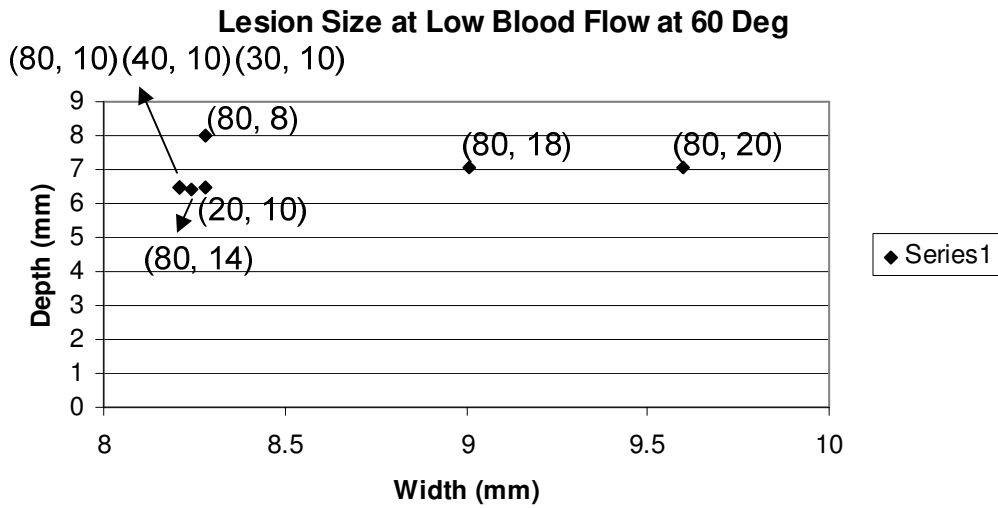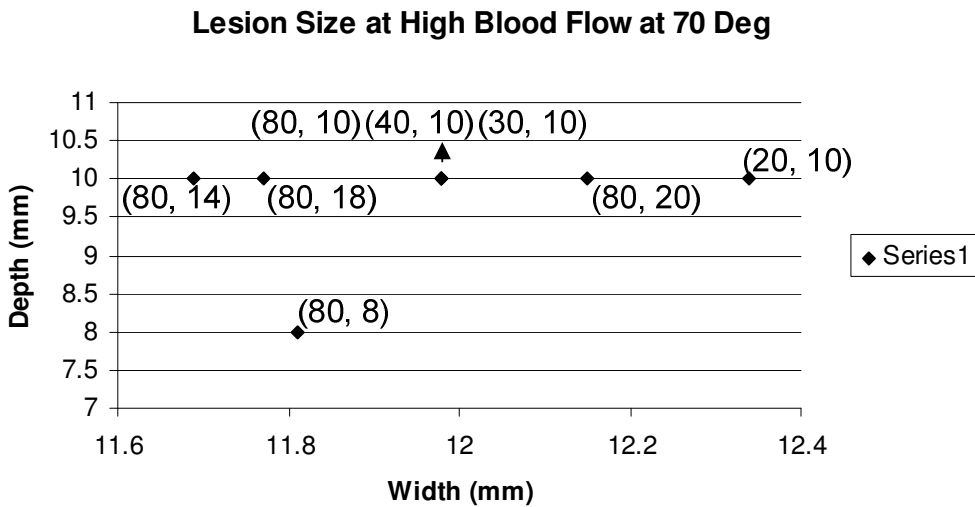
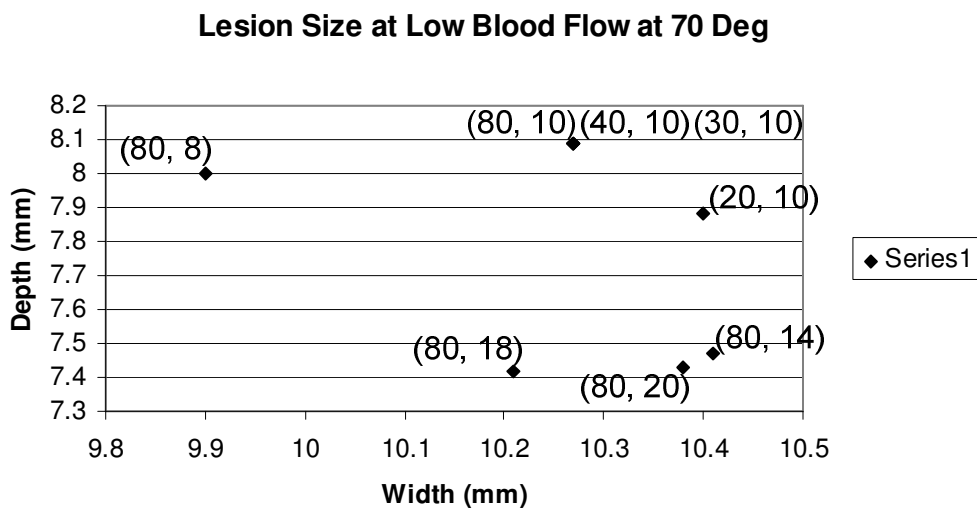**Lesion Size at Low Blood Flow at 70 Deg**

Fig. 10. Results at 90 s in different myocardial widths and thickness at low flow at 70 $^{\circ}$C target temperature. The numbers in the labels (W, T) represent the width and thickness of the cardiac tissue in mm.

Lesion Size at High Blood Flow at 50 Deg

Fig 11. Results at 90 s in different blood–electrode and blood–myocardium convective coefficients in high blood flow at 50 $^{\circ}$C target temperature. The numbers in the labels, (BM, BE), represent increment percentages of the blood–myocardium and blood–electrode to their respective base values.

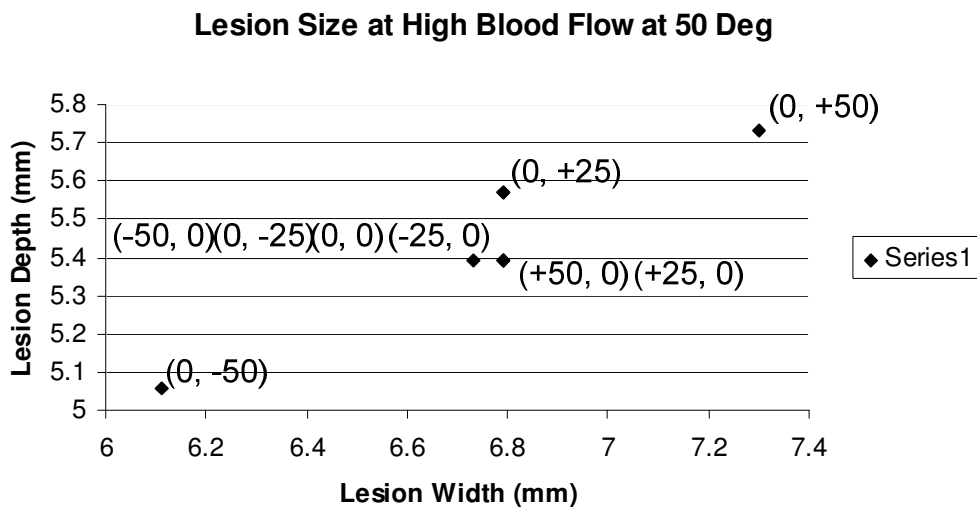**Lesion Size at Low Blood Flow at 50 Deg**

Fig 12. Results at 90 s in different blood–electrode and blood–myocardium convective coefficients in low blood flow at 50 $^{\circ}$C target temperature. The numbers in the labels, (BM, BE), represent increment percentages of the blood–myocardium and blood–electrode to their respective base values.

Lesion Size at High Blood Flow at 60 Deg

Fig 13. Results at 90 s in different blood–electrode and blood–myocardium convective coefficients in high blood flow at 60 ^{o}C target temperature. The numbers in the labels, (BM, BE), represent increment percentages of the blood–myocardium and blood–electrode to their respective base values.
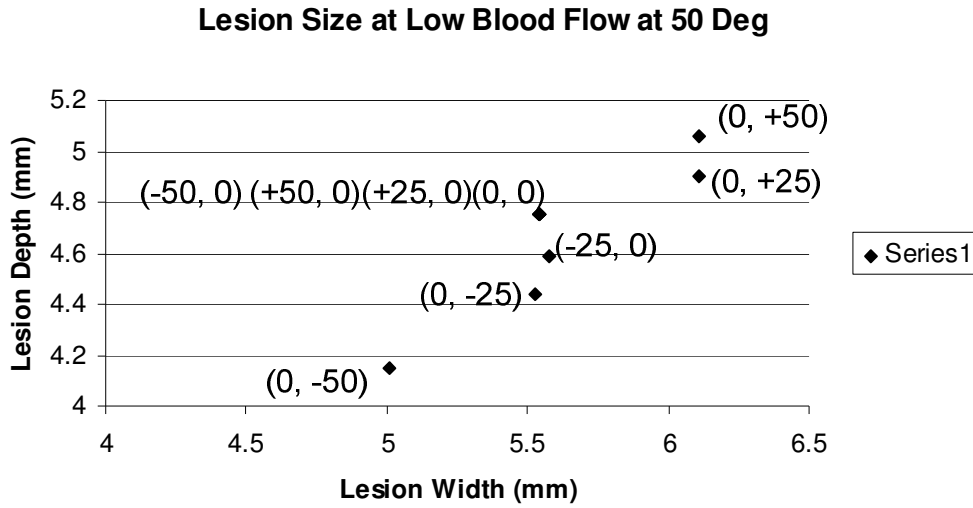
Lesion Size at Low Blood Flow at 60 Deg

Fig 14. Results at 90 s in different blood–electrode and blood–myocardium convective coefficients in low blood flow at 60 ^{o}C target temperature. The numbers in the labels, (BM, BE), represent increment percentages of the blood–myocardium and blood–electrode to their respective base values.

Lesion Size at High Blood Flow at 70 Deg

Fig 15. Results at 90 s in different blood–electrode and blood–myocardium convective coefficients in high blood flow at 70 ^{o}C target temperature. The numbers in the labels, (BM, BE), represent increment percentages of the blood–myocardium and blood–electrode to their respective base values.
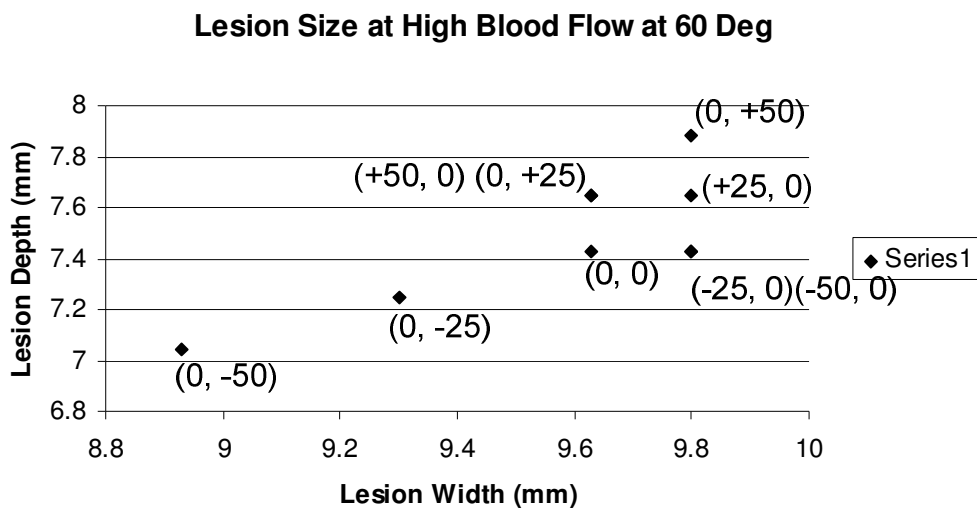
Lesion size at Low Blood Flow at 70 Deg

Fig 16. Results at 90 s in different blood–electrode and blood–myocardium convective coefficients in low blood flow at 70 $^{\circ}$C target temperature. The numbers in the labels, (BM, BE), represent increment percentages of the blood–myocardium and blood–electrode to their respective base values.
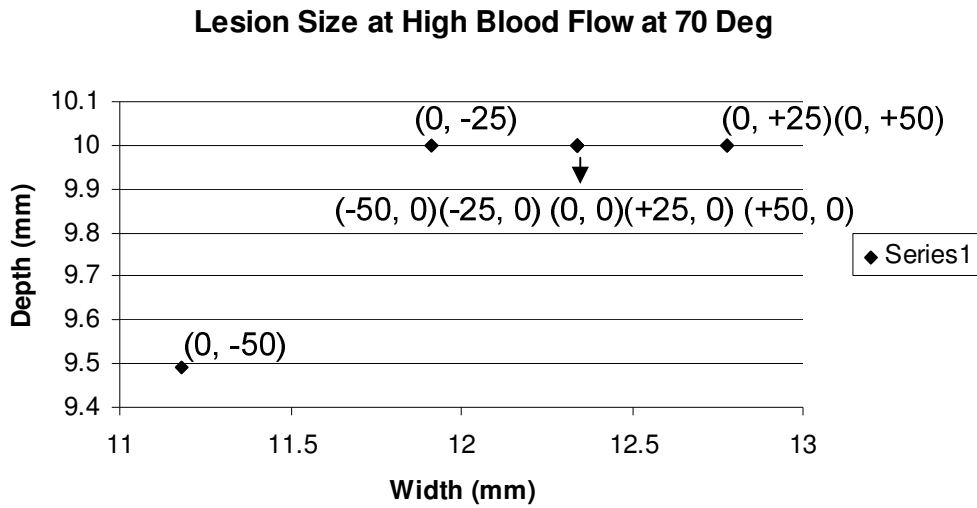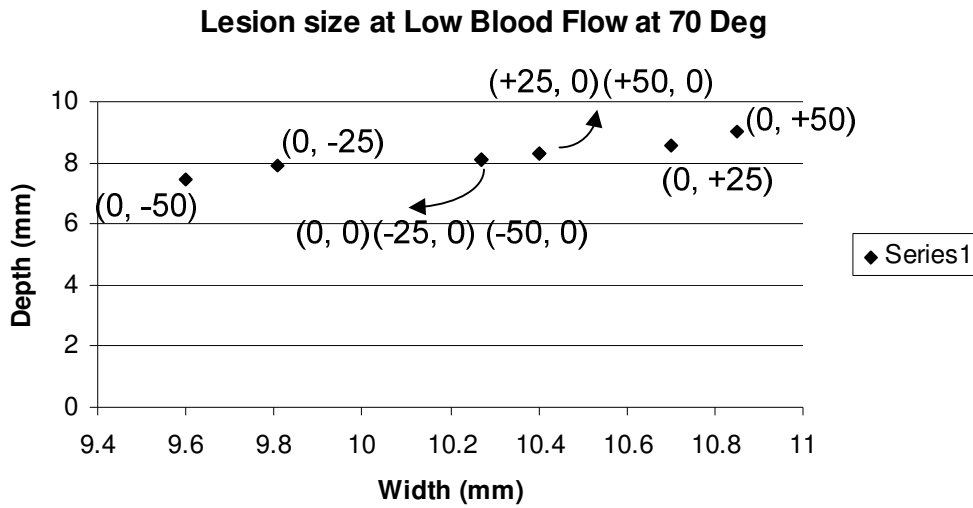
Table 1. The number of nodes and elements contained in each model with different widths in mm.

Width	# of Elements	# of nodes
20	4118	8208
30	4282	8496
40	4352	8604
80	3273	6546

Table 2. The number of nodes and elements contained in each model with different thicknesses in mm.

Thickness	# of Elements	# of nodes
8	2157	4294
14	2392	4749
18	2387	4739
20	3678	7206

Table 3. The convective coefficient sets were constructed by fixing the convective coefficient at the blood–electrode interface when changing the convective coefficient at the blood–myocardium interface with increments of 50%, 25%, 0, –25%, –50%.

Set	**High blood flow region**		**Low blood flow region**	
	h_{bm}* [W/(m^2·K)]	h_{be}** [W/(m^2·K)]	h_{bm} [W/(m^2·K)]	h_{be} [W/(m^2·K)]
1	10650	6090	5025	2081
2	8875	6090	4187.5	2081
3***	7100	6090	3350	2081
4	5325	6090	2512.5	2081
5	3550	6090	1675	2081

* h_{bm}: convective coefficient at blood–myocardium interface
** h_{be}: convective coefficient at blood–electrode interface
*** The set is used in our lesion size estimator

Table 4. The convective coefficient sets were constructed by fixing the convective coefficient at the blood–myocardium interface when changing the convective coefficient at the blood–electrode interface with increments of 50%, 25%, 0, –25%, –50%.

Set	High blood flow region		Low blood flow region	
	h_{bm}* [W/(m^2·K)]	h_{be}** [W/(m^2·K)]	h_{bm} [W/(m^2·K)]	h_{be} [W/(m^2·K)]
1	7100	9135	3350	3121.5
2	7100	7612.5	3350	2601.25
3***	7100	6090	3350	2081
4	7100	4567.5	3350	1560.75
5	7100	3045	3350	1040.5

* h_{bm}: convective coefficient at blood–myocardium interface
** h_{be}: convective coefficient at blood–electrode interface
*** The set is used in our lesion size estimator

CHAPTER 3

LESION SIZE ESTIMATOR BY CONSIDERING THE APPLIED LOCATION, DURATION AND TARGET TIP TEMPERATURE

Abstract—Finite element (FE) analysis has become a common method to analyze the lesion formation during temperature-controlled radiofrequency (RF) cardiac ablation. We present a process of FE modeling a system including blood, myocardium, and an ablation catheter with a thermistor embedded at the tip. The simulation uses a simple proportional-integral (PI) controller to control the entire process operated in temperature-controlled mode. Several factors affect the lesion size such as target temperature, blood flow rate, and application time. We simulated the time response of RF ablation at different locations by using different target temperatures. The applied sites were divided into two groups each with a different convective heat transfer coefficient. The first group was high-flow such as the atrioventricular (AV) node and the atrial aspect of the AV annulus, and the other was low-flow such as beneath the valve or inside the coronary sinus. Results showed the change of lesion depth and lesion width with time, under different conditions. We collected data for all conditions and used it to create a database. We implemented a user-interface, the lesion size estimator, where the user enters set temperature and location. Based on the database, the software estimated lesion dimensions during different applied durations. This software could be used as a first-step predictor to help the clinical electrophysiologists choose treatment parameters.

I. INTRODUCTION

Because of the efficacy, controllability, and minimal invasiveness, radiofrequency (RF) catheter ablation has proven an effective method to treat some cardiac arrhythmias, such as atrioventricular node re-entry, atrial tachycardia, atrial flutter, and fascicular ventricular tachycardias [1]–[3]. Several research groups also suggest that it may be a good method for palliative suppression of ventricular tachycardias [3]–[5].

In order to analyze the relationship between the set temperature in temperature-controlled mode and lesion size in the cardiac tissue during RF ablation, we solve the bioheat equation. Commercial software (ABAQUS 6.2), a common FE bioheat equation solver, is used to determine the temperature distribution in the myocardium. FE modeling takes into account myocardial properties (electrical conductivity, thermal conductivity, density, and specific heat capacity) and the convection of the blood flow. Thus it has been demonstrated that it is a useful tool in qualitative assessment of lesion dimensions created by RF ablation [6]–[8]. Early simulations such as Tungjitkusolmun et al. [8] used trial and error adjustment of the applied voltage at each time step to control the tip temperature at the set value. Haemmerich et al. [9] implemented a simple PI controller for hepatic ablation simulation. In this study, we adjusted the control coefficients to fit cardiac characteristics. In temperature-controlled mode, the controlled temperature is sensed from an insulated thermistor in contact with the endocardium at the tip of the catheter and feedbacks to the PI controller. The PI controller increases the applied power gradually and lets the tip temperature approach the set value with minimum overshoot at the set temperature. This is similar to the commercial ablation generator. Thus, we expect to obtain similar temporal behavior as in the *in-vivo* experiments. In addition, with the aid of the computer, we can also set the time-step shorter to make the simulation more precise.

In addition to the set temperature, the blood flow in the heart chambers also plays an important role in lesion formation during RF ablation. The blood flow carries heat away from the endocardium and from the electrode by convection. It has a cooling effect on the myocardium and has a large impact on the final lesion size [7], [10], [11]. The blood velocities are significantly different at different locations inside the heart. So the cooling effect due to blood convection differs at different ablation locations. Even though the tip temperature is set at the same temperature, different lesion sizes result at different locations.

Thus, our objective was to quantify the effect of changing ablation catheter tip temperature, in different locations in the heart chamber with different blood velocities on the FE calculation of the lesion size as a function of the applied ablation time.

II. SIMULATION PROCESS

Fig. 1. shows the entire simulation procedure. The initial conditions including application time, period of each simulation step, data exported period, applied target tip temperature, input model file having the data of all thermal, electrical properties are fed into the simulation controller to generate the ABAQUS script file for the FE solver. Then the program sends the script file to the FE solver. The FE solver finds the solution numerically for each time step and outputs a data file containing temperature and potential distribution. The data collection analyzes the data file to extract temperature at the thermistor for the controlling algorithm to set up the applied voltage in the next-step script file. The data collection also saves the data file for fixed times for the creation of the database for the lesion size estimator. The next-script file is fed to the FE solver again. This process continues until the simulation time reaches the preset applied time.

We implement the simulation controller in a C++ program by using a proportional integral (PI) algorithm. The controller determines the applied voltage at each uniform step time (0.5 s) by comparing the set temperature and the temperature at the thermistor. The thermistor temperature was read from the resulting file created by ABAQUS 6.2 when it finished the simulation of each time step.

III.   Result and Discussion

A. Data collection and lesion size measurement

Fig. 2. shows the 2D model which is used for the entire simulation. Fig. 3. shows the entire data collection process by using our PI controller and the ABAQUS FE solver. We ran the left part for two different blood flows and different applied temperatures. We simulated temperature-controlled ablation at temperatures of 50, 55, 60, 65, 70, 75, and 80 °C in different blood flow states. We acquired the temperature distribution at 10, 20, 30, 40, 50, 60, 70, 80, and 90 s after start of the ablation simulation for each set temperature.

Nath [12] observed that when the tissue temperature reached 50 °C, irreversible myocardial injury occurred during RF cardiac ablation. The cells lost electrical excitability and the re-entrant pathways were interrupted. Thus 50 °C is usually considered as the threshold for lesion formation. We implemented a C++ program to search the temperature distribution in the system to find those points exceeding the critical temperature of 50 °C. Fig. 4 shows a typical shape of the lesion formed by RF ablation. *W* is the maximum width of the lesion, and *D* is the maximum depth of the lesion. The user interface estimates the *W* and *D* values from the temperature distribution.

The results are shown in Figs. 5, 6, 7, 8. The width of the lesion increases rapidly at the beginning of the ablation and then reaches a plateau for the high flow state at 30 s, and the low flow state at 40 s. The depth also grows rapidly at the beginning, and then gradually in the middle of simulation until it penetrates the entire depth of the cardiac tissue. The slope of the high flow state is steeper than that of the low flow state.

B. Comparison to the commercial control algorithm

In this simulation, we implemented the PI controller to increase the applied power monotonically at the beginning of the ablation. When the temperature approached the target temperature, the applied power decreased to maintain the monitored temperature at the target temperature so that it yielded minimum overshoot at the set temperature. This is similar to the commercial ablation generator. Thus, we expected to obtain similar temporal behavior as in the *in-vivo* experiments. However, the real commercial machine monitors the temperature, power, and impedance of the tissue at the same time. Because the hot spot would not appear at the tip of the electrode, the commercial algorithm should be able to predict the temperature at the hot spot from the temperature at the thermistor and prevent the occurrence of further injury of the myocardium such as popping. The implemented details of the machine are a commercial secret. We attempted to imitate the controlling strategy of the commercial device.

C. Comparison to the results in in-vitro experiments

Table 2 shows the comparisons of the lesion sizes between the FE simulations and *in-vitro* experiments after applying 90 s of RF ablation. First, because of the 50 W power limit in the RF generator, the highest achievable target temperature was about 73 °C at the high blood-flow region. Thus, the process at 80 °C could not achieve the expected result. Second, the predictions in lesion width by FE simulations were almost the same as the experimental results for lesion width. Third, there were prediction errors in lesion depth between simulation and experimental results, but the prediction errors were fixed at about 2.5 mm for all cases. These differences may have resulted from the catheter–myocardium contact conditions such as insertion depth, insertion angle, and deformation due to the catheter insertion.

IV.   USER INTERFACE

When clinical electrophysiologists apply RF ablation to a patient, they must estimate the lesion size by considering all the variables that will affect the result. In this study, we also created the preliminary architecture of software to ease the burdening of combining the affecting factors together. We created a user interface to allow the user to input the target tip temperature and the applied location. After looking up the temperature distribution database, it showed the estimates of the lesion dimensions to the user. It could be used as the first-step predictor to estimate the possible lesion formation in different settings. The interface should be extended to include additional parameters. Fig. 9. shows a screenshot of the user interface.

V. CONCLUSION

Previously published papers describe the effect of the ablation time [6], tip temperature [6], control algorithm [9], and blood flow effect [8] separately. However, when clinical electrophysiologists want to apply RF ablation to a patient, they must estimate the lesion size by considering all the variables that will affect the result. In addition, none of these papers present the relation between applied time and the formation of lesions. We created the preliminary architecture of software where the user can enter set temperature, ablation time and ablation location. The software shows estimates of the lesion dimensions to the user. It could be used as a first-step predictor to estimate the possible lesion formation in different settings.

However, we only used two convective heat transfer coefficients to model the different applied locations and have assumed contact of 2 mm penetration in the cardiac model during the simulation. In real life, the situation is not so simple. Thus the following may be limitations to the precision of estimation:

(1). In real life, the variation of the contact has a quantitative effect on the formation of the lesion. Modeling different penetration depths and angles would improve the precision.

(2). Although blood flow in the cardiac chamber is very complex and varies from 5 L/min to almost 0 L/min, we simply divided the applied locations into high blood flow (3 L/min) and low blood flow (1 L/min). With improved knowledge of blood flow at each location, we could obtain an improved estimation of the formation of the lesion.

(3). We used a control program that improved efficiency without human interaction during the simulation. The accuracy of the control method could be improved by determining the dynamic response of the increased tissue temperature to applied voltage during *in-vivo* experiments. With information about the control methods used in the commercial generators, we could more precisely simulate process of RF ablation in the operating room.

REFERENCES

[1] S. K. S. Huang and D. J. Wilber, Eds., *Radiofrequency Catheter Ablation of Cardiac Arrhythmias: Basic Concepts and Clinical Applications*, 2nd ed., Armonk, NY: Futura, 2000.

[2] D. P. Zipes and M. Haïssaguerre, *Catheter Ablation of Arrhythmias*. 2nd ed. Armonk, NY: Futura, 2002.

[3] F. Morady, "Drug therapy: radio-frequency ablation as treatment for cardiac arrhythmias," *N. Engl. J. Med*., vol. 340, pp. 534-544, 1999.

[4] D. Panescu, "Intraventricular electrogram mapping and radiofrequency cardiac ablation for ventricular tachycardia," *Physiol. Meas*., vol. 18, pp. 1-38, 1997.

[5] H. Nakagawa, K. J. Beckman, and J. H. McClelland, "Radiofrequency catheter ablation of idiopathic left ventricular tachycardia guided by a Purkinje potential," *Circulation*, vol. 85, pp. 1666-1674, 1992.

[6]. Tungjitkusolmun, S., Woo, E. J., Cao, H., Tsai, J.-Z., Vorperian, V. R., and Webster, J. G., "Thermal-electrical finite element modeling for radio-frequency cardiac ablation: effects of changes in myocardial properties," *Med. Biol. Eng. Comput.*, vol. 38, pp. 562-568, 2000.

[7]. H. Cao, V. R. Vorperian, S. Tungjikusolmun, J.-Z. Tsai, D. Haemmerich, Y. B. Choy, and J. G. Webster, "Flow effect on lesion formation in RF cardiac catheter ablation, *IEEE Trans. Biomed. Eng.*, vol. 48, pp. 425-433, 2001.

[8]. S. Tungjitkusolmun, V. R. Vorperian, N. Bhavaraju, H. Cao, J.-Z. Tsai, and J. G. Webster, "Guidelines for predicting lesion size at common endocardial locations during radio-frequency ablation," *IEEE Trans. Biomed. Eng.*, vol. 48, pp. 194-201, 2001.

[9] D. Haemmerich, J. G. Webster, "Automatic control of finite element models for temperature-controlled radiofrequency ablation", Biomed. Eng. Online, 4(1):42, 2005.

[10]. D. Panescu, J. G. Whayne, S. D. Fleischman, M. S. Mirotznik, D. K. Swanson and J. G. Webster, "Three-dimensional finite element analysis of current density and temperature distributions during radio-frequency ablation," *IEEE Trans. Biomed. Eng.*, vol. 42, pp. 879-890, 1995.

[11]. H. H. Peterson, X. Chen, A. Pietersen, J. H. Svendsen, S. Hauns, "Lesion dimensions during temperature-controlled radiofrequency catheter ablation of left ventricular porcine myocardium: impact of ablation size, electrode size and convective cooling," *Circulation*, vol. 99, pp. 319-325, 1999.

[12] S. Nath, C. Lynch, J. G. Whayne, D. E. Haines, "Cellular electrophysiological effects of hyperthermia on isolated guinea pig papillary muscle implication for catheter ablation," *Circulation*, vol. 88, part 1, pp. 1826-1831, 1993.

Fig. and Table Captions:

Fig. 1. The FE simulation collects data for the creation of the lesion size estimator database.

Fig. 2. The geometry of the standard size ablation electrode in millimeters.

Fig. 3. The PI controller adjusts the applied voltage to maintain the tip temperature constant.

Fig. 4. Lesion volume is calculated from depth *D* and width *W*.

Fig. 5. Simulation result in lesion width increases with ablation time at high flow.

Fig. 6. Simulation result in lesion depth increases with ablation time at high flow.

Fig. 7. Simulation result in lesion width increases with ablation time at low flow.

Fig. 8. Simulation result in lesion depth increases with ablation time at low flow.

Fig. 9. A screenshot of the user interface

Table 1. Convective heat transfer coefficient and flow state in different applied locations

Table 2. Comparisons between final ablation result in FE simulations and in *in-vitro* experiments.
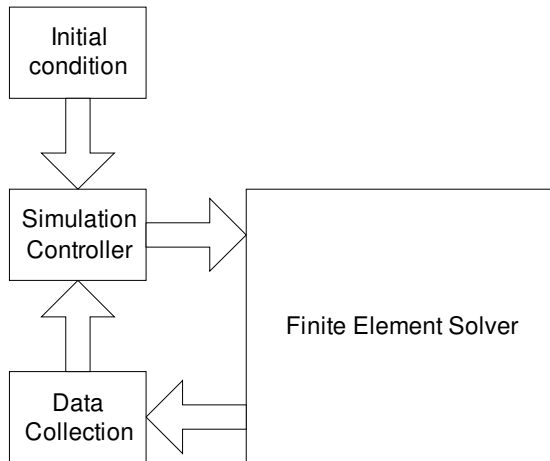
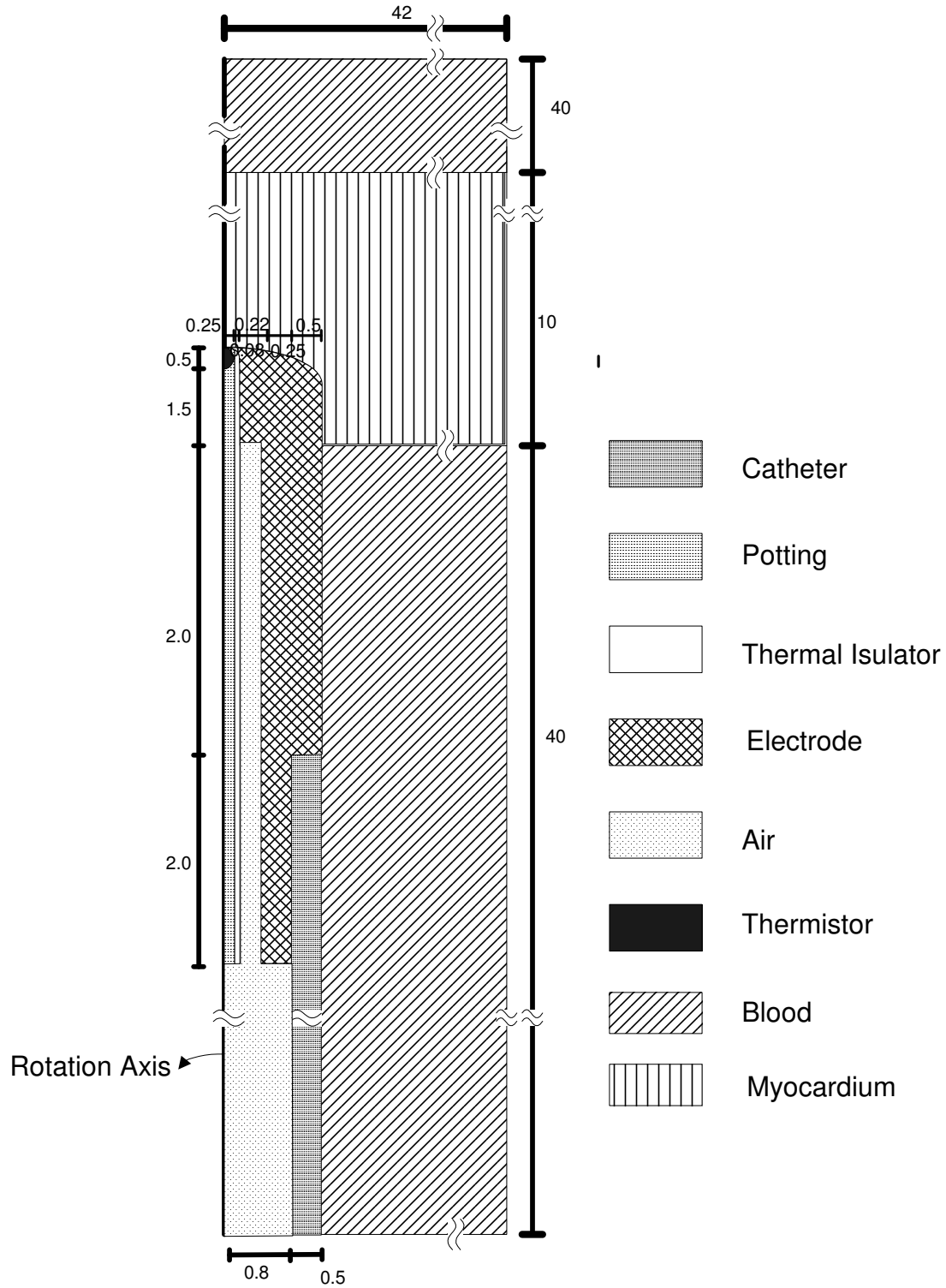**Fig. 1.** The FE simulation collects data for the creation of the lesion size estimator database.

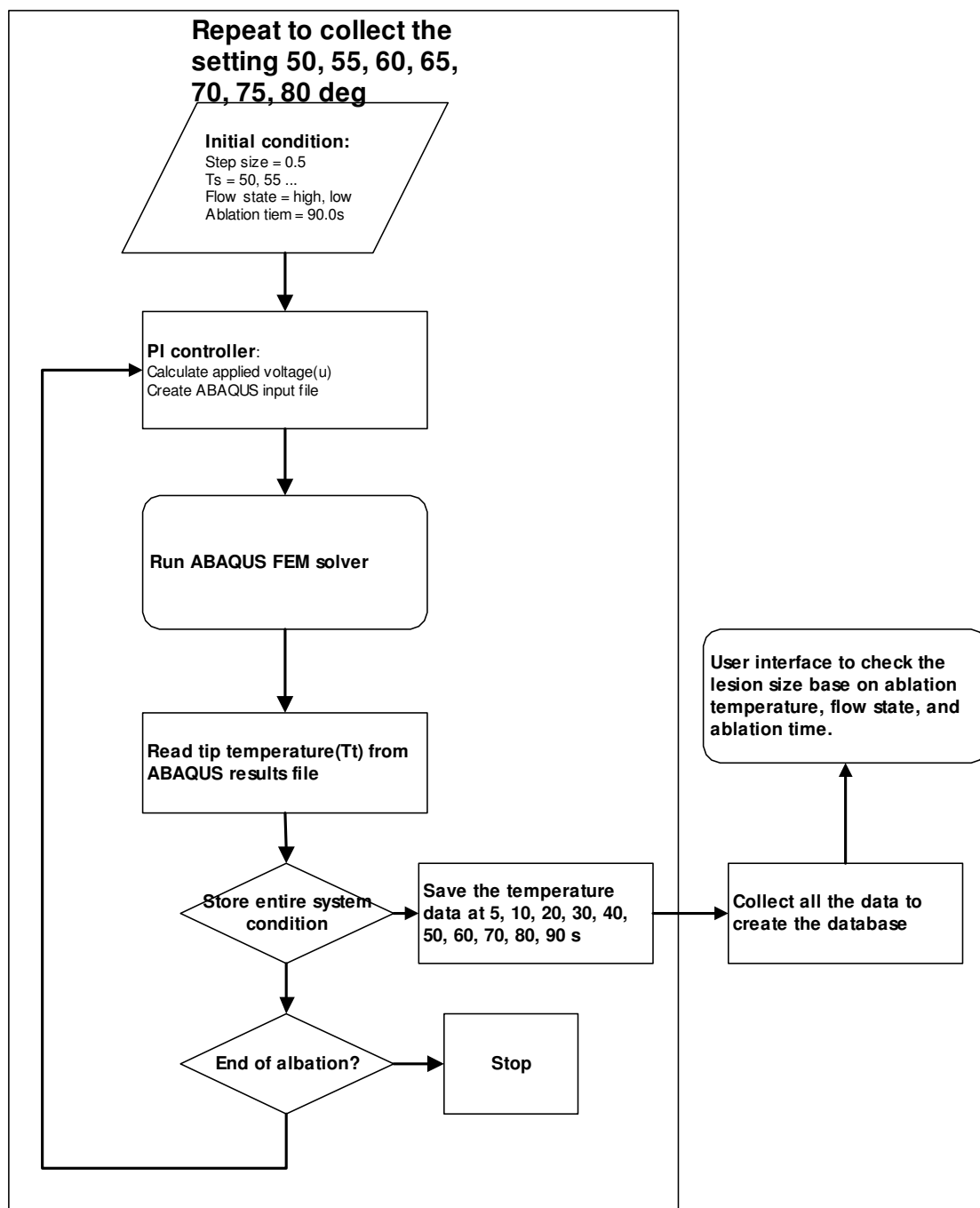**Fig. 1**. The geometry of the standard size ablation electrode in millimeters.

Fig. 3 The PI controller adjusts the applied voltage to maintain the tip temperature constant.
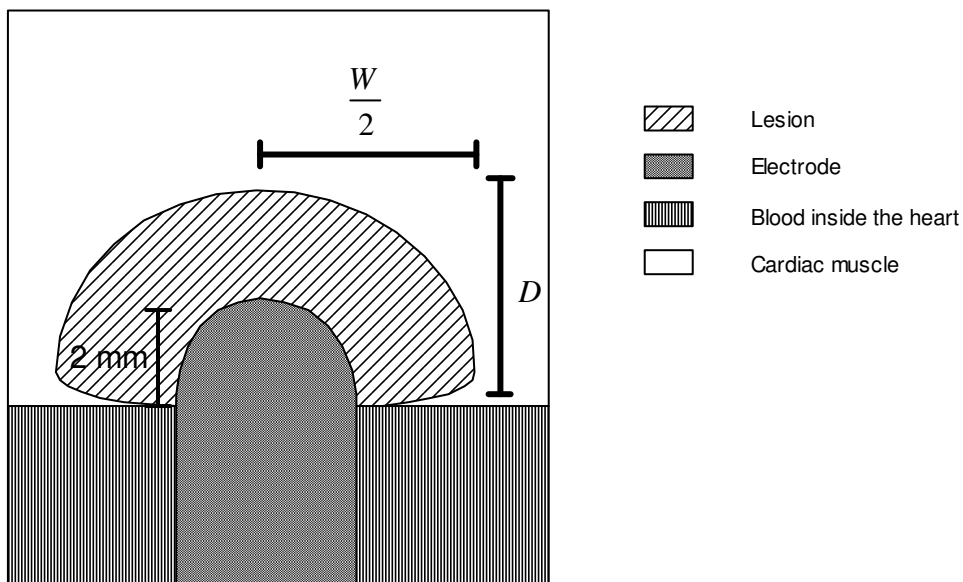
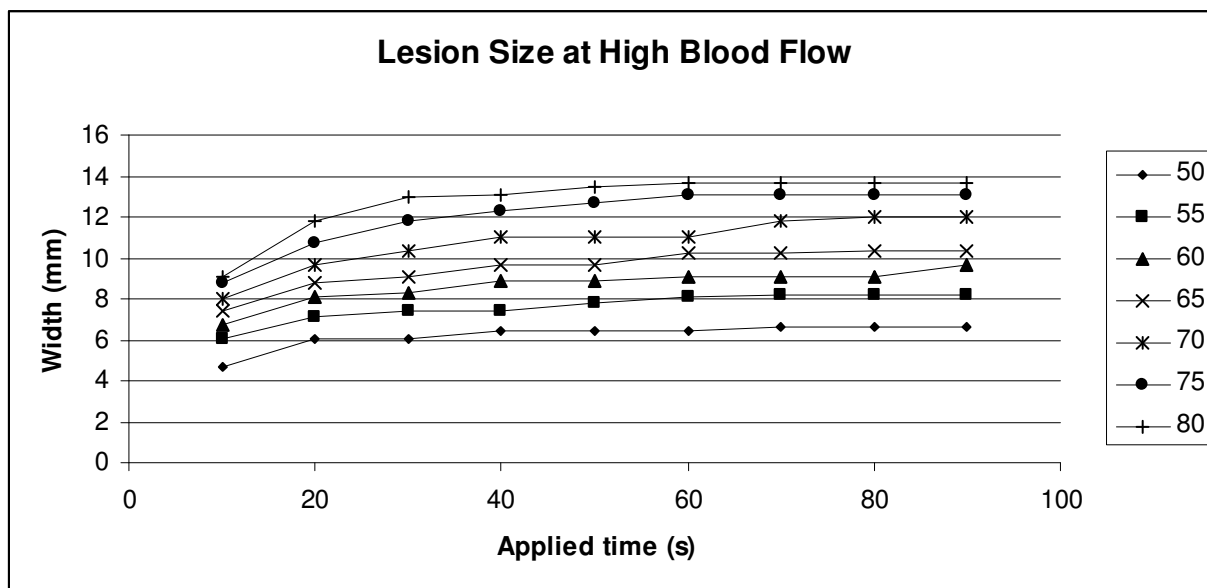**Fig. 4** Lesion volume is calculated from depth *D* and width *W*.

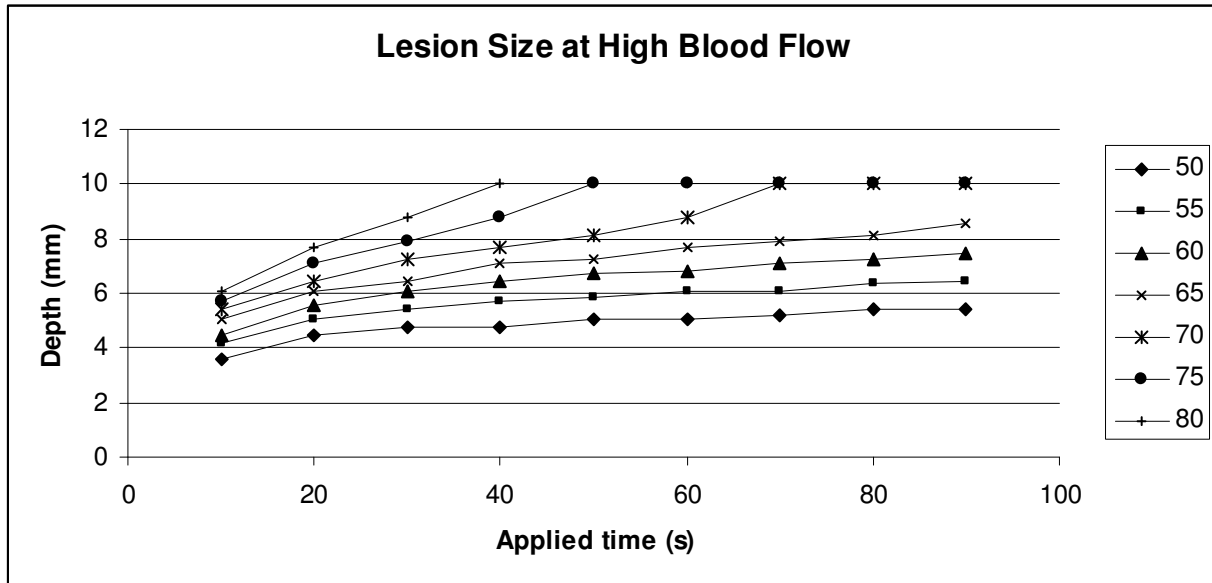**Fig. 5** Simulation result in lesion width increases with ablation time at high flow.

Fig. 6 Simulation result in lesion depth increases with ablation time at high flow.
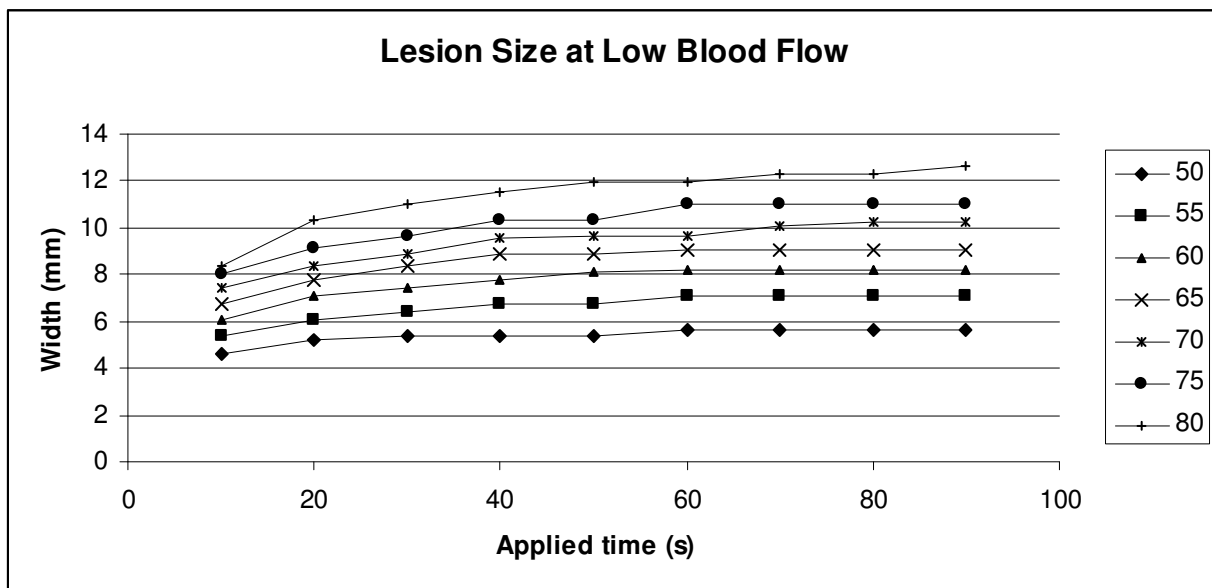

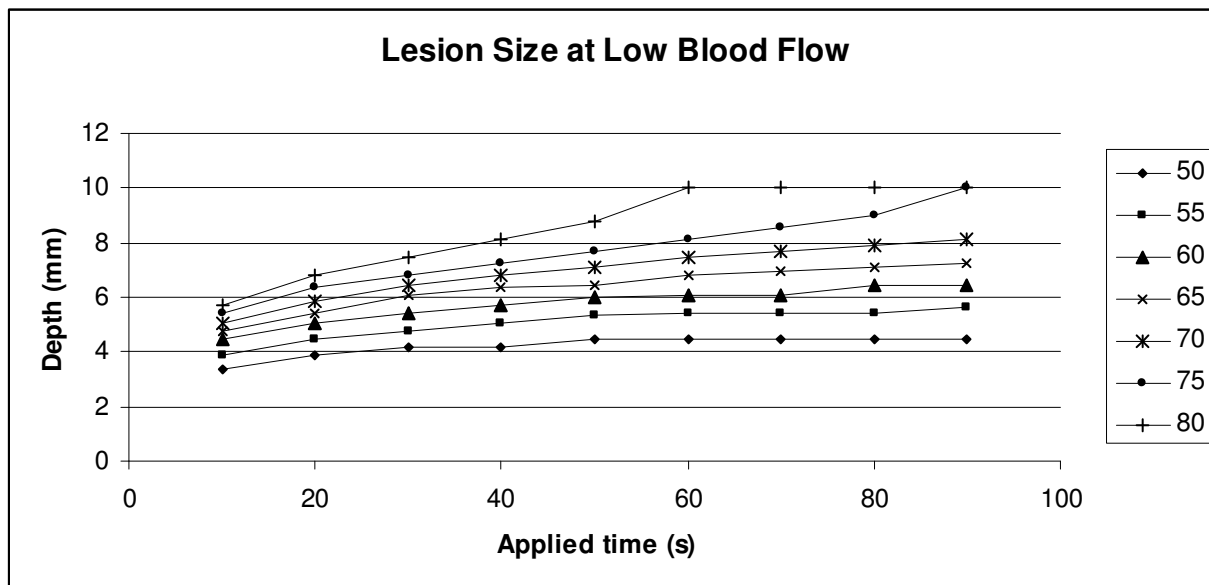**Fig. 7** Simulation result in lesion width increases with ablation time at low flow.

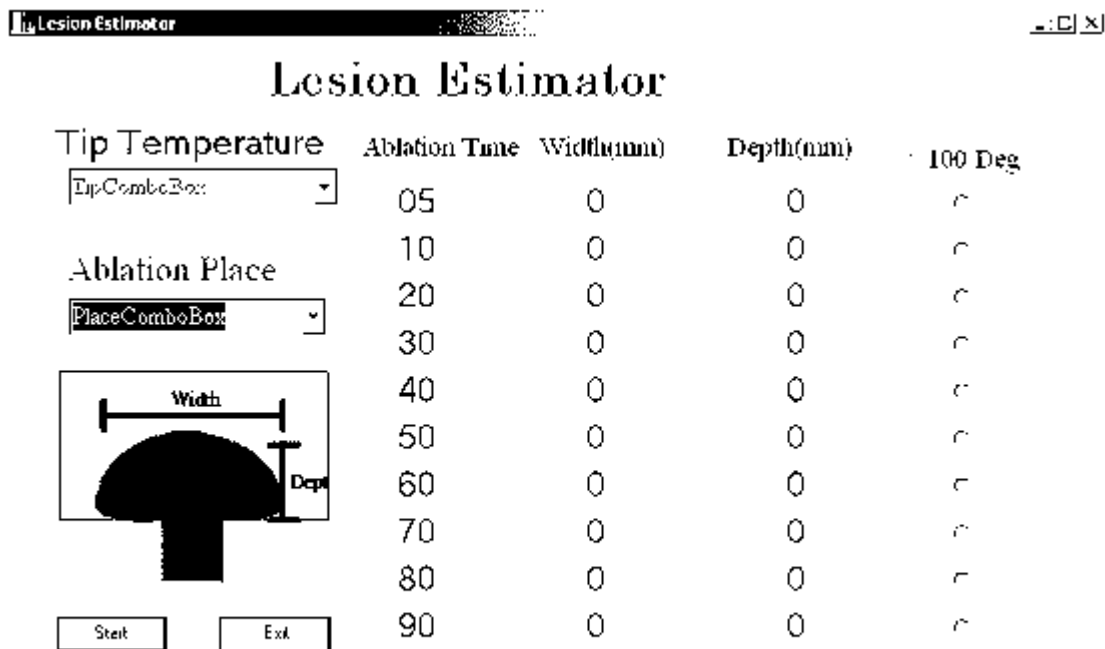**Fig. 8** Simulation result in lesion depth increases with ablation time at low flow.

Fig. 9 A screenshot of the user interface.

Table 1 Convective heat transfer coefficient and flow state in different applied locations

Location	Blood flow	h_b at blood-myocardium interface [W/(m^2·K)]	h_{be} at blood-electrode interface [W/(m^2·K)]
AV node	High	7100	6090
CS	Low	3350	2081
Atrial AP	High	7100	6090
Ventricular AP	Low	3350	2081
RV outflow VT	High	7100	6090

Table 2. Comparisons between final ablation result in FE simulations and in *in-vitro* experiments.

Target temperature	Blood flow	Width (mm) in FE	Width (mm) in *in-vitro*	Depth (mm) in FE	Depth (mm) in *in-vitro*
60	High	9.6	10.54	7.4	5.92
	Low	8.2	7.61	6.45	3.9
70	High	11.98	12.38	10	7.14
	Low	10.3	9.96	8.09	5.3
80	High	13.7	13.63	10	7.67
	Low	12.6	11.65	10	6.45

CHAPTER 4

IN-VITRO EXPERIMENT FOR THE LESION SIZE ESTIMATOR

Abstract— This study investigated the effect of blood flow, target temperature, and applied duration on the lesion formation during radiofrequency cardiac ablation. The target temperature directly affects the power delivered into the myocardium. In addition, the blood flow in heart chambers carries heat away from the electrode and from the myocardium. This cooling effect requires more power from the ablation generator to maintain target temperature. As a result, it also causes a larger lesion. A flow system simulated the different flow rates inside the heart chamber. *In-vitro* ablation performed on bovine myocardium with two different flow rates (1 and 3 L/min) targeted two different temperatures (60 and 70 °C) under temperature-controlled mode with nine different applied durations (10, 20, 30, 40, 50, 70, 80, and 90 s). The lesion dimensions (represented with maximum depth, maximum width) were larger with 12.38 mm in width and 7.41 mm in depth in high-flow applied sites at high target temperatures.

I. INTRODUCTION

Since the 1980s, due to its efficacy, controllability, and minimal invasiveness, radiofrequency cardiac ablation has become a preferable treatment for cardiac arrhythmias such as atrioventricular node re-entry, atrial tachycardia, atrial flutter, and fascicular ventricular tachycardias [1]–[3]. It is also a promising method to treat ventricular tachycardias and associated coronary diseases [3]–[5].

During RF catheter ablation, the clinical electrophysiologist applies an electric current with a frequency between 300 kHz and 1 MHz between the catheter electrode (~2.6 mm in diameter) in contact with the endocardium and a rectangular dispersive electrode (~15 cm × 9 cm) attached to the back of the patient. Fig. 1 shows the heat interaction between electrode, myocardium, and blood flow. The electric current directly heats the myocardium around the

ablation electrode by Joule heat generation. Other cardiac tissue is heated by conduction of the heat. In addition, the blood flow carries heat away from the myocardium, and from the electrode. As a result, when the tissue temperature reaches 50 °C [6], irreversible myocardial injury occurs. At this temperature, the cells lose electrical excitability and the re-entrant pathways are interrupted. Thus 50 °C is usually considered as the threshold for lesion formation.

Commercial RF ablation units often provide two modes of operation, power- and temperature-controlled modes. In power-controlled ablation, a constant power is delivered to the ablation electrode. On the other hand, the temperature-controlled mode controls the temperature at the ablation electrode tip at a constant value. An insulated thermistor located at the tip of the catheter monitors the temperature at the point of the contact in the endocardium. The controller of the generator controls the inserted power by reading the tip temperature from this thermistor, and this forms a closed loop control. To ensure safety, there are limits of allowed maximum power and allowed maximum catheter tip temperature to avoid charring of the endocardium. Since catheter ablation is a heating process, the temperature-controlled mode ablation provides better control of lesion size than the power-controlled mode ablation [8], [14].

The formation of the RF lesion is affected by many factors such as the electrical and thermal properties of the ablation catheter, the myocardium, the blood, the duration of energy application, the catheter-endocardial contact, the catheter geometry, the blood flow around the ablation site, the applied power, and the target temperature [7]–[10]. For the temperature-controlled mode, the RF generator supplies power (not more than the set maximum power) to the electrode, in order to achieve the target temperature. The control algorithm in the RF generator tries to maintain the tip temperature for the rest of the ablation duration by varying the amount of current delivered to the electrode tip. The higher the set target temperature, the more power is delivered to the cardiac tissue.

In addition to the set temperature, the blood flow in the heart chambers also plays an important role in lesion formation during RF ablation. The blood flow carries heat away from the endocardium and from the electrode by convection. It has a cooling effect on the myocardium and has a large impact on the final lesion size [10]–[12].

Cao et al. [10] discuss the flow effect on the formation of lesions. They focused on the relation between flow rate and lesion dimension by applying the ablation for 120 s. However, they did not investigate the time response of the lesion dimension at different target temperatures in their experiment. Thus, our objective was to quantify the effect of the target temperature and application duration at different locations in the heart chamber with different blood velocities on the lesion size by *in-vitro* cardiac RF ablation.

We set up a circulation system to simulate the flow rate inside the heart chambers and carried out *in-vitro* catheter ablation on bovine myocardium. We performed *in-vitro* ablation on bovine myocardium with two different flow rates (1 L/min and 3 L/min) representing two commonly seen ablation blood flow groups. The entire ablation process used the temperature-controlled mode by setting different target temperatures (60, 70 °C) with different applied durations (10, 20, 30, 40, 50, 60, 70, 80, 90 s).

II. THEORY

During RF ablation, an electric current is applied between the catheter electrode, which is inserted into the myocardium, and the dispersive electrode. The injected RF power directly heats up the tissue adjacent to the catheter tip. Moreover, the majority of thermal injury is produced by heat conduction from the high-temperature rim to the surrounding myocardium [14]. At the same time, the blood remains at 37 °C during ablation. There exists a temperature difference between the ablated myocardium and blood flow in the heart chamber. As a result, heat transfers from the

endocardium to the blood by heat convection. Furthermore, the same phenomenon happens on the electrode surface. As heat is carried away from these surfaces, the temperature at the endocardial surface is lower than the temperature inside the myocardium. Consequently, the lesion diameter on the surface is smaller than the maximum lesion diameter inside the myocardium as shown in Fig. 3.

The cooling effect at the electrode surface causes the ablation generator to maintain the target temperature by providing more power. The rate of heat transfer by convection is dependent on the flow rate around the catheter. The higher the flow is, the more heat is carried away by convection. Therefore, it takes more power to maintain the catheter at a target temperature under high flow conditions. The ablation generator delivers more electric current to the catheter. This increase in power has several effects on lesion formation.

1) It increases the current density and the Joule heat generation inside the myocardium. As a result, the Joule-heated rim rises to a higher temperature and becomes larger. It conducts more heat to the surrounding tissue to a larger boundary due to the higher temperature gradient. Thus, it raises the myocardial temperature in other regions and causes a larger lesion.

2) The higher the delivered power is, the faster the myocardial temperature rises, especially in the directly heated rim. It has more time to conduct heat into the surrounding myocardium and reaches a larger boundary. This also increases the lesion dimensions.

Thus, the entire effect is to make the lesion size larger.

III. METHOD

A. Flow System Setup

Fig. 2 shows the flow system that simulates the different flow conditions inside the heart chamber [10] for *in-vitro* catheter ablation on bovine myocardium. The myocardial block sits on a Plexiglas frame immersed in a plastic container filled with 0.5% saline. The catheter, attached to a depth meter, contacts the tissue surface at a normal angle (90°). The depth meter controls the electrode's insertion depth. A pump circulates the saline between the plastic container and a 12 L water bath (Model 180, Precision Scientific, Winchester, VA) to keep the saline at 37±1 °C. A flow meter (7200 series, King Instrument, Huntington Beach, CA) regulates the flow rate from 0 to 6 L/min. The hose injecting saline to the tissue has an 18 mm inside diameter, which corresponds to 250 mm^2 area and is comparable to the areas of the mitral and tricuspid valves. The bottom of the injecting hose aperture and the surface of myocardium are at the same level. The distance from the hose to the catheter is 18 mm.

B. Ablation and Lesion Measurement

We used an EPT-1000XP ablation unit and a Blazer II 7-Fr catheter with a 2.6 mm diameter and 4 mm length electrode, both from EP Technologies (San Jose, CA). We performed *in-vitro* ablation on bovine myocardium with two different flow rates (1 L/min and 3 L/min), which correspond to the two common application groups and two target temperatures (60 and 70 °C) and 9 intervals (10, 20, 30, 40, 50, 60, 70, 80, 90 s). Furthermore, we performed 4 ablations at each setting.

We obtained bovine heart from the local butcher shop. We cut the myocardium into 3.0 × 3.0 × 1.0 cm blocks. We aligned the catheter electrode at the center of the myocardial block and inserted the catheter 2 mm perpendicularly into the myocardium for ablation. After ablation,

we dissected the myocardium through the center and then immersed it in p-nitro blue tetrazolium solution for about 10 min to distinguish the live (blue) and dead (pale) tissue. The staining solution changes the color of normal cardiac tissues into dark blue while keeping the color of lesions pale. We then used a digital camera to take pictures of lesions with a ruler scale on the lesion surface as shown in Fig. 3(b).

Six observers measured the dimensions independently without knowing the ablation settings so that we could avoid subject bias. We averaged their measurements to yield the dimensions for each lesion and determined the variability of the measurement. The result is measured as D = maximal depth, W = maximal diameter as shown in Fig. 3(a).

For correction and convenience, we also developed a user interface shown in Fig, 3(b) to measure the lesion dimensions. Before using it, we first calibrated the ratio between real distance in the world and the pixel distance in a picture by using the ruler scale in it. After calibration, the user only needed to point the mouse cursor at the top, bottom, left, and right of the lesion. The computer calculated the width and depth automatically. It was easier and more accurate than manually measured through the ruler in the picture.

C. Statistical Analysis

1. Analyze whether target tip temperature and flow rate have significant effects on the lesion formation

(1) Target tip temperature effect:

When the flow rate was fixed, we measured the outcomes (width or thickness of lesions) of different temperature groups at different time points. We wanted to determine whether target tip temperature effect on the lesion formation depended on

the time points based on the two-way ANOVA (analysis of variance) method using R software. The hypothesis was as follows:

$H_0 : \mu_{60°,t} = \mu_{70°,t}$ where $t = 10, 20, 30, 40, 50, 60, 70, 80, 90$ s

H_1:otherwise

(2) Blood Flow effect:

When the target tip temperature was fixed, we measured the outcomes (width or thickness of lesions) of different blood flow rate groups at different time points. We wanted to determine whether the blood flow rate effect on the lesion formation depended on the time points based on the two-way ANOVA. The hypothesis was as follows:

$H_0 : \mu_{High,t} = \mu_{Low,t}$ where $t = 10, 20, 30, 40, 50, 60, 70, 80, 90$ s

H_1 : otherwise

2. Analyze the prediction ability of our simulation and experimental data

The experimental data were statistical but the simulated data were deterministic. Therefore, these two types of data could not be treated simultaneously in a statistical model. Instead, the statistical analysis employed differences between experimental values and corresponding simulated values i.e. $\Delta W = W_{experiment} - W_{simulate}$ and $\Delta D = D_{experiment} - D_{simulate}$ as a function of temperature, flow rate, and time. Thus, negative difference indicated that the simulated values overestimated the observed values from the experiments. If the simulated values were perfectly accurate, all differences would be equal to zero, and a regression model using $x = time$ as the explanatory variable and $y = differences$ would have an intercept of zero

and a slope of zero. Hence, tests of the regression intercept and slope coefficients, individually and in combination, would show no statistical significance.

A.

IV. RESULTS

Table 1 shows the final result of the ablation after applying ablation 90 s for the 6 lesion groups. Based on the results of two-way ANOVA, we concluded that the target tip temperature and the blood flow rate affected the size of lesion formation significantly at the 5% significant level (p-value < 0.05).

Figs. 3 to 6 show the time response of the lesion size for cardiac ablation of different tip temperatures at different locations and also show the comparisons between FE simulations and *in-vitro* experiments of time responses in lesion sizes of different target tip temperatures at different flow states.

Tables 2 and 3 show the results of individual regressions for lesion width and depth under different flow rates with different target temperatures. Each regression splits into two rows indicated as "intercept" and "slope". If the intercept or slope in the regression model is statistically significantly different from zero, the related information in the corresponding row is printed with bold. These indicate significant bias between the simulated data and experimental data. The Regression Standard Error shown in the fourth column is a measure of the average distance of ΔW or ΔD from the computed regression line. The R^2 statistic gives the fraction of variation in the ΔW or ΔD explained by time. Perfect simulation results would result in an R^2 statistic of zero. Thus, a small value is better. In the tables, we can observe that R^2 in ΔW ranges from 0.05 to 0.41 and R^2 in ΔD ranges from 0.01 to 0.35. We get a small R^2 when slope is not significant in the regression model.

V. DISCUSSION

A. *Lesion Dimension vs. Target Tip Temperature*

The lesion dimensions (maximum depth and maximum diameter) of the higher target temperature (70 °C) are larger than those of the lower target temperatures (60 °C). The increase in target tip temperature causes the increases in lesion width and depth. As discussed in THEORY, the target tip temperature affects the power applied from the generator to the electrode. As a result, this showed that the target set temperature played a critical role in lesion dimension.

B. *Lesion Dimension vs. Flow Rate*

Table 1 also shows that at the same target temperature setting, the lesion dimension grew significantly as the flow rate increased. The cooling effect due to blood convection increased the delivered power. A higher the blood flow yielded a higher convection effect. The power delivered to the myocardium increased dramatically as the blood flow increased. Even though the target temperature was set at the same temperature, the final result was different at various locations, dependent on the local blood flow. For those high flow rate locations (such as near the mitral and tricuspid valve surfaces), a low temperature setting may result in a larger lesion. A similar result can happen if we manually introduce a cooling effect at the catheter tip by artificially injecting a constant temperature saline, and then also achieve a larger lesion at the same target temperature setting. Thus a saline-irrigated electrode is helpful to create larger lesions for ventricular arrhythmias.

C. The Time Response of Lesion Dimensions

Figs. 3 to 6 show the time response of the lesion size for cardiac ablations for different tip temperatures at different locations. The lesion dimensions grew rapidly at the beginning because the generator would apply as much power as possible to achieve the target temperature, and the temperature gradient between the Joule heating region and conduction heating region was large. After about 60 s, the heating process almost achieves equilibrium; the temperature inside the myocardium maintains a constant temperature. Thus the increase in lesion dimensions almost stops. The time responses of the lesion width and depth suggest that instead of using 120 s as an application duration, we can use 60 to 80 s to achieve a similar size of lesion but reduce the time when the catheter penetrates the cardiac tissue.

We expected that the increment in the lesion width and depth would be monotonic. The experimental data show that there are several exceptional points existing in the results such as the data point at 40 s targeted at 60 °C at high blood flow and the data point at 70 s targeted at 70 °C at high blood flow. However, the entire time response curves show the increment trend. There are several possible causes of these deviations: (1) the electrical and thermal properties of cardiac tissue may vary from piece to piece. (2) the control of the flow meter sometimes fluctuated during the experiment. (3) the real penetration depth may be different. (4) the penetration angle may not be perpendicular to the cardiac tissue because the cut of the tissue is not perfect. (5) different pieces of cardiac tissue may have a little different deformation which affects the energy delivery and cooling effect. (6) the size of the cardiac tissue may have a little deviation from the specification. (7) the pictures taken may be under different lighting condition and this may cause the deviation in measurement. (8) the time cardiac tissue remains in p-nitro blue tetrazolium may vary and also the thickness of the dissected cardiac tissue may cause the variation in color distribution. (9) the distance between the top of the cardiac tissue surface and saline flow from

the hose may vary. (10) when we dissect the cardiac tissue to slice and dip it in the p-nitro blue, the slice edge may not pass through the center of ablation and the cut may not be perpendicular to the top surface, this may cause an offset. In addition to the variation in the ablation process, we use different observers to measure the set of lesion picture dimensions on different monitors. There are several factors which may affect the measurement results: the visual sensitivity difference among observers, the ability of monitors to show correct color, and the lighting condition for each picture. In order to reduce the experimental variation, we minimized the possible variations in the experimental setting such as to create a model to help us dissect the cardiac tissue into desired dimension with the top of the surface as smooth as possible, to record the flow rate through the entire ablation process and to discard the data when the flow fluctuation is large, to carefully place the cardiac tissue and locate the hose just above the top surface of the cardiac tissue, and to examine the basic thermal, electrical and physical properties of the cardiac tissue and to avoid those cardiac tissue with large variations in the properties. For future work, we also propose two methods to reduce the bias caused by the human observers:

First, before we conduct the entire experiment, we could first check the repeatability, reproducibility between technicians, and reproducibility between labs of the experiment to evaluate the variability caused by human observers and try to standardize a measurement process. Because the lighting of the pictures may affect the observer's decision at picking the proper boundary, we could create a color template from p-nitro blue tetrazolium dying patterns of a standard ablation process and use this template to calibrate the color in pictures taken later to minimize the bias caused by the change of lighting.

Second, we could develop an algorithm to do automatic measurement by using computers. In the computer vision community, segmentation is a common and mature technique.

If we could choose a proper criterion to do the segmentation automatically, we could prevent the bias caused by the difference in human observers' color sensitivities.

We believe that after carefully setting up the measurement and experimental environment as we discussed in this section that if we reconducted the experiment with more ablations per data point, we could get a smoother monotonic-increasing curve without the exceptional points.

D. Comparison of the formation of the lesions between FE simulations and in-vitro experiments

First, Figs. 3 to 6 show that the shapes of the curves between FE simulation and *in-vitro* experiment are similar. They all have a saturation time after which the growth of the lesion is negligible. This confirms that there exists a saturation time for the ablation process as presented previously [14]. Second, the prediction of lesion width is close to the corresponding results in the *in-vitro* experiment.

The statistical regression analysis shows that in all experiments we obviously have a significant additive error for predictions in lesion width and lesion depth for different flow rates with different target temperatures. In the predictions of the lesion width, except for the case of low blood flow with target temperature 60 °C, the differences also contain proportionate error related to time. As evidenced by the statistically significant slopes, in the predictions of the lesion depth, except in the case of high blood flow with target temperature 70 °C, we only have significant additive errors. The next section provides possible factors to analyze the cause and possible modification of our model to improve its prediction of the lesion formation.

E. Future Direction

There are several possible factors to cause the difference between simulated data and experimental data. The deviation in prediction may result from the deformation of cardiac tissue near the site where the electrode penetrated, which may affect the blood cooling effect and energy delivery, the applied voltage control mechanism, the convective coefficients used for simulation, and properties of tissue. The critical temperature is based on the experimental results of cardiac tissue losing the activity but not when the p-nitro blue shows as color transition. Through cross-regression model analysis, we know that flow rate is an important factor for the deviation. However, in our model, we use two convective coefficients to model the convection effect introduced by the blood flow. This may be too simple to represent the convective effect on the cardiac surface. We propose some future research directions to modify our FE model to more precisely predict the experimental results. Since there are deviations between the simulation results and the *in-vitro* experimental results, we believe that there are some important factors that have not been modeled by our FE model.

First, we examine other important factors of the lesion formation such as penetration depth and penetration angle. By using our original parameters and assumptions, we could compare the effects of other parameters on the lesion formation with our simulation results. The comparison could give us a qualitative concept about how important these factors are on the lesion formation.

Second, we could use the data collected in the experiment to improve the simulation to increase the precision of the prediction.

    1) From simulation and experiment, we knew that the blood flow rate is a very important factor on the lesion formation. In the simulation, we use blood–electrode and blood–myocardium convective coefficients to model the blood flow effect. The values used

were collected using *in-vivo* experiments and theoretical calculations may be different from the values presented in the flow system. Thus, if we could collect the blood–electrode and blood–myocardium convective coefficients during the experiment, we could have a set of values which are more close to the *in-vitro* experimental conditions.

2) The electrical and thermal properties of cardiac tissue have an important effect on lesion formation. If we could measure the electrical and thermal properties of a piece of tissue from the same bovine heart, we could have more similar properties related to the experiment.

3) Our simple control algorithm may be different from the real control algorithm. The generator allows us to collect the applied voltage during the ablation process. We could modify our control algorithm to use this collected voltage as input during the simulation process. Then we would have a control algorithm which is close to the real one.

4) Cao et al. [10] embedded thermocouples at a certain depth in the meat and measured the temperature variation profile of the ablation process. We could use a similar method to obtain a temperature profile for different depths inside the cardiac tissue. We could use this depth temperature profile to compare the boundary of lesion measured from p-nitro blue to obtain a better temperature for choosing the critical temperature for our simulation.

5) In our model, we assumed that the blood has a constant temperature. We could measure the temperature just above the cardiac tissue inside the saline solution to confirm the validity of this assumption.

Third, we could also review the validity of our assumptions for the flow simulation system. We assumed that the heat loss due to the blood perfusion outside the epicardium was negligible compared to the heat loss due to the blood flow inside the heart chamber. We could verify this assumption by measuring the blood–myocardium convective coefficients on the outside of the cardiac tissue (different from the ablation inside) and then use these values in our simulation model to check the deviation caused by these values.

Fourth, we could put all the important factors together into a more complex and precise model. There are several important factors such as target tip temperature, blood flow rate, tissue properties, and the deformation at the penetration site. There may be more and we could consider the importance of them and try to put them into a more complex and precise model. Then, we could compare the simulation result with the experimental results through the same procedure provided in this paper.

Fifth, the analysis of differences between experimental values and simulated values shows that flow rate is more important than the target temperature. We used two convective coefficients to model the entire flow effect and this may simplify the simulation too much. We could consider a more complex and better model to model this complex effect which may be critical for the correctness of simulation.

VI. CONCLUSION

The size of the lesions is the result of a combination of several factors such as applied tip temperature, application time, applied location, myocardial properties, etc. We investigated the effect of combining three important factors, the tip temperature, the applied duration, and the flow rate that corresponds to the applied location. These factors are more controllable than the tissue properties and blood impedance. By examining the time response of the lesion size at different tip temperatures, we concluded that higher tip temperatures create larger lesion sizes

within the maximally allowed power. There will be a maximally possible lesion size for each ablation setting when the heat transfer reached equilibrium. Thus we could not achieve a larger lesion by applying a longer duration. The cooling effect of the blood flow is affected by the flow rate. As a result, the power delivered by the generator is also affected. A higher flow rate, yields a larger cooling effect, which results in more power delivered, and a larger lesion size formed. The cooling effect generated larger lesions as required to cure ventricular tachycardia (VT).

REFERENCES

[1] S. K. S. Huang and D. J. Wilber, Eds., *Radiofrequency Catheter Ablation of Cardiac Arrhythmias: Basic Concepts and Clinical Applications*, 2nd ed., Armonk, NY: Futura, 2000.

[2] D. P. Zipes and M. Haïssaguerre, *Catheter Ablation of Arrhythmias*. 2nd ed. Armonk, NY: Futura, 2002.

[3] F. Morady, "Drug therapy: radio-frequency ablation as treatment for cardiac arrhythmias," *N. Engl. J. Med.*, vol. 340, pp. 534–544, 1999.

[4] D. Panescu, "Intraventricular electrogram mapping and radiofrequency cardiac ablation for ventricular tachycardia," *Physiol. Meas.*, vol. 18, pp. 1–38, 1997.

[5] H. Nakagawa, K. J. Beckman, and J. H. McClelland, "Radiofrequency catheter ablation of idiopathic left ventricular tachycardia guided by a Purkinje potential," *Circulation*, vol. 85, pp. 1666–1674, 1992.

[6] S. Nath, C. Lynch, J. G. Whayne, D. E. Haines, "Cellular electrophysiological effects of hyperthermia on isolated guinea pig papillary muscle implication for catheter ablation," *Circulation*, vol. 88, part 1, pp. 1826–1831, 1993.

[7] J. J. Lamberg, M. Gallagher, S. A. Strickberger, and O. Amirana, "Temperature-guided radio-frequency catheter ablation with very large distal electrodes," *Circulation*, vol. 88, pp. 245–249, 1993.

[8] D. Panescu, J. G. Whayne, S. D. Fleischman, M. S. Mirotznik, D. K. Swanson, and J. G.Webster, "Three-dimensional finite element analysis of current density and temperature distributions during radio-frequency ablation," *IEEE Trans. Biomed. Eng.*, vol. 42, pp. 879–890, Sept. 1995.

[9] I. D. McRury and D. E. Haines, "Ablation for the treatment of arrhythmias," *Proc. IEEE*, vol. 84, pp. 404–416, Mar. 1996.

[10]. H. Cao, V. R. Vorperian, S. Tungjitkusolmun, J.-Z. Tsai, D. G. Haemmerich, Y. B. Choy, and J. G. Webster, "Flow effect on lesion formation in RF cardiac catheter ablation," *IEEE Trans. Biomed. Eng.*, vol. 48, pp. 425–433, Apr. 2001.

[11]. H. H. Peterson, X. Chen, A. Pietersen, J. H. Svendsen, S. Hauns, "Lesion dimensions during temperature-controlled radiofrequency catheter ablation of left ventricular porcine myocardium: impact of ablation size, electrode size and convective cooling," *Circulation*, vol. 99, pp. 319–325, 1999.

[12]. S. Tungjitkusolmun, V. R. Vorperian, N. Bhavaraju, H. Cao, J.-Z. Tsai, and J. G. Webster, "Guidelines for predicting lesion size at common endocardial locations during radio-frequency ablation," *IEEE Trans. Biomed. Eng.*, vol. 48, pp. 194–201, 2001.

[13]. D. Haines. The biophysics of radiofrequency catheter ablation in the heart: the importance of temperature monitoring, *PACE*, vol. 16, pp. 596–591, 1993.

[14]. Y. C. Lai, Y. B. Choy, D. Haemmerich, V. R. Vorperian, J. G. Webster, "Lesion size estimator of cardiac radiofrequency ablation at different common locations with different tip temperatures", *IEEE Trans. Biomed. Eng.,* vol. 51, pp. 1859–1864, 2004.
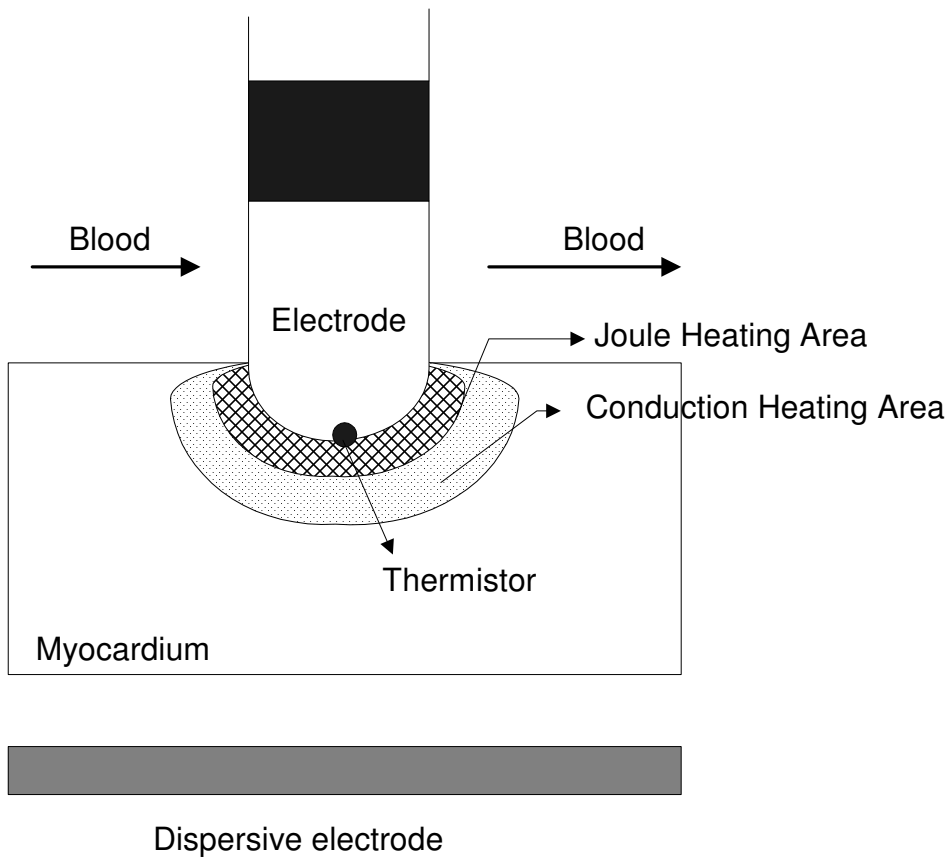
Fig. and Table Captions:

Fig. 1. Simplified diagram of catheter ablation. The catheter is perpendicular to the myocardium. There is an electric current applied between the catheter electrode and the dispersive electrode. The myocardium adjacent to electrode is mainly heated by the Joule effect. The myocardium in the conduction heating region is mainly heated by heat conduction. The blood flow carries the heat away from the myocardium and the catheter by convection.

Fig. 2. The flow simulation system consisted of a plastic container and a 12 L constant temperature water bath used to maintain the saline temperature. The flow meter regulated the flow rate from 0 L/min to 6 L/min. The foil dispersive electrode was put at the bottom of the container. The myocardium was put on a frame attached to the bottom of the container. The catheter was fixed to a depth meter so that the insertion depth was well controlled.

Fig. 3. (a) Myocardium deformation during ablation. (b) A screen shot of the measurement user interface. In the center is the sample of ablated myocardium after p-nitro tetrazolium blue staining. This case is 80 °C with 3 L/min after 10 s ablation. The smallest unit on the ruler is 1 mm. The ruler is used to calibrate the ratio between the real length and the pixel length. The lesion size can be easily obtained by using the mouse cursor to point at the top, bottom, left and right of the lesion after calibrating the distance ratio.

Fig. 4. Lesion width increased with ablation time at high flow. Lesion width also increased with the target temperature. However due to the limitation of maximal power, the width increase is less when tip temperature increases from 70 to 80 °C.

Fig. 5. Lesion depth increased with ablation time at high flow. Lesion depth also increased with the target temperature. However, the depth seems not to increase any more when tip temperature increases from 70 to 80 °C due to the limitation of maximal power.

Fig. 6. Lesion width and depth increased with ablation time at low flow targeted at 70 °C for simulation and experimental data.

Fig. 7. Lesion width and depth increased with ablation time at low flow targeted at 70 °C for simulation and experimental data.

Table 1. The lesion dimensions for different target temperatures expressed in width and depth after applying 90 s ablation for high blood flow and low blood flow.

Table 2. The statistical regressions of the differences between the experimental values and the simulated values of lesion width.

Table 3. The statistical regressions of the differences between the experimental values and the simulated values of lesion depth.

Fig. 1. Simplified diagram of catheter ablation. The catheter is perpendicular to the myocardium. There is an electric current applied between the catheter electrode and the dispersive electrode. The myocardium adjacent to electrode is mainly heated by the Joule effect. The myocardium in the conduction heating region is mainly heated by heat conduction. The blood flow carries the heat away from the myocardium and the catheter by convection.
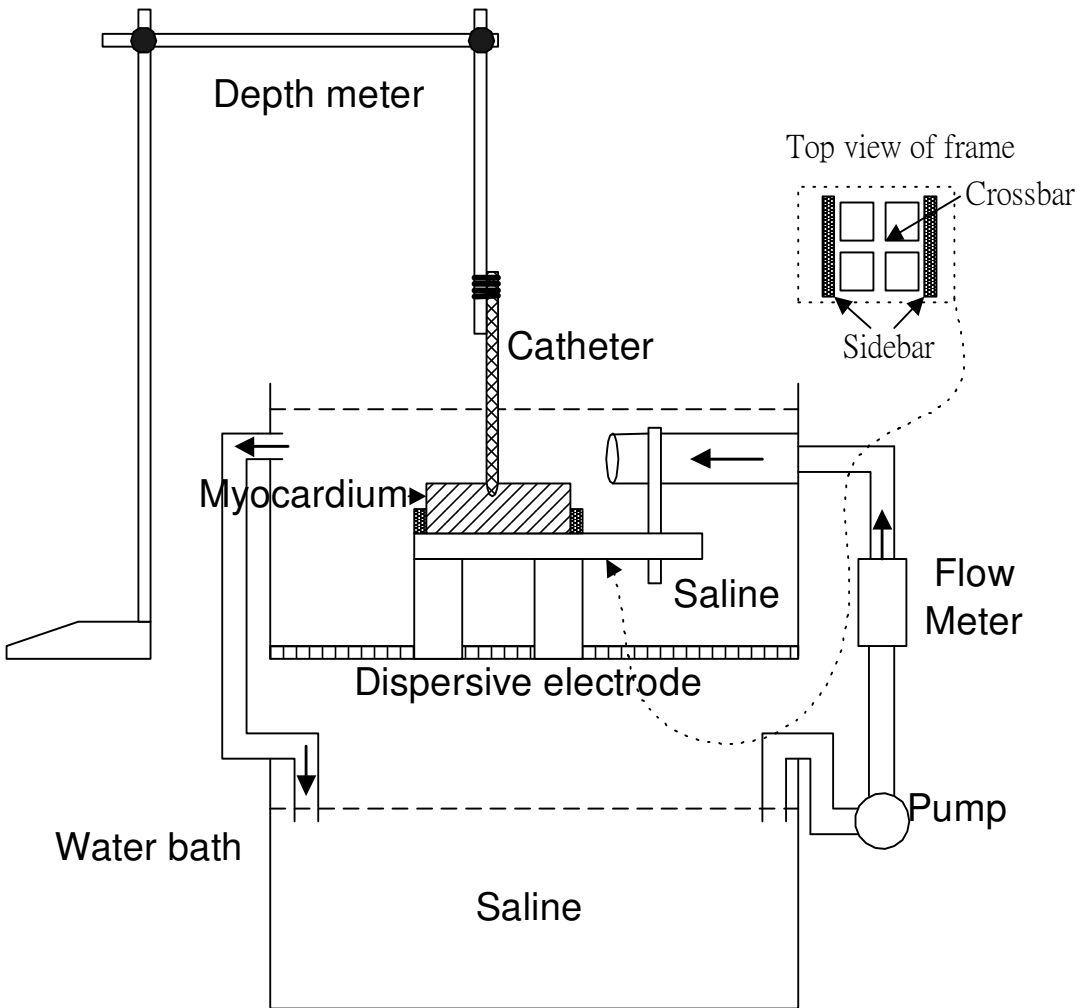
Fig. 2. The flow simulation system consisted of a plastic container and a 12 L constant temperature water bath used to maintain the saline temperature. The flow meter regulated the flow rate from 0 L/min to 6 L/min. The foil dispersive electrode was put at the bottom of the container. The myocardium was put on a frame attached to the bottom of the container. The catheter was fixed to a depth meter so that the insertion depth was well controlled.

Fig. 3. (a) Myocardium deformation during ablation. (b) A screen shot of the measurement user interface. In the center is the sample of ablated myocardium after p-nitro tetrazolium blue staining. This case is 80 °C with 3 L/min after 10 s ablation. The smallest unit on the ruler is 1 mm. The ruler is used to calibrate the ratio between the real length and the pixel length. The lesion size could be easily obtained by using the mouse cursor to point at the top, bottom, left and right of the lesion after calibrating the distance ratio.
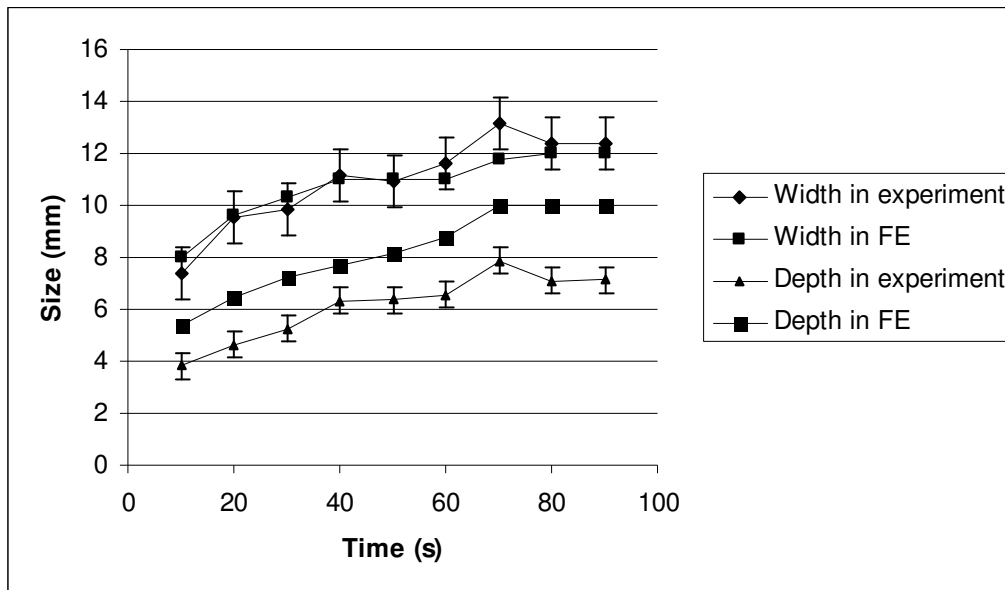
Fig. 4. Lesion width and depth increased with ablation time at high flow targeted at 70 °C for simulation and experimental data. The deviation is about 1.0 for the measurement in lesion width and about 0.4 for the measurement in lesion depth
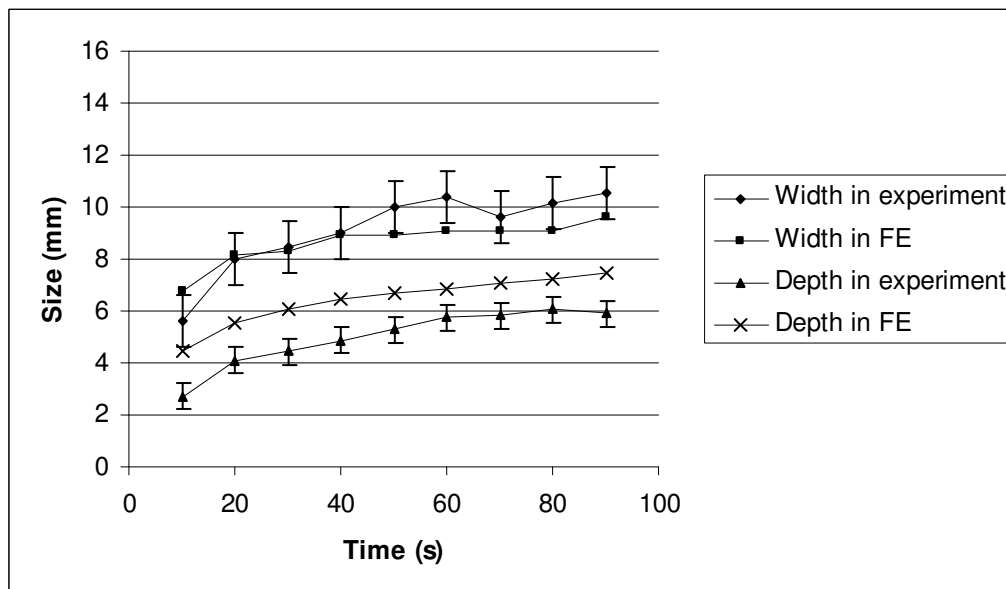
Fig. 5. Lesion width and depth increased with ablation time at high flow targeted at 60 °C for simulation and experimental data.
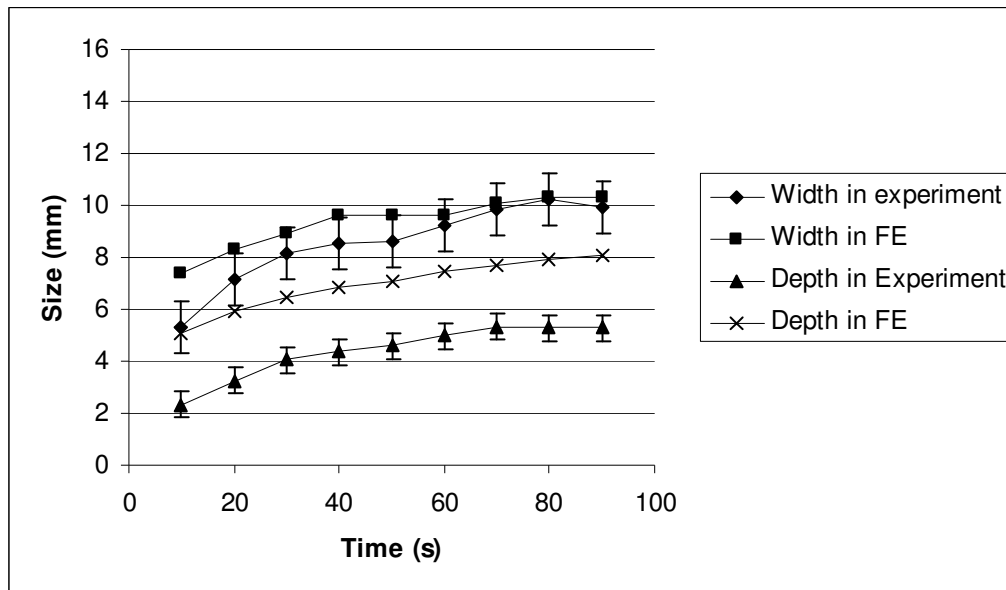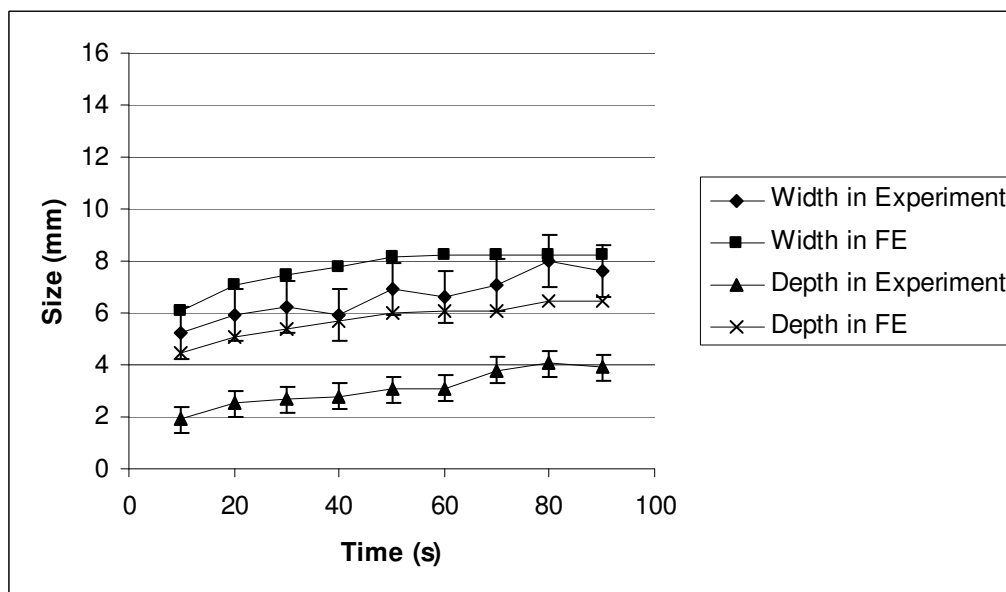
Fig. 6. Lesion width and depth increased with ablation time at low flow targeted at 70 °C for simulation and experimental data.

Fig. 7. Lesion width and depth increased with ablation time at low flow targeted at 70 °C for simulation and experimental data.

Table 1. The lesion dimensions for different target temperatures expressed in width and depth after applying 90 s ablation for high blood flow and low blood flow.

Target temperature (°C)	Blood flow	Width (mm)	Depth (mm)
60	High	10.54	5.92
	Low	7.61	3.9
70	High	12.38	7.14
	Low	9.96	5.3

Table 2. The statistical regressions of the differences between the experimental values and the simulated values of lesion width.

Target temperature (°C)	Blood flow	R^2	Std. Error of Entire	Term	Coeff	Std. Error for term	t	p-value
60	High	.41	.85	Inter.	**-.839**	**.309**	**-**	**.0104**
				Slope	**.027**	**.005**	**4.89**	**<.0001**
	Low	.05	.82	Inter.	**-**	**.299**	**-**	**<.0001**
				Slope	.221	.167	1.323	.1945
70	High	.17	1.13	Inter.	-.665	.410	-	.1138
				Slope	**.019**	**.007**	**2.651**	**.0121**
	Low	.24	.96	Inter.	**-**	**.349**	**-**	**<.0001**
				Slope	**.020**	**.006**	**3.266**	**.0025**

Table 3. The statistical regressions of the differences between the experimental values and the simulated values of lesion depth.

Target temperature (°C)	Blood flow	R^2	Std. Error of Entire	Term	Coeff	Std. Error for term	t	p-value
60	High	.06	.51	Inter.	**-**	**.185**	**-**	**<.0001**
				Slope	.005	.003	1.412	.1669
	Low	.01	.65	Inter.	**-**	**.235**	**-**	**<.0001**
				Slope	.096	.171	.565	.5761
70	High	.35	.59	Inter.	**-**	**.215**	**-**	**<.0001**
				Slope	**-.588**	**.139**	**-**	**.0002**
	Low	.05	.47	Inter.	**-**	**.170**	**-**	**<.0001**
				Slope	.217	.167	1.296	.2036

CHAPTER 5

LESION SIZE DEPENDS ON PENETRATION DEPTH

Abstract—The penetration depth affects the effective amount of energy delivered from the electrode into the cardiac tissue, which is an important factor for lesion formation. If the penetration depth is too shallow or too deep, the effective amount of energy delivered into cardiac tissue is low. As a result, the formation of lesion is small. This study presents a process of FE modeling a system that includes blood, myocardium, and an ablation catheter with a thermistor embedded at the tip with different penetration depths for two different flow states. The entire process is operated in a temperature-controlled mode. It explores the relationship between the penetration depth and lesion formation for different flow states. We found that the maximum lesion volume occurs at the penetration depth of about 2.0 mm to 3.0 mm for both high blood flow and low blood flow.

I. INTRODUCTION

Because of the efficacy, controllability, and minimal invasiveness, radiofrequency (RF) catheter ablation has proven an effective method to treat some cardiac arrhythmias, such as atrioventricular node re-entry, atrial tachycardia, atrial flutter, and fascicular ventricular tachycardias [1]–[3]. Several research groups also suggested that it may be a good method for palliative suppression of ventricular tachycardias [3]–[5].

Good electrode–endocardial contact ensures that heat is conducted to the myocardium instead of being carried away by the surrounding blood flow because most of the lesion is formed as a result of heat conduction from the Joule heating region, which is limited to a relatively small region next to the electrode. The electrode–endocardial contact includes two aspects: the penetration depth and the penetration angle between the electrode and endocardial surface [19]. Some reported experimental results indicated that lesion dimensions changed significantly as the penetration depth was increased within a certain range [7], [19]. During cardiac ablation, the catheter must penetrate the cardiac tissue. If the penetration depth is

shallow, a large portion of the electrode is exposed to the blood flow. Thus, most energy from the generator dissipates to the blood and the lesion formation is small. If the penetration depth is deep, the blood convection is small and, as a result, the cooling effect on the thermistor is small. Therefore, only a small amount of energy is applied to the system in the temperature-controlled mode. The lesion size is small also.

During the entire process, the physician cannot actually see the electrode and the cardiac tissue. Therefore, the penetration depth is also an uncertain variable. Cao et al. [7] set a penetration of 2.0 mm to explore the effects of blood flow on the lesion formation. Tungjitkusolmun et al. [8] used a penetration of 1.3 mm at low blood flow region and 3.0 mm at high blood flow region to explore the effects of different blood flow on the lesion formation under two different ablation modes, temperature-controlled and power-controlled modes. However, we have been unable to find any previous research revealing the differences caused by these different penetration depths. We set up a system for two flow states with different insertion depths to quantify the effect of the insertion depths on the formation of lesions.

In order to analyze the relationship between the penetration depths and the lesion size in the cardiac tissue during RF ablation, we solved the bioheat equation. The commercial software (ABAQUS), a common FE bioheat equation solver, was used to determine the temperature distribution in the myocardium. FE modeling takes into account the myocardial properties (electrical conductivity, thermal conductivity, density, and specific heat capacity) and the convection of the blood flow. Thus it has been demonstrated that it is a useful tool in qualitative assessment of lesion dimensions created by RF ablation [6]–[8].

We created several 2D axisymmetric FE models with different penetration depths with a constant width and thickness for two flow states in order to investigate the effect of different insertion depths on the lesion formation.

II. SIMULATION PROCESS

For all of the simulations, the ablation electrode was of standard size used in clinical practice (4 mm long, and 2.6 mm diameter). A temperature-sensing thermistor was embedded at the electrode tip. Similar to Tungjikusolmun et al. [6], the system was modeled by an axisymmetric model. The catheter tip was pushed into the myocardium at a set of different distances of 0.7, 1.3, 2.0, 2.5, 3.0, and 3.5 mm. The blood pool extended 40 mm beyond the myocardium. It was used to model the body fluid outside the epicardium. The heat loss due to the blood perfusion outside the epicardium is negligible compared to the heat loss due to the blood flow inside the heart chamber. Thus, we assumed that the convective heat loss at outside the epicardium due to fluid flow was negligible. The only heat transfer in this region was thermal conduction. We set the temperature of the blood on the boundary of the model to 37 °C, the same as the blood temperature in the cardiac chamber. Using the Dirichlet boundary conditions, we assumed that the voltages on the outer surfaces of the model were 0 V. The electrical and thermal properties of all the materials used in the electrode were taken from the values listed in [19]. The electrical conductivity of the myocardium varies with the temperature. Tsai et al. [15] measured it using the four-terminal method at 500 kHz every degree from 20 to 100 °C. We used the temperature-dependent thermal conductivity and the specific heat of the myocardium from Foster and Schwan [16] and Bhavaraju and Valvano [17].

The cooling effect of blood depends on the location in the cardiac chambers. There are several common locations where clinical electrophysiologists apply ablation, such as the atrioventricular node, AV valve annulus, and right ventricular outflow tract. We divided these locations into two blood flow states. One is the high blood flow state (3 L/min) such as the atrioventricular node, and the other is the low blood flow state (1 L/min) beneath the mitral

valve. The flow state was modeled by the convective heat transfer coefficient h_b. The values of h_b at the blood–myocardium and at the blood–electrode interfaces are different. We used h_b for the blood–myocardium interfaces from Tangwonsan et al. [18], who measured the *in-vivo* convective heat transfer coefficients by directly inserting the measurement catheter into the pig heart. At the blood–electrode interface, we chose convective heat transfer coefficients which Tungjitkusolmun et al. [7] derived from the blood velocity measured by ultrasound doppler [18]. Table 2 lists the convective heat transfer coefficients for different blood flow at the blood–myocardium interface and the blood–electrode interface used in this study.

We used a proportional-integral (PI) controller similar to that implemented for hepatic ablation developed by Haemmerich et al. [11]. By analyzing the cardiac ablation system, we set the PI control coefficient to be $K_p = 0.5$ and $K_i = 0.3$ to minimize overshoot of the controlled temperature. The PI controller was implemented by a C++ program. The controller determined the applied voltage at each uniform step time (0.5 s) by comparing the set temperature and the temperature at the thermistor. The thermistor temperature was read from the resulting file created by ABAQUS when it finished the simulation of each time step.

Fig. 1 shows the simplified diagram of the geometry of the ablation electrode model and the tissue at different penetration depths. Fig. 1 of Ch. 3 shows the detail of the geometry information for the simulation system. Table 1 lists the total number of nodes and elements in each model. Fig. 1 shows the simplified diagram that defines the penetration depth. The same data collection procedure by using a PI controller and the ABAQUS FE solver suggested by Lai et al. [18] was followed. Simulated temperature-controlled ablation at temperatures of 60, 70, and 80 °C at different blood flow states were used. The temperature distributions at 10, 20, 30, 40, 50, 60, 70, 80, and 90 s after start of the ablation simulation for each set were acquired.

Nath [13] observed that when the tissue temperature reaches 50 °C, irreversible myocardial injury occurs during RF cardiac ablation. The cells lose electrical excitability and the re-entrant pathways are interrupted. Thus 50 °C is usually considered as the threshold for lesion formation. A C++ program was implemented to search the temperature distribution in the system to find those points exceeding the critical temperature of 50 °C. Fig. 1 also shows a typical shape of the lesion formed by RF ablation. *Width* is the maximum width of the lesion, *Depth* is the maximum depth of the lesion and *Depth under tip* is the maximum depth of the lesion measured from the electrode tip.

III. RESULTS

The relationship between penetration and lesion formation was investigated, and a similar phenomenon among the sets with different target temperatures at different flow states was found. Only the results of the simulation targeted at 60 °C at high blood flow region are shown. Figs. 2 and 3 show the results for lesion width and lesion depth. The complete set of time responses for all different settings of simulations can be found in Appendix B. Figs. 4 and 5 show the shapes of the lesion formations at 90 s for target tip temperature at 60 °C for the high and low blood flow regions.

When we observed the voltage applied to the electrode by the PI controller at 89 s, the case of the penetration depth of 0.7 mm had the highest applied voltage of 22.84 V at high blood flow and 21.69 V at low blood flow and the case of the penetration depth of 3.5 mm had the lowest applied voltage of 16.02 V at high blood flow and 13.97 V at low blood flow. The voltage applied decreased with the increase in the penetration depth.

Fig. 1 and 2 show that the smallest lesion width and depth occurred at the penetration depth of 0.7 mm. The width increased when the penetration depth increased. The width reached a

maximum value at the penetration depth of about 2.0 to 2.5 mm. The width decreased when the penetration depth increased after a penetration depth of 2.5 mm. The lesion depth showed a similar pattern. The maximum depth appeared at a penetration of 3.0 mm. Thus, the maximum lesion volume occured at a penetration depth of about 2.0 to 3.0 mm.

III. DISCUSSION

A. *Penetration depth vs. applied voltage.*

Temperature-controlled ablation depends on the temperature measured by the thermistor at the tip of the electrode to determine how much energy needs to be delivered into the system, i.e. the voltage applied to the electrode. If the penetration depth is shallow, the blood cooling effect carries a large amount of heat away from the electrode and tissue surrounding the thermistor. This effectively reduces the heat conveyed to the thermistor. The system has to deliver more energy to heat up the thermistor. Thus, the results show that the maximal value of voltage applied to the electrode appeared at the penetration depth of 0.7 mm and the minimal value of voltage applied to the electrode appeared at the penetration depth of 3.5 mm.

B. *Penetration depth vs. lesion size.*

The energy delivered by the power source is not the only factor to affect the formation of the lesion. Heat loss due to blood convection at the blood–electrode interface plays another important role in the formation of the lesion. When the penetration is shallow, the portion of the electrode exposed to blood flow is large. Thus the convection region on the electrode is large. In addition, the effective contact area between the electrode and the myocardium is small. As a result, most of the energy from the power system is carried away by the blood flow instead of being delivered into the cardiac tissue. Thus, the smallest lesion width and depth occurs at the penetration depth of 0.7 mm.

With an increase in the penetration depth, the area of the electrode contacting the blood decreases and the area contacting the cardiac tissue increases. Consequently, the energy taken away by the blood decreases and the energy effectively delivered into the system increases. Although the energy delivered by the power source decreases due to the reduction in the blood convection, the total effective energy delivered into the myocardium still increases. Therefore, the lesion width steadily increases as the penetration depth increases. In the high blood flow region, this effect is much more obvious.

However, when we push the electrode too deep, the blood cooling effect at the thermistor is insignificant. As a consequence, the power system does not need to deliver extra power to maintain the tip temperature. The result is that the total energy delivered into the myocardium by the system is small, and the width of the lesion is small.

As a result, there is a tradeoff between the ratio of energy delivered into the cardiac tissue and the energy injected into the electrode. As shown in the results section, a penetration depth of about 2.0 to 3.0 mm produces the maximum lesion volume.

IV. CONCLUSION

During cardiac ablation, the contact between the ablation electrode and the cardiac tissue plays an important role in the formation of the lesion. The effect of penetration depth on the formation of the lesion was investigated. The maximum ablation volume appears at a penetration of 2.0 to 3.0 mm. In this range, the blood cooling effect on the thermistor is large enough to induce a large amount of power into the system. And also, the power carried away by blood convection at the blood–electrode and blood–myocardium interface is relatively small. As a result, a larger amount of the energy is transmitted into the cardiac tissue, and the size of the lesion is maximized.

REFERENCES

[1] S. K. S. Huang and D. J. Wilber, Eds., *Radiofrequency Catheter Ablation of Cardiac Arrhythmias: Basic Concepts and Clinical Applications*, 2nd ed., Armonk, NY: Futura, 2000.

[2] D. P. Zipes and M. Haïssaguerre, *Catheter Ablation of Arrhythmias*. 2nd ed. Armonk, NY: Futura, 2002.

[3] F. Morady, "Drug therapy: radio-frequency ablation as treatment for cardiac arrhythmias," *N. Engl. J. Med.*, vol. 340, pp. 534–544, 1999.

[4] D. Panescu, "Intraventricular electrogram mapping and radiofrequency cardiac ablation for ventricular tachycardia," *Physiol. Meas.*, vol. 18, pp. 1–38, 1997.

[5] H. Nakagawa, K. J. Beckman, and J. H. McClelland, "Radiofrequency catheter ablation of idiopathic left ventricular tachycardia guided by a Purkinje potential," *Circulation*, vol. 85, pp. 1666–1674, 1992.

[6]. Tungjitkusolmun, S., Woo, E. J., Cao, H., Tsai, J.-Z., Vorperian, V. R., and Webster, J. G., "Thermal-electrical finite element modeling for radio-frequency cardiac ablation: effects of changes in myocardial properties," *Med. Biol. Eng. Comput.*, vol. 38, pp. 562–568, 2000.

[7]. H. Cao, V. R. Vorperian, S. Tungjikusolmun, J.-Z. Tsai, D. Haemmerich, Y. B. Choy, and J. G. Webster, "Flow effect on lesion formation in RF cardiac catheter ablation, *IEEE Trans. Biomed. Eng.*, vol. 48, pp. 425–433, 2001.

[8]. S. Tungjitkusolmun, V. R. Vorperian, N. Bhavaraju, H. Cao, J.-Z. Tsai, and J. G. Webster, "Guidelines for predicting lesion size at common endocardial locations during radio-frequency ablation," *IEEE Trans. Biomed. Eng.*, vol. 48, pp. 194–201, 2001.

[9] D. Haemmerich, J. G. Webster, "Automatic control of finite element models for temperature-controlled radiofrequency ablation", Biomed. Eng. Online, 4(1):42, 2005.

[10]. D. Panescu, J. G. Whayne, S. D. Fleischman, M. S. Mirotznik, D. K. Swanson and J. G. Webster, "Three-dimensional finite element analysis of current density and temperature distributions during radio-frequency ablation," *IEEE Trans. Biomed. Eng.*, vol. 42, pp. 879–890, 1995.

[11]. H. H. Peterson, X. Chen, A. Pietersen, J. H. Svendsen, S. Hauns, "Lesion dimensions during temperature-controlled radiofrequency catheter ablation of left ventricular porcine myocardium: impact of ablation size, electrode size and convective cooling," *Circulation*, vol. 99, pp. 319–325, 1999.

[12] S. D. Edwards and R. A. Stern, *Electrode and Associated Systems Using Thermally Insulated Temperature Sensing Elements*, U. S. Patent 5 688 266, 1997.

[13]. K. R. Foster and H. P. Schwan, "Dielectric properties of tissues and biological materials: A critical review," *CRC Crit. Rev. Biomed. Eng.*, vol. 17, pp. 25-104, 1989.

[14] N. C. Bhavaraju and J. W. Valvano, "Thermophysical properties of swine myocardium," *Int. J. Thermophys.*, vol. 20, pp. 665–676, 1999.

[15]. C. Tangwongsan, J. A. Will, J. G. Webster, K. L. Meredith Jr., D. M. Mahvi, "*In vivo* measurement of swine endocardial convective heat transfer coefficient", *IEEE Trans. Biomed. Eng.*, 51, 1478-1486,

[16]. A. B. Houston and I. A. Simpson, Eds, *Cardiac Doppler ultrasound: A clinical perspective*. Boston: Wright, 1988.

[17] S. Nath, C. Lynch, J. G. Whayne, D. E. Haines, "Cellular electrophysiological effects of hyperthermia on isolated guinea pig papillary muscle implication for catheter ablation," *Circulation*, vol. 88, part 1, pp. 1826–1831, 1993.

[18]. Y. C. Lai, Y. B. Choy, D. Haemmerich, V. R. Vorperian, J. G. Webster, **"**Lesion size estimator of cardiac radiofrequency ablation at different common locations with different tip temperatures", *IEEE Trans. Biomed. Eng.,* vol. 51, pp. 1859-1864, 2004.

[19] H., Cao, S. Tungjitkusolmun, Y. B. Choy, J.-Z. Tsai, V. R. Vorperian, and J. G. Webster, "Using electrical impedance to predict catheter–endocardial contact during RF cardiac ablation", *IEEE Trans. Biomed. Eng.,* vol. 49, pp. 247-253, 2002.

[20] S. D. Edwards and R. A. Stern, "Electrode and associated systems using thermally insulated temperature sensing elements", U. S. Patent 5 688 266, 1997.

Fig. and Table Captions:

Fig. 1. The penetration depth is the length of electrode inserted into the cardiac tissue and its value is the vertical distance between the tip and the blood-cardiac interface. The width and depth are the maximum extensions in *X* and *Y* direction. The depth value from the tip which is the vertical distance from the tip to the vertical maximal extent in the *Y* direction is measured in order to yield further understanding of the effect of different penetration on lesion size formation.

Fig. 2. Simulation of time response for width for different insertion depths for high blood flow targeted at 60 °C

Fig. 3. Simulation of time response for depth for different insertion depths for high blood flow targeted at 60 °C

Fig. 4. The shape of lesion gathered from simulation data at 90 s for different insertion depths for high blood flow targeted at 60 °C
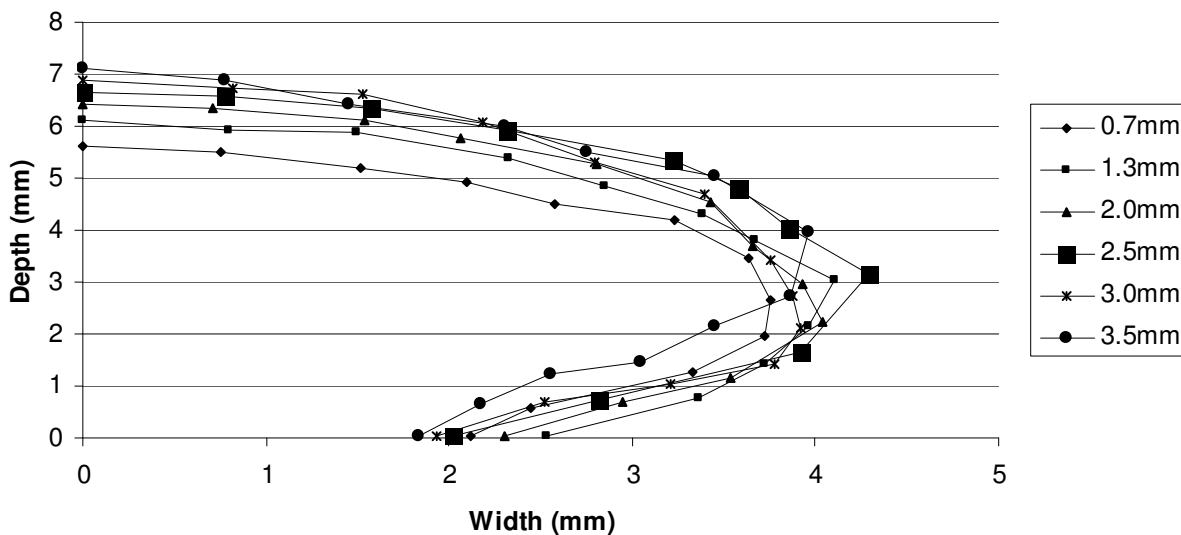
Fig. 5. The formation of lesions for different insertion depths at 90 s after starting applying the cardiac ablation at high blood flow targeted at 60 °C.

Table 1 The total number of nodes and elements in each FE model for different insertion depths

Table 2 Convective heat transfer coefficient and flow state in different applied locations

Fig. 1. The penetration depth is the length of electrode inserted into the cardiac tissue and its value is the vertical distance between the tip and the blood-cardiac interface. The width and depth are the maximum extensions in *X* and *Y* direction. The depth value from the tip which is the vertical distance from the tip to the vertical maximal extent in the *Y* direction is measured in order to yield further understanding of the effect of different penetration on lesion size formation.

Fig. 2. Simulation of time response for width for different insertion depths for high blood flow targeted at 60 °C

Fig. 3. Simulation of time response for depth for different insertion depths for high blood flow targeted at 60 °C

Fig. 4. The shape of lesion gathered from simulation data at 90 s for different insertion depths for high blood flow targeted at 60 °C

Fig. 5. The shape of lesion gathered from simulation data at 90 s for different insertion depths for low blood flow targeted at 60 °C

Table 1 The total number of nodes and elements in each FE model for different insertion angles

Penetration depth	# of Elements	# of Nodes
0.7 mm	2325	4650
1.3 mm	2319	4435
2.0 mm	3273	11216
2.5 mm	2286	4344
3.0 mm	2304	4395
3.5 mm	2266	4319

Table 2 Convective heat transfer coefficient and flow state in different applied locations

Location	Blood flow	h_b at blood-myocardium interface [W/(m²·K)]	h_{be} at blood-electrode interface [W/(m²·K)]
AV node	High	7100	6090
CS	Low	3350	2081
Atrial AP	High	7100	6090
Ventricular AP	Low	3350	2081
RV outflow VT	High	7100	6090

CHAPTER 6

CARDIAC ABLATION LESION SIZE DEPENDS ON THE ELECTRODE INSERTION ANGLE

Abstract—Cardiac ablation electrode insertion angle affects the blood cooling effect and the efficiency of energy delivered from electrode into cardiac tissue. This study investigates the effect of the changes in the insertion angle on the formation of the lesion. This can give clinical electrophysiologists more information about the probable success of cardiac ablation. We developed several 3D FE models to simulate temperature-controlled myocardial ablation at different insertion angles. We found that there is an interesting changing pattern in the lesion formation as the insertion angle decreases.

I. INTRODUCTION

Because of the efficacy, controllability, and minimal invasiveness, radiofrequency (RF) catheter ablation has proven an effective method to treat some cardiac arrhythmias, such as atrioventricular node re-entry, atrial tachycardia, atrial flutter, and fascicular ventricular tachycardias [1] – [3]. Several research groups also suggest that it may be a good method for palliative suppression of ventricular tachycardias [3] – [5].

In order to analyze the relationship between the set temperature in the temperature-controlled mode and the lesion size in the cardiac tissue during RF ablation, we solved the bioheat equation. Commercial software (ABAQUS), a common FE bioheat equation solver, was used to determine the temperature distribution in the myocardium. FE modeling took into account the myocardial properties (electrical conductivity, thermal conductivity, density, and specific heat capacity) and the convection of the blood flow. FE modeling is a useful tool in the qualitative assessment of the lesion dimensions created by RF ablation [6] – [8].

During cardiac ablation, the catheter must penetrate the cardiac tissue. The insertion angle is an important factor that affects the formation of the lesion during the application of RF ablation. The relative impact of the blood flow around the electrode compared to electrode–tissue

contact, as exemplified by parallel vs. perpendicular electrode orientation, has not been fully explored. Generally, increasing either electrode-endocardial contact area or electrode cooling area in a constant blood flow yields a larger lesion volume. For specific electrode geometry, an increase in the electrode–tissue contact area is usually accompanied by a decrease in the cooling area and vice versa. Since varying the electrode orientation impacts both the electrode-endocardial contact and the convection at the blood–electrode interface, we investigated how these factors affect the lesion formation for a given electrode geometry. Perpendicular and parallel orientations are the two extreme cases. An investigation of the effects of the changes in the insertion angle on the formation of the lesion would give the clinical electrophysiologist more information to evaluate the probable success of cardiac ablation. We developed several FE models to represent different insertion angles and used them to simulate temperature-controlled myocardial ablation for two blood flow states. We computed lesion sizes from the set of temperature distributions collected during the simulations to analyze the effects of the changes in the insertion angle on the lesion size.

Our objective was to quantify the effect of changing orientation of the catheter tip under different blood velocities on the lesion size as a function of the applied ablation duration.

II. METHOD

The formation of the RF ablation lesion depends on the temperature distribution inside the tissue. The temperature change during the process inside the myocardium is governed by the bioheat equation [6]. Because it is not practical to solve the coupled problem analytically, we use FE modeling to solve it numerically.

When the electrode is not perpendicular to the myocardium, the system is no longer axisymmetric to the central axis of the catheter. We need to use 3D FE models to investigate the

effects of the change in the insertion angle on the lesion size. Fig. 1(b) shows a schematic diagram of the values and variables used in this simulation. The thickness of the myocardial tissue was chosen as 10 mm consistent with previous studies. The depth meter in *in-vitro* experiment was used to control the insertion at 2 mm. Therefore, we specified the insertion length as 2 mm. The insertion length was defined as the distance between the tip of the catheter and the intersection points between the blood–myocardium interface and the central axis of the catheter. The angle, θ, is the angle between the central axis of the applied catheter and the normal direction of the blood–myocardium interface. This is illustrated in Fig. 1. Next, we also wanted to investigate seven different insertion angles, 0, 15, 30, 45, 60, 75, and 90° measured from the perpendicular direction of the blood–myocardium interface, where 90° means that the catheter is parallel to the blood–myocardium interface and 0° means that the catheter is perpendicular to the blood–myocardium interface. We used the same control algorithm to control the entire simulation using the temperature-controlled mode. We investigated the effects for high blood flow and low blood flow for a single target temperature 60 °C

In all of the simulations, the ablation electrode was of standard size used in clinical practice (4 mm long, and 2.6 mm diameter). A temperature-sensing thermistor was embedded at the electrode tip. To model the liquid-containing tissue beyond the myocardium, we kept the model simple by placing 40 mm of blood outside the myocardium with no convective heat loss. The heat loss due to the blood perfusion in tissue outside the epicardium is negligible compared to the heat loss due to the blood flow inside the heart chamber. Thus, the only heat transfer in this region was thermal conduction. We set the temperature of the blood on the boundary of the model to 37 °C, the blood temperature in the cardiac chamber. Using the Dirichlet boundary conditions, we assumed that the voltages on the outer surfaces of the model were 0 V. The electrical and thermal properties of all the materials used in the electrode were taken from the

values listed in [14]. The electrical conductivity of the myocardium varied with the temperature.

Tsai et al. [15] measured it using the four-terminal method at 500 kHz every degree from 20 °C

to 100 °C. We used the temperature-dependent thermal conductivity and the specific heat of the

myocardium from Foster and Schwan [16] and Bhavaraju and Valvano [17].

The cooling effect of blood depends on the location in the cardiac chambers. There are

several common locations where clinical electrophysiologists apply ablation, such as near the

atrioventricular node, AV valve annulus, and right ventricular outflow tract. We divided these

locations into two blood flow states. One was the high blood flow state (3 L/min) such as near

the atrioventricular node, and the other was the low blood flow state (1 L/min) beneath the mitral

valve. The flow state was modeled by the convective heat transfer coefficients, h_b. The values of

h_b at the blood–myocardium and at the blood–electrode interfaces were different. We used h_b for

the blood–myocardium interfaces from Tangwonsan et al. [18], who measured the *in-vivo*

convective heat transfer coefficients by directly inserting the measurement catheter into the pig.

At the blood–electrode interface, we chose convective heat transfer coefficients, which

Tungjitkusolmun et al. [7] derived from the blood velocity measured by doppler ultrasound [18].

Table 1 lists the convective heat transfer coefficients for different blood flows at the blood–

myocardium interface and the blood–electrode interface used in this study.

We used a proportional-integral (PI) controller similar to that implemented for hepatic

ablation developed by Haemmerich et al. [11]. By analyzing the cardiac ablation system, we set

the PI control coefficient to be $K_p = 0.5$ and $K_i = 0.3$ to minimize overshoot of the controlled

temperature. The PI controller was implemented by a C++ program. The controller determined

the applied voltage at each uniform step time (0.5 s) by comparing the set temperature and the

temperature at the thermistor. The thermistor temperature was read from the resulting file created

by ABAQUS when it finished the simulation of each time step.

The entire data collection process using our PI controller and the ABAQUS FE solver proposed by Lai et al. [22] was used in this study. We simulated temperature-controlled ablation at different insertion angles of 0, 15, 30, 45, 60, 75, and 90° meashured from the perpendicular direction of the blood–myocardium interface with the target tip temperature of 60 °C for different blood flow states. We acquired the temperature distribution at 10, 20, 30, 40, 50, 60, 70, 80, and 90 s after the start of the ablation simulation for each set temperature.

Nath [13] observed that when the tissue temperature reaches 50 °C, irreversible myocardial injury occurs during RF cardiac ablation. The cells lose electrical excitability and the re-entrant pathways are interrupted. Thus, 50 °C is usually considered as the threshold for lesion formation. We implemented a C++ program to search the temperature distribution in the system to find those points exceeding the critical temperature of 50 °C. Fig. 2(a) also shows a typical shape of the lesion formed by RF ablation. *Width* is the maximum length of the lesion in the direction parallel to the blood–myocardium interface, and *Depth* is the maximum length of the lesion measured from the blood–myocardium interface in the direction perpendicular to the interface.

Table 1 lists the total number of nodes and elements contained in each model for different insertion angles.

III. RESULTS

The relationship between penetration angle and lesion formation was investigated, and a similar phenomenon for the low blood flow state was found. Only the results of the simulation targeted at 60 °C at high blood flow region are shown. Figs. 3 and 4 show the results for lesion width and lesion depth. Fig. 5 shows the shape of the lesions projected on the plane constructed by two vectors; the first vector's origin is at the tip of the electrode with its direction parallel to

the central axis of the catheter, and the other origin is at the tip of the electrode with its direction parallel to the normal direction of the blood–myocardium interface at 90 s for different insertion angles. Fig. 6 shows the applied voltages at 90 s for different insertion angles.

III. DISCUSSION

Generally, increasing either electrode-endocardial contact area or blood cooling effect at the thermistor under a constant blood flow yields a larger lesion. The larger the contact area is, the larger the percentage of the power that is conducted to the myocardium instead of being lost in the blood flow. The larger the blood cooling effect is, the larger the power is delivered by the power system to maintain the thermistor temperature. Furthermore, the cooling effect at the thermistor depends both on the total number of heat-transport paths from the blood to the thermistor and the length of each path.

As the insertion angle changes from 0 to 15° measured from the perpendicular direction of the blood–myocardium interface, the electrode–contact area and electrode–myocardium contact area maintain the same value as shown at the top of Fig. 2(b). Thus, the length of the heat-transport path from the blood to the thermistor on the blood exposed side becomes shorter. As a result, a larger blood cooling effect is induced into the ablation process. The generator needs to apply a larger voltage to maintain the tip temperature and the lesion size formed at 15° is larger than that at 0°.

When increasing from about 25 to 90° measured from the perpendicular direction of the blood–myocardium interface, the blood–myocardium interface cut through the spherical part of the electrode as shown at the bottom of Fig. 2(b). Thus, as insertion angle increases, the electrode–myocardium contact area becomes larger and the electrode–blood contact area

becomes smaller. As a result, when the insertion angle changes from 15 to 30° measured from the perpendicular direction of the blood–myocardium interface, the reduction in the electrode–blood contact area causes the total number of the heat-transport paths reaching the thermistor from the blood to decrease. Although the length of transport paths on the myocardium side decreases, the reduction in the electrode–blood contact area has a more important effect on the blood cooling. Thus, the applied voltage is smaller. The lesion size formed at 30° is smaller than the lesion size formed at 15°.

When the angle increases over 30° measured from the perpendicular direction of the blood–myocardium interface, the thermistor is much closer to the blood flow on the blood side of the electrode. Consequently, the reduction in the length of the transport paths becomes more significant than the reduction of the electrode–blood contact area in the blood cooling effect. This requires the power system to deliver more power to maintain a constant temperature and generates a larger lesion depth. In addition to the larger cooling effect, the larger electrode–myocardium contact area introduces an even larger lesion width. For large insertion angles over 75° mearesured from the perpendicular direction of the blood–myocardium interface, the thermistor directly contacts the blood flow. The blood carries away heat directly from the thermistor. The power system needs to infuse a large amount of energy to maintain the target tip temperature. In other words, the system heats up by an unreasonable amount in the control algorithm. Therefore, the formation of the lesion is impossibly large. This is not allowed to happen in real life to prevent creating an unnecessarily large lesion in the patent's heart. It is controlled by the limit of the power generator.

We also observed that to simulate a case in 2D is much more efficient than to simulate in 3D. This is because creating a model in 2D takes about 1 day, and creating a model in 3D takes about 1 week. In addition, to simulate a case in a 2D model requires only 10 minutes on average

while to simulate a case in a 3D model used similar density of mesh as the corresponding 2D model requires about 48 hours with similar mesh density. Thus, the 2D model permits a quick check of the feasibility of different design ideas for a different set of parameters.

IV. CONCLUSION

During cardiac ablation, the catheter must penetrate the cardiac tissue. The insertion angle is an important variable during the application of RF ablation. The results of simulation at different insertion angles show an interesting pattern. When the insertion angle changes from 0 to 15° measured from the perpendicular direction of the blood–myocardium interface, the lesion size increases due to the reduction in the length of heat-transport paths from the thermistor to the blood. When the insertion angle changes from 15 to 30° measured from the perpendicular direction of the blood–myocardium interface, the lesion formation becomes smaller because the reduction in the blood–electrode contact area is the dominant factor for the blood cooling effect and the input power decreases. However, when the angle increases from 30° to 60° measured from the perpendicular direction of the blood–myocardium interface, the lesion formation grows again because the reduction in the length of heat-transport paths from the thermistor to the blood becomes significant in blood cooling. However, when applying a large insertion angle, more than 75° measured from the perpendicular direction of the blood–myocardium interface, we take the risk of overheating the cardiac tissue because the cooling effect becomes so large that the power supply induces too much energy causing the popping effect. This is what clinical electrophysiologists try to avoid. In addition, it is hard to insert the catheter to reach the designed depth, and the contact between the electrode and cardiac tissue is also hard to maintain at a high insertion angle.

REFERENCES

[1] S. K. S. Huang and D. J. Wilber, Eds., *Radiofrequency Catheter Ablation of Cardiac Arrhythmias: Basic Concepts and Clinical Applications*, 2nd ed., Armonk, NY: Futura, 2000.

[2] D. P. Zipes and M. Haïssaguerre, *Catheter Ablation of Arrhythmias*. 2nd ed. Armonk, NY: Futura, 2002.

[3] F. Morady, "Drug therapy: radio-frequency ablation as treatment for cardiac arrhythmias," *N. Engl. J. Med.*, vol. 340, pp. 534-544, 1999.

[4] D. Panescu, "Intraventricular electrogram mapping and radiofrequency cardiac ablation for ventricular tachycardia," *Physiol. Meas.*, vol. 18, pp. 1-38, 1997.

[5] H. Nakagawa, K. J. Beckman, and J. H. McClelland, "Radiofrequency catheter ablation of idiopathic left ventricular tachycardia guided by a Purkinje potential," *Circulation*, vol. 85, pp. 1666-1674, 1992.

[6]. Tungjitkusolmun, S., Woo, E. J., Cao, H., Tsai, J.-Z., Vorperian, V. R., and Webster, J. G., "Thermal-electrical finite element modeling for radio-frequency cardiac ablation: effects of changes in myocardial properties," *Med. Biol. Eng. Comput.*, vol. 38, pp. 562-568, 2000.

[7]. H. Cao, V. R. Vorperian, S. Tungjikusolmun, J.-Z. Tsai, D. Haemmerich, Y. B. Choy, and J. G. Webster, "Flow effect on lesion formation in RF cardiac catheter ablation, *IEEE Trans. Biomed. Eng.*, vol. 48, pp. 425-433, 2001.

[8]. S. Tungjitkusolmun, V. R. Vorperian, N. Bhavaraju, H. Cao, J.-Z. Tsai, and J. G. Webster, "Guidelines for predicting lesion size at common endocardial locations during radio-frequency ablation," *IEEE Trans. Biomed. Eng.*, vol. 48, pp. 194-201, 2001.

[9]. D. E. Haines, "The biophysics of radiofrequency catheter ablation in the heart: The importance of temperature monitoring," *PACE*, vol. 16, pp. 596-591, Mar. 1993.

[10]. D. E. Haines, and D. D. Watson, "Tissue heating during radiofrequency catheter ablation: A thermodynamic model and observation in isolated perfused and superfused canine right ventricular free wall," *PACE*, vol. 12, pp. 962-976, June 1989.

[11] D. Haemmerich, J. G. Webster, "Automatic control of finite element models for temperature-controlled radiofrequency ablation", *Biomed. Eng. Online*, 4(1):42, 2005.

[12]. D. Panescu, J. G. Whayne, S. D. Fleischman, M. S. Mirotznik, D. K. Swanson and J. G. Webster, "Three-dimensional finite element analysis of current density and temperature distributions during radio-frequency ablation," *IEEE Trans. Biomed. Eng*. vol. 42, pp. 879-890, 1995.

[13]. H. H. Peterson, X. Chen, A. Pietersen, J. H. Svendsen, S. Hauns, "Lesion dimensions during temperature-controlled radiofrequency catheter ablation of left ventricular porcine myocardium: impact of ablation size, electrode size and convective cooling," *Circulation*, vol. 99, pp. 319-325, 1999.

[14] S. D. Edwards and R. A. Stern, *Electrode and Associated Systems Using Thermally Insulated Temperature Sensing Elements*, U. S. Patent 5 688 266, 1997.

[15]. J.-Z. Tsai, *Measurement of in vivo and in vitro swine myocardial resistivity*, PhD Dissertation, Univ. of Wisconsin-Madison, May 2001

[16] K. R. Foster, and H. P. Schwan, "Dielectric properties of tissues and biological materials: a critical review," *CRC Crit. Rev. Biomed. Eng*., vol. 17, pp. 25-104, 1989.

[17] N. C. Bhavaraju and J. W. Valvano, "Thermophysical properties of swine myocardium," *Int. J. Thermophys*., vol. 20, pp. 665-676, 1999.

[18]. A. B. Houston and I. A. Simpson, Eds, *Cardiac Doppler ultrasound: A clinical perspective*. Boston: Wright, 1988

[19] N. C. Bhavaraju, *Heat Transfer Modeling During Radiofrequency Cardiac Ablation in Swine Myocardium*, Ph. D. Dissertation, Univ. Texas, Austin, Mar. 2000.

[20] S. Nath, C. Lynch, J. G. Whayne, D. E. Haines, "Cellular electrophysiological effects of hyperthermia on isolated guinea pig papillary muscle implication for catheter ablation," *Circulation*, vol. 88, part 1, pp. 1826-1831, 1993.

[21]. C. Tangwongsan, J. A. Will, J. G. Webster, K. L. Meredith Jr., D. M. Mahvi, "*In vivo* measurement of swine endocardial convective heat transfer coefficient", *IEEE Trans. Biomed. Eng.*, 51, 1478-1486, 2004.

[22]. Y. C. Lai, Y. B. Choy, D. Haemmerich, V. R. Vorperian, J. G. Webster, **"**Lesion size estimator of cardiac radiofrequency ablation at different common locations with different tip temperatures", *IEEE Trans. Biomed. Eng.,* vol. 51, pp. 1859-1864, 2004.

.

Fig. and Table Captions:

Fig. 1. (a) Insertion of electrode into the myocardium. (b). Different values used for the FE model including the thickness of the myocardial tissue, the insertion depth, and also the angle of insertion.

Fig. 2. (a) The electrode enters the myocardium at an angle θ and generates a lesion with width W and depth D. (b) The top shows that when the blood−myocardium interface passes through the cylinder part, the reduction in electrode−myocardium contact area on the left of the central axis is equal to the increase on the right. The bottom shows that when the blood−myocardium interface passes through the sphere part, the reduction in the left hand side is smaller than the increase in the right hand side.

Fig. 3. Simulation of lesion width increases with ablation time for high flow for different insertion angles at target tip temperature 60 °C.

Fig. 4. Simulation of lesion depth increases with ablation time for high flow for different insertion angles at target tip temperature 60 °C.

Fig. 5. The lesion shape at 90 s for different insertion angles at high blood flow at target tip temperature 60 °C.

Fig. 6. The voltage applied at 90 s for different insertion angles at target tip temperature 60 °C.

Table 1 Convective heat transfer coefficient and flow state for different applied locations.

Table 2 The total number of nodes and elements in each FE model for different insertion angles.
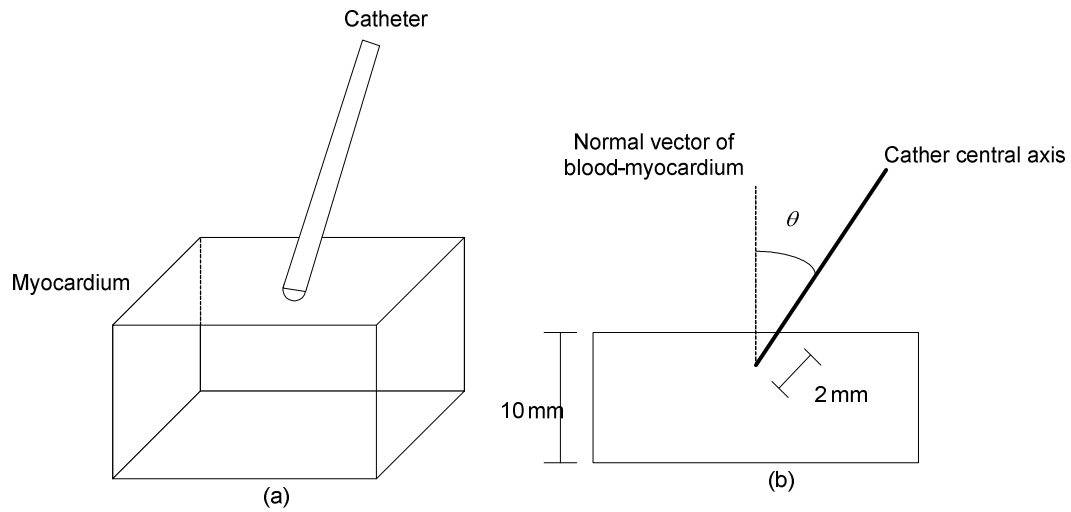
Fig. 1. (a) Insertion of electrode into the myocardium. (b). Different values used for the FE model including the thickness of the myocardial tissue, the insertion depth, and also the angle of insertion which is measured from the perpendicular direction of the blood–myocardium inteface.
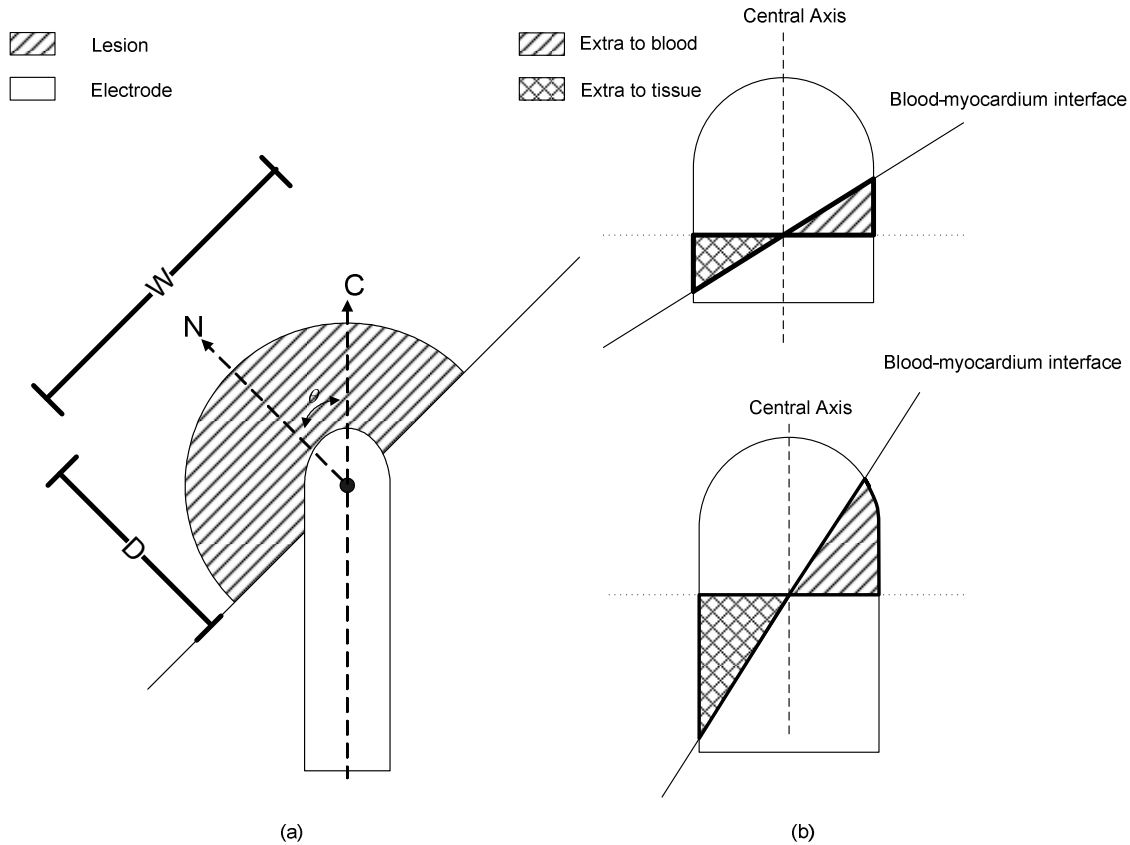
Fig. 2. (a) The electrode enters the myocardium at an angle θ and generates a lesion with width *W* and depth *D*. (b) The top shows that when the blood−myocardium interface passes through the cylinder part, the reduction in electrode−myocardium contact area on the left of the central axis is equal to the increase on the right. The bottom shows that when the blood−myocardium interface passes through the sphere part, the reduction in the left hand side is smaller than the increase in the right hand side.
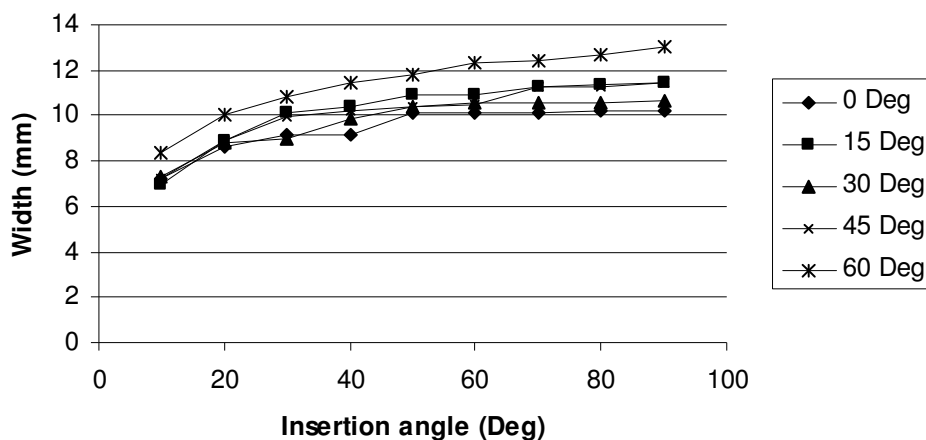
Fig. 3. Lesion width increases with ablation time for high blood flow for different insertion angles at target tip temperature 60 °C.
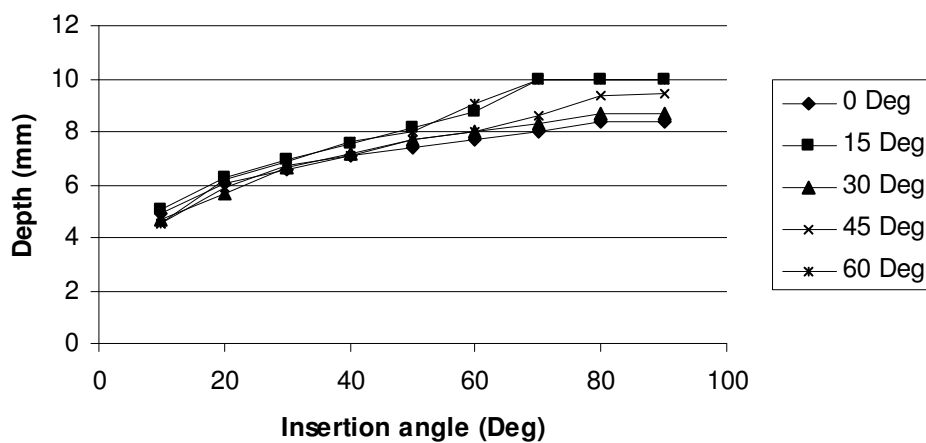
Fig. 4. Lesion depth increases with ablation time for high blood flow for different insertion angles at target tip temperature 60 °C.
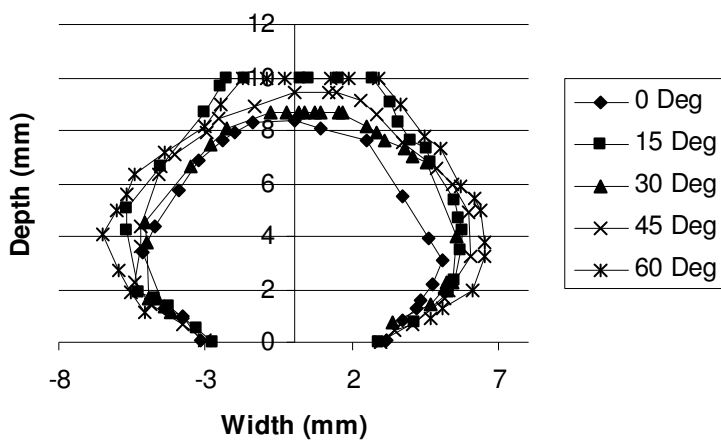
Fig. 5. The lesion shape at 90 s for different insertion angles at high blood flow at target tip temperature 60 °C.
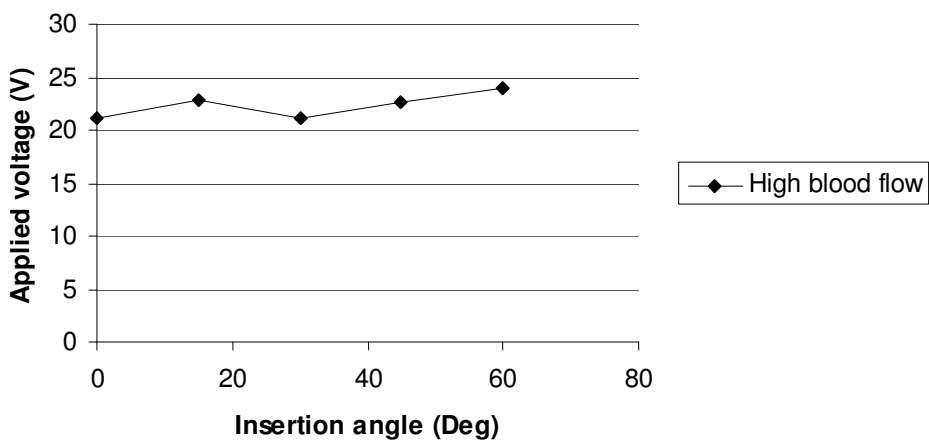
Fig. 6. The applied voltage at 90 s for different insertion angles for high blood flow rate at target tip temperature 60 °C.

Table 1 Convective heat transfer coefficient and flow state for different applied locations

Location	Blood flow	h_b at blood-myocardium interface [W/(m^2·K)]	h_{be} at blood-electrode interface [W/(m^2·K)]
AV node	High	7100	6090
CS	Low	3350	2081
Atrial AP	High	7100	6090
Ventricular AP	Low	3350	2081
RV outflow VT	High	7100	6090

Table 2 The total number of nodes and elements in each FE model for different insertion angles

Insertion angle	# of Elements	# of Nodes
0	212732	36433
15	210148	36168
30	184957	31384
45	193957	34188
60	222284	38316
75	207078	33433
90	201104	32123

CHAPTER 7

CONCLUSION

The size of the formed lesions is the result of a combination of factors such as applied tip temperature, application time, applied location, myocardial properties, penetration depth, insertion angle, and so on. In this thesis, for lesion formation the studies of the effects of changes in dimension of cardiac tissue including the width and thickness, convective coefficients on blood–electrode and blood–tissue interfaces, applied location which is related to blood flow rate, penetration depth, and penetration angle were presented. All these are numerically studied by FE methods either in 2D axisymmetric or 3D models. We implemented an automatic temperature-controlled system to control the tip temperature at a constant target tip temperature and collect a set of the temperature distribution data during the process. A C++ program was used to extract the dimensions of the lesion formation automatically. We also conducted *in-vitro* experiments to verify the numerical results for the lesion size estimator. We showed that every factor has different effects on the lesion formation. At the end of each chapter we provide a quantitative description of the estimated lesion size according to the application conditions.

However, we only used a limited set of possible parameters in our studies. In real life, the situation is more complex. Thus the following may be limitations to the precision of estimation:

(1). In real life, the variation of the contact area has a quantitative effect on the formation of the lesion. Modeling deformation of the cardiac tissue would improve the precision.

 (2). Although blood flow in the cardiac chamber is very complex and varies from 5 L/min to almost 0 L/min, we simply divided the applied locations into high blood flow (3 L/min) and low blood flow (1 L/min). With improved knowledge of blood flow at each location, we could obtain an improved estimation of the formation of the lesion.

(3). We used a control program that improves efficiency without human interaction during the simulation. The accuracy of the control method could be improved by determining the dynamic response of the increased tissue temperature to applied voltage during *in-vivo*

experiments. With information about the control methods used in the commercial generators, we could more precisely simulate process of RF ablation in the operating room.

Through the entire dissertation, three important factors for the formation of lesion were observed. The first is target tip temperature which affects the applied voltage on the electrode from the radiofrequency generator. The second is cooling effect on the thermistor which also affects the applied voltage. In addition, the cooling effect is affected by three factors: the velocity of the blood flow, the contact area between the blood and the electrode, and the length of conducting paths from the thermistor to the electrode. The last is efficiency of energy delivery which affects the size of Joule heating rim. It is affected by the contact area between the electrode and the cardiac tissue. However, the area of the electrode is fixed. Thus, there is a tradeoff between the blood–electrode and myocardium–electrode contact area. In other words, there is a tradeoff between the cooling effect and the energy delivery efficiency.

In this dissertation, we presented a procedure to create a database for predicting the formation of the lesion by collecting time response data of the lesion formation by using different FE models for different application conditions. The database is created for predicting the lesion formation of the standard 7 Fr cardiac ablation catheter. However, similar processes can be extended for other types of cardiac catheters. We demonstrated how to use this database to predict the size of the lesion formation by using two parameters, lesion width and lesion depth, because shapes of the lesions created by the standard 7 Fr catheter are similar. This prediction of the lesion formation demonstrated one way to use this database. There are several different extensions to the usage of the database. First, an animation of the growth of the lesion related to certain specific application conditions could be created in order to let clinical electrophysiologists gain the sense of cardiac ablation during application process. Second, a much larger database could be created by collecting more simulation data from all different types

of cardiac ablation catheters. The shape of the lesion when using different types of catheter could be predicted by using the larger database. Finally, the database could be used to answer an important question: if a specific shape and size of lesion would like to be created, what kind of catheter should be used, what target tip temperature should be set, how much penetration is needed for a specific applied location. In other words, clinical electrophysiologists specify the target size and shape of the lesion and other specific conditions such as applied locations. The database should be able to list several proper applied conditions such as how large the penetration depth should be, what the target tip temperature should be, and what the penetration angle should be. The clinical electrophysiologists could then choose a proper one and apply the designed cardiac ablation to a patient.

APPENDIX A

IN-VITRO EXPERIMENT TO COMPARE LESION SIZES WHEN CONDUCTING EXPERIMENTS IN DIFFERENT SALINE SOLUTIONS.

I. INTRODUCTION

As most cell membranes are freely permeable to water and do not possess water pumps in their membranes, cells will shrink or swell in response to changes in the ionic concentration of the environment. However, for *in-vitro* cardiac ablation experiments, we must use a saline solution whose impedance matches the impedance of the blood. In Ch. 4, we conducted the entire experiment with 0.5% saline. According to cell physiology, this concentration causes an increment of water pumped into cardiac tissues and the growth of the volume of each cell. The extra water content and the increment in cell volume may have effects on the heat conduction during the ablation process. In this appendix, we present an experiment to verify that the concentration of the saline solution does not have significant effects on the ablation results.

II. METHOD

Fig. 1 shows the environment which simulates the blood pool in the heart chamber. The myocardial block sits on a Plexiglas frame immersed in a plastic container filled with two different saline solutions which are listed in Table 1. Solution 1 is a 0.5% saline solution used in our previous *in-vitro* experiment. In addition to 0.5% NaCl, we add extra glucose into Solution 2 to match the total ion concentration with the blood (equivalent to a 0.89% saline solution). The catheter, attached to a pressure measurement meter, contacts the tissue surface at a normal angle (90°). The electrode is the standard Chilli II from BioScience. Since the electrode is internally cooled, there is little difference in lesion size at different flow rates with this type of catheter. As a result, there is no external flow. The target temperature is set at 40 °C, which is the standard clinical setting for this type of internally cooled catheter. Initial power is 2 W, and slowly ramped up over the first 30 to 45 s of the ablation, usually to around 18 to 20 W max. The total time for each ablation is 120 s.
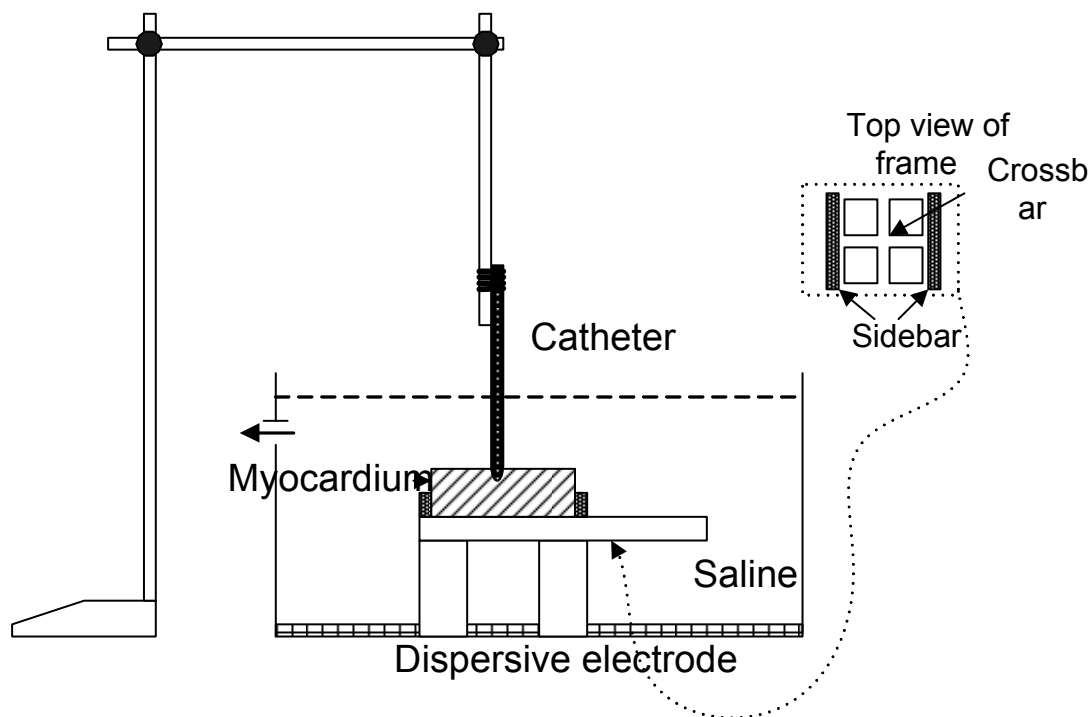
Fig. 1. The experiment environment simulates the heart chamber without external
flow.

Components	NaCl (g/L)	$C_6H_{12}O_6$ (g/L)
Solution 1	5	0
Solution 2	5	32.83

Table 1 Components used in solutions

We obtained bovine heart from the local butcher shop. We cut the myocardium into 3.0
$\times 3.0 \times 1.0$ cm blocks. We aligned the catheter electrode at the center of the myocardial block
and inserted the catheter perpendicularly into the myocardium for ablation. The contact force
was ~15 g. The myocardium deformed into a bowl shape as shown in Fig. 2. After ablation, we
dissected the myocardium through the center and then immersed it in p-nitro blue tetrazolium
solution for about 10 min to distinguish the live (blue) and dead (pale) tissue. The staining
solution changed the color of normal cardiac tissues into dark blue while keeping the color of
lesions pale. We then used a digital camera to take pictures of lesions with a ruler scale on the
lesion surface. We then measured the parameters *A*, *B*, *C*, *D* to calculate the width, depth, and
volume of the lesion.
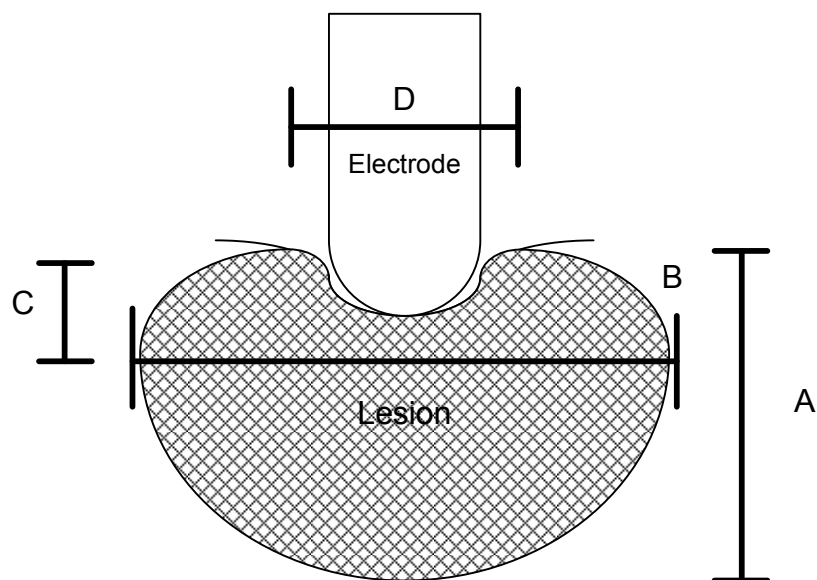
Fig. 2 The traditional shape of the lesion. *A* is the maximal depth, and *B* is the maximal diameter. In addition, *A*, *B*, *C*, and *D* are used to calculate the volume of the lesion.

III. RESULT

We measured maximal depth and maximal diameter as shown in Fig. 2. We also calculated the volume of the lesion size by using the equation: $V = \frac{2}{3}\pi\left(\frac{B}{2}\right)^2 A + \frac{1}{3}\pi\left(\frac{D}{2}\right)^2 C$.

The influence of concentration of solution was accessed by the t-test using Microsoft Excel. Values of $p > 0.95$ computed were considered statistically insignificant different.

Table 2 shows the results.

Solution 1	Experiments	1	2	3	4	5	Avg	Dev
	Width (mm)	11.77	12.01	11.71	11.31	11.03	11.56	0.452
	Depth (mm)	7.20	6.94	6.57	6.95	6.54	6.84	0.279
	Volume (mm^3)	586.51	591.2	524.68	533.72	495.59	546.34	41.31
Solution 2	Experiments	1	2	3	4	5	Avg	Dev
	Width (mm)	11.71	12.02	10.89	11.47	11.78	11.58	0.427
	Depth (mm)	6.90	6.24	7.10	7.05	6.94	6.84	0.350
	Volume (mm^3)	542.74	542.31	503.80	572.58	574.33	547.15	28.76

Table 2. Maximal depth and maximal diameter of lesions.

Table 2 shows that the results measured in the width, depth, and volume are close enough. Thus, we conclude that the deviation caused by the concentration of the saline solution is insignificant compared to other factors.

APPENDIX B

***COMPLETE STATISTICAL ANALYSS OF IN-VITRO* EXPERIMENT**

The results section of Ch. 4 presents the statistical regression analysis. In addition to the regression model analysis, we have done more analysis of the relation between the experimental data and the simulated data. This appendix provides the statistical analysis and some description of statistical terms used in Ch. 4 and this appendix.

BASICAL INFORMATION

In this section, we introduce the several basic concepts and terms used in Ch. 4 and this appendix

Error Types

When we analyze differences between the simulated values and experimental values, we fit the difference into a first order regression model. If the simulation is perfect, we should get a straight line with zero slope and zero interception. However, the result may not be so simple. We need to understand the meaning of different types of error.
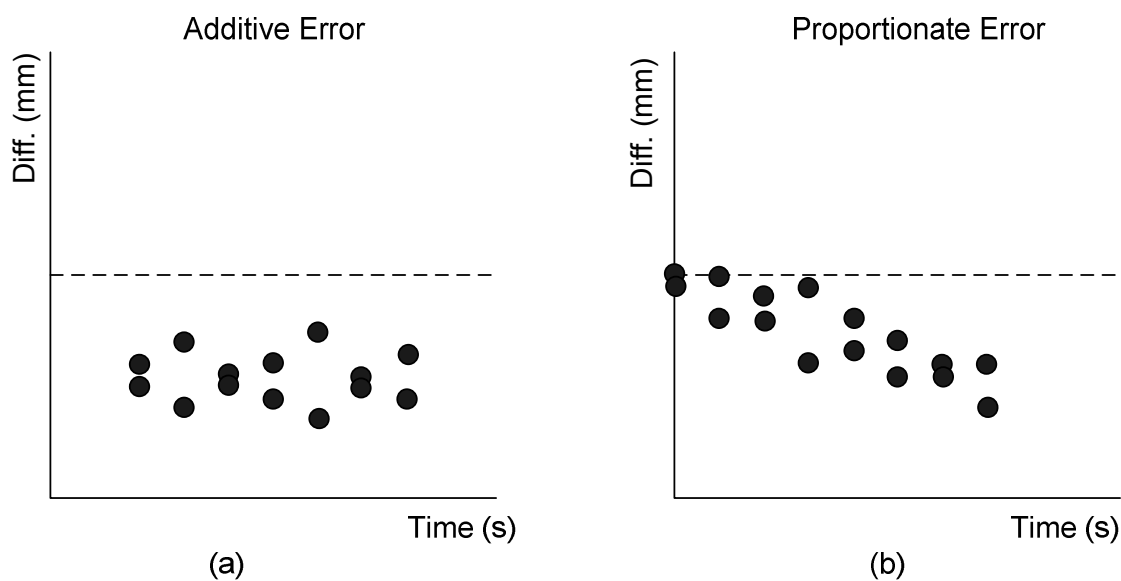
Fig. 1. (a) an example for additive error. (b). an example for proportionate error.

Additive Error

Figure 1.a shows an example of additive error. The slope of the regression is still zero but all the data points shift down; and there is a constant difference between the reference line and the regression line. Under this condition, we can model the actual data as $f(t) + \alpha$ where α is the additive error. In this situation, factors independent of time causing the bias from the reference line are neglected in our model.

Proportionate Error

Figure 1.b shows an example of proportionate error. The intercept of the regression line is zero, but there is negative slope. We can model the actual data as $\alpha \bullet f(t)$ where α is the proportionate error. Under this condition, there probably exist factors dependent on time which are neglected in our model.

Whiskers Box Plot
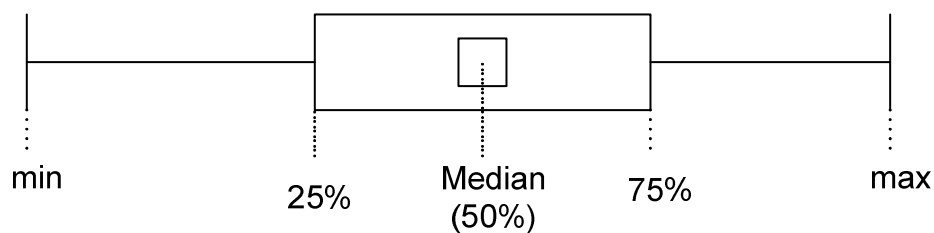
Fig. 2. A box and whisker plot.

Fig. 2 shows a box and whisker plot. To the left and right, a line extends to the minimum and maximum measures. The middle shows a box representing the interquartile range (equal to the difference between the 75% and 25% quartiles). This shows the distribution of the differences of the experimental values and simulated values.

Verifying the Human Observers Measure Process

We wish to verify the possible human error. Three tests are used in experiment to verify that these human-caused errors are low

Repeatability

We use the same sample, which is the lesion picture taken during one ablation on the cardiac tissue under a specific blood flow with specific target temperature. We ask the same observer to measure the lesion size on the same monitor several times. The standard deviation of these measures is called the repeatability.

Between-Technician Reproducibility

We use the same sample and ask several different observers to measure the lesion size on the same monitors several times. The standard deviation is called the between-technician reproducibility.

Between-Lab Reproducibility

We use the same sample to ask several different observers to measure the lesion size on different monitors several times. The standard deviation is called the between-lab reproducibility

DATA ANALYSIS

This experiment had a balanced design in temperature and flow rate, with two temperatures, 60 and 70 °C, and two flow rates, high and low. For each of the four combinations of temperature and flow rate, four experimental and four simulated values were obtained for each time period from 10 s to 90 s, taken at 10 s intervals. Thus, there were a total of $2 \times 2 \times 9 \times 4 = 144$ observations.

The actual data were derived from experiments, and hence were subject to experimental error. That is, the experimental data is statistical in nature. The simulated observations, being derived from a computer algorithm, are not statistical in nature. Therefore, these two types of data cannot be treated simultaneously in a statistical model. Instead, the statistical analysis employed differences between experimental and simulated values as a function of temperature, flow rate and time. These differences are given by experimental values—simulated values, so that a negative difference indicates that the simulated values overestimated the observed values from the experiments. If the simulated values were perfectly accurate, then all differences would equal zero.

Figs. 3a to 3d show the lesion width differences for each combination of temperature and flow rate. The reference line at Diff = 0 indicates *experimental result = simulation result*. The width simulations had mixed differences. At the high flow rate the simulations are reasonably unbiased, with some above and some below the reference line. For low flow rates, most differences are negative, indicating that the simulated values are higher than the experimental results. The statistical significance of these differences is addressed in Ch. 4.

The plots in Figs. 4a to 4d show the lesion depth differences for each combination of temperature and flow rate. The differences are negative for all comparisons for the depth

simulations. At the high flow rate, the typical bias is –1.5, and grows to –2.5 for the low flow rates. It appears that the bias for all figures depends more on flow rate (FR) than on temperature (*T*). We also use a regression model of $y = \alpha + \beta_1 T + \beta_2 \mathrm{FR} + \beta_3 T \times \mathrm{FR}$ to analyze the significance of each parameter. The result agrees with our conclusion that the flow rate has a more significant effect on the deviation.

For each of Figs. 3 and 4, four Whiskers box plots are given. The boxes extend one standard deviation on either side of the mean, and the whiskers extend to 1.96 standard deviations on either side of the mean. In order, the plots are for high Flow Rate, Temperature = 60 and 70 °C, followed by a similar pair for low Flow Rate. The four plots in Fig. 3(a) represent experimental values. Simulated values are presented in the four plots in Fig. 3(b). (Note that the vertical axes have identical scales.) Figs. 3(a) and 3(b) show that lesion width variability increases slightly with temperature, for both experimental and simulated values. Simulated values have less variability than experimental values, as one would expect.

Fig. 3(c) represents $\Delta W = W_{\mathrm{experiment}} - W_{\mathrm{simulation}}$, and Fig. 3(d) represents the percentage of ΔW to the experimental value, $W_{\mathrm{experiment}}$. Figs. 3(c) and 3(d) indicate bias, which is negligible for high flow rate, but negative (simulated values are too high) for low flow rate. Some simulated values exceed actual values by nearly 50% (where the bottom whiskers extend to –0.5). Improved lesion width simulations should focus on the low flow rate.

Comparing Figs. 4(a) and 4(b), shows that lesion depth simulations have a strong bias, with quite large overestimations. Fig. 4(d) indicates that the average simulated value is overestimated by 100%, with some values overestimated by 200%. The data tables at the end of this report show that there is not a single instance of a simulated depth value that is lower than any experimental outcome. Clearly, improving the simulations requires a much better job of simulating lesion depth.

Figs. 5a – 5d show the scatter plots of the width differences, and Figs. 6a – 6d show the scatter plots of the depth differences.
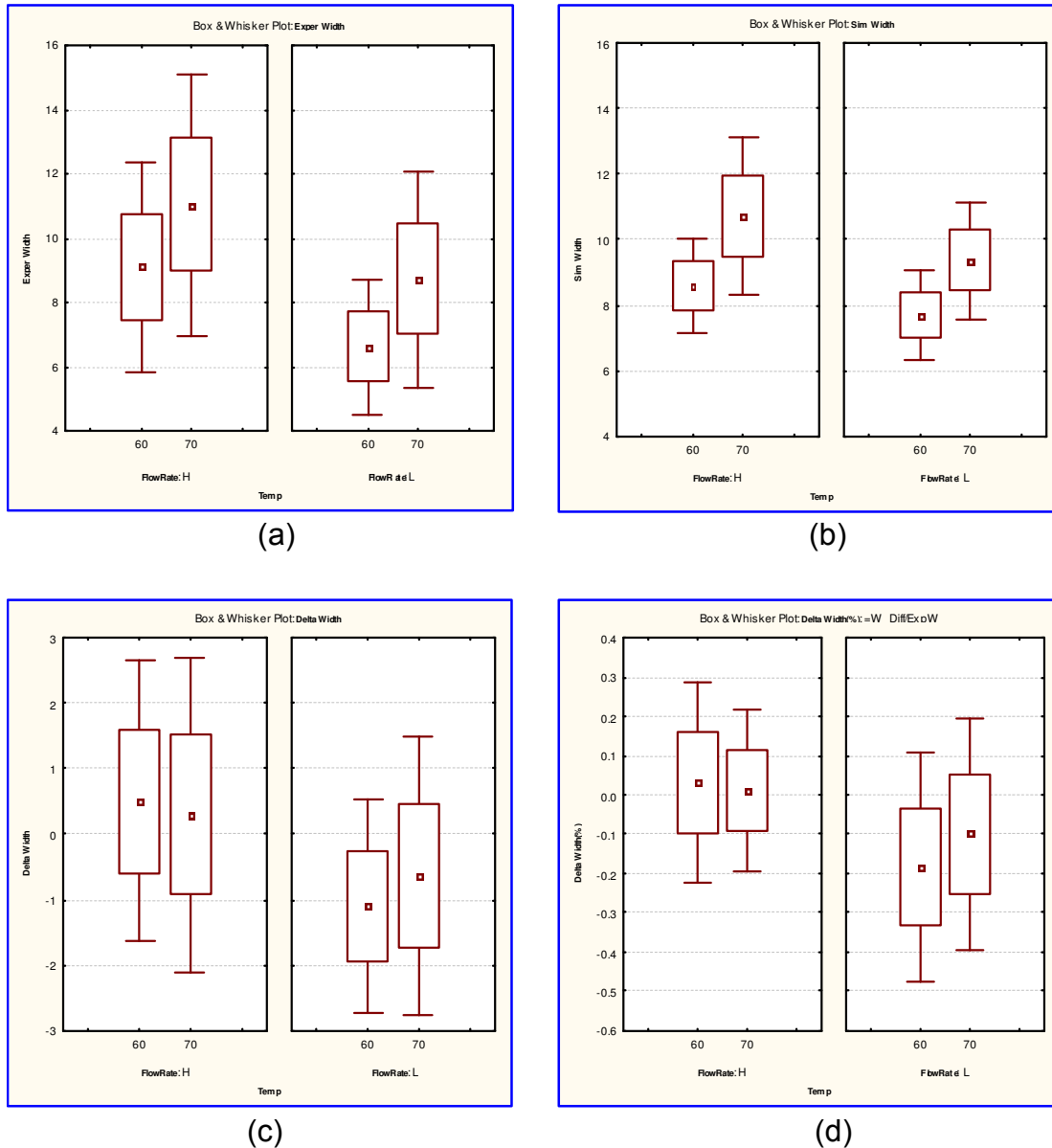
Fig. 3. Whiskers box plots of lesion width. (a) experimental data distribution for different flows at different time intervals with different target temperatures (b) simulated data distribution for different flow at different intervals with different target temperatures (c) the distribution of the difference between simulated data and experimental data for different flow at different intervals with different target temperatures (d) the distribution of the difference in percentage with respect to the experimental data value.
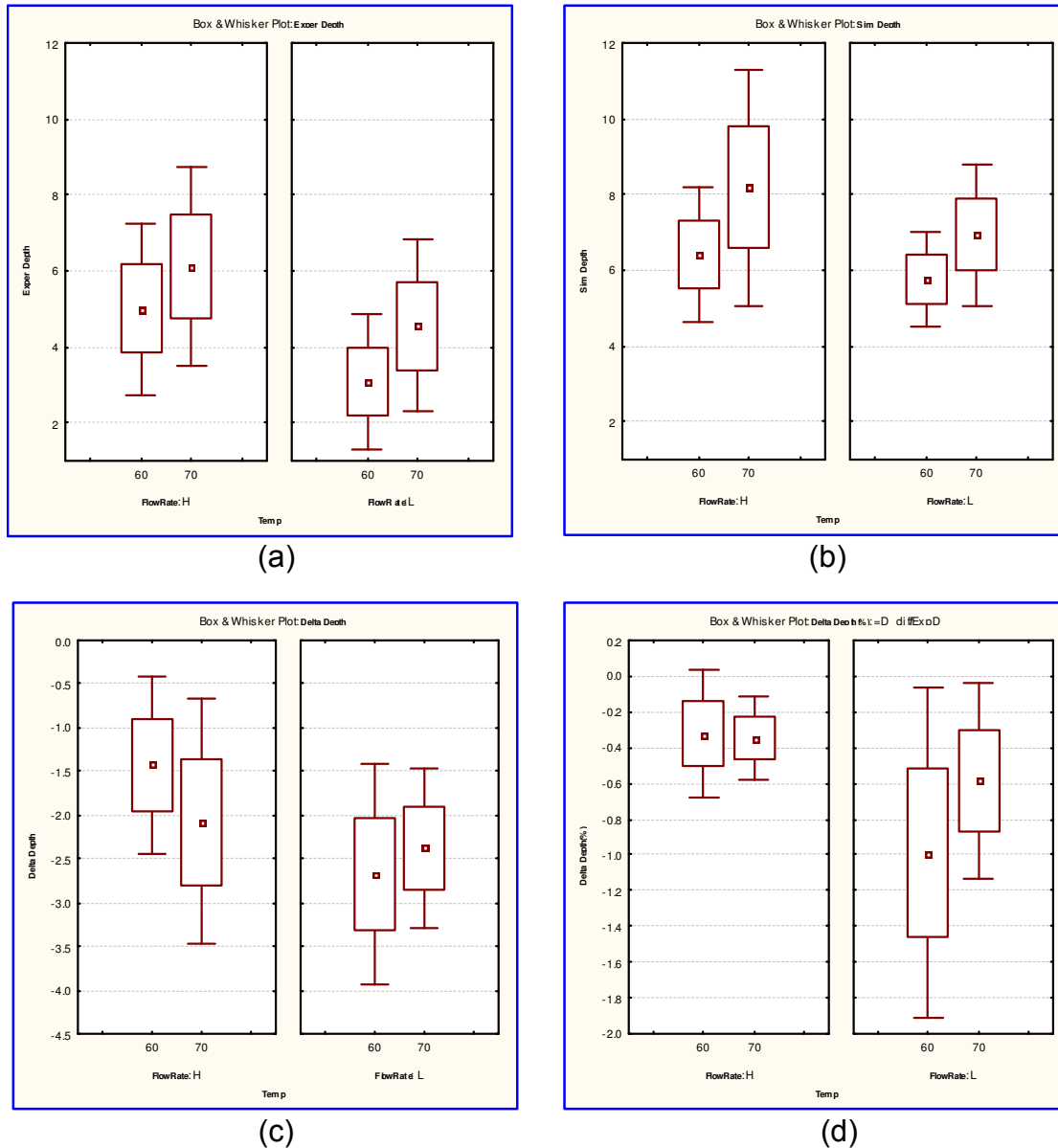
Fig. 4. The Whiskers box plot of lesion depth. (a) experimental data distribution for different flows at different time intervals with different target temperatures (b) simulated data distribution for different flow at different intervals with different target temperatures (c) the distribution of the difference between simulated data and experimental data for different flow at different intervals with different target temperatures (d) the distribution of the difference in percentage with respect to the experimental data value.
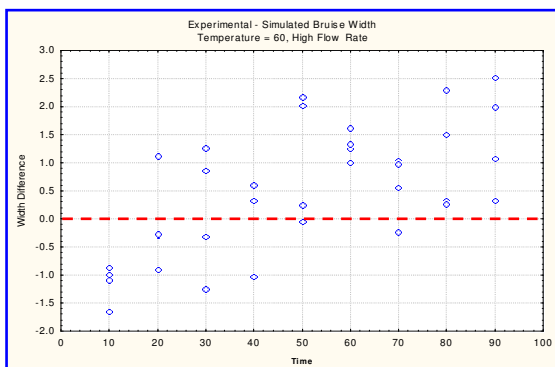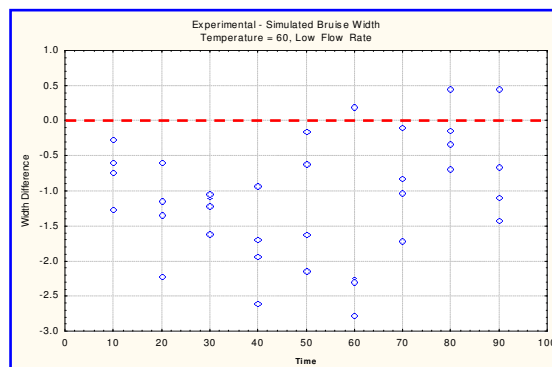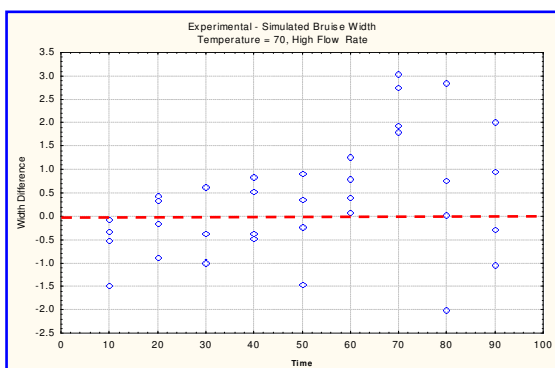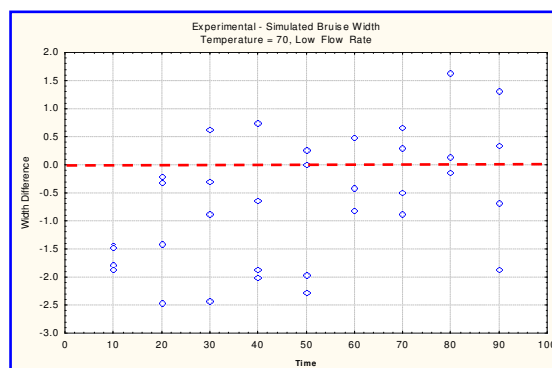
Fig. 5. The scatter plots of the difference of width between simulated data and experimental data at different applied time. (a) the scatter plot for data at high blood flow with target temperature 60 °C. (b) the scatter plot for data at low blood flow with target temperature 60 °C. (c) the scatter plot for data at high blood flow with target temperature 70 °C. (d) the scatter plot for data at low blood flow with target temperature 70 °C.
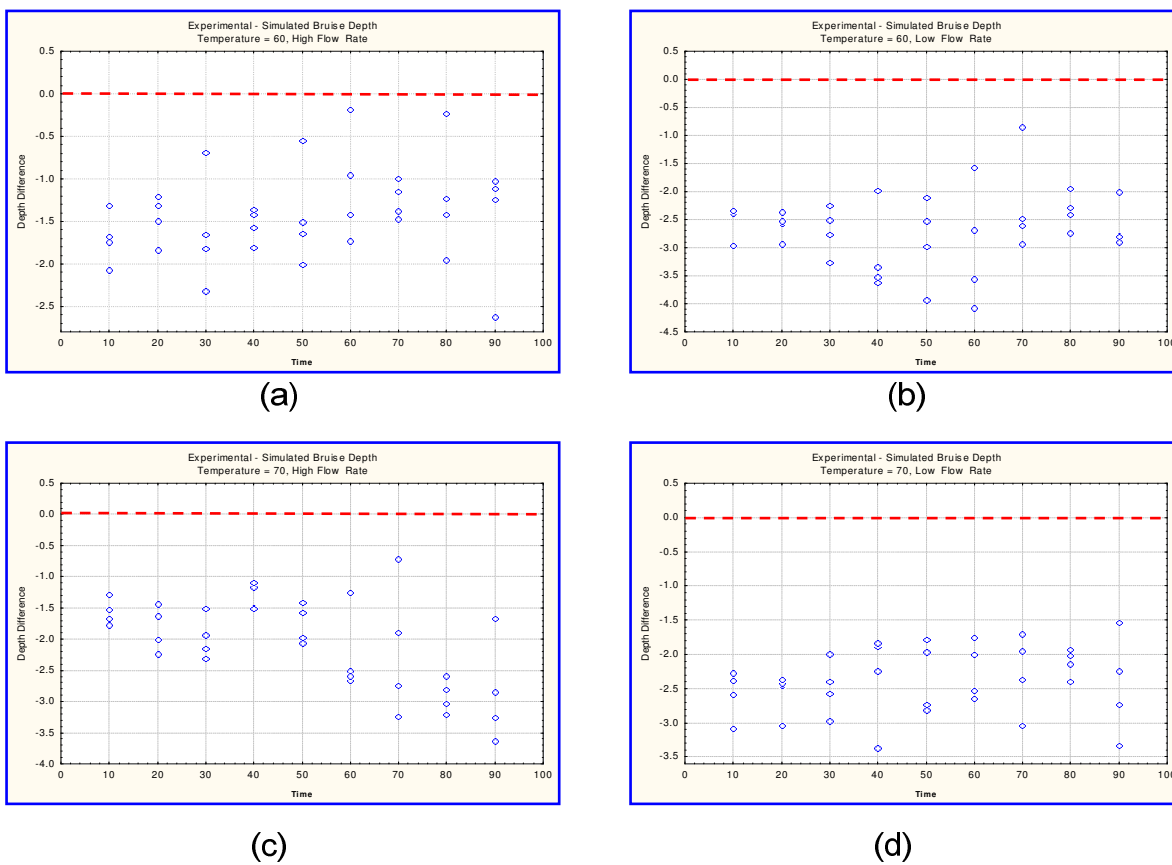
Fig. 6. The scatter plots of the difference of depth between simulated data and experimental data at different applied time. (a) the scatter plot for data at high blood flow with target temperature 60 °C. (b) the scatter plot for data at low blood flow with target temperature 60 °C. (c) the scatter plot for data at high blood flow with target temperature 70 °C. (d) the scatter plot for data at low blood flow with target temperature 70 °C.

APPENDIX C

SUPPORT MATERIAL FOR CHAPTER 5

Ch. 5 shows only the time responses of the lesion width, lesion depth, and lesion depth for different penetration depths under the tip for high blood flow targeted at 60 °C and the lesion shapes for different penetration depths at 90 s after starting the ablation targeted at 60 °C for high blood flow and for low blood flow to illustrate the relationship between penetration angle and lesion formation. Below are additional collected time responses for penetration depths of 0.7, 1.3, 2.0, 2.5, 3.0, and 3.5 mm targeted at temperatures of 60, 70, and 80 °C for two different blood flow states. Figs. 1 to 12 in this appendix represent the results of different penetration depths targeted at different temperatures for different flow rates. Figs. 13 and 14 show the power applied to the electrode at 90 s for different penetration depths for high blood flow and low blood flow.
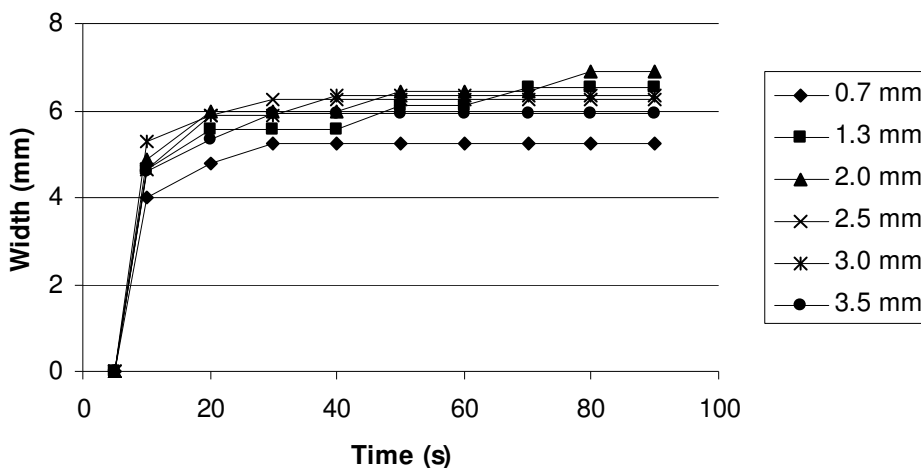
Fig. 1. Simulation of time response for width for different insertion depths for high blood flow targeted at 50 °C
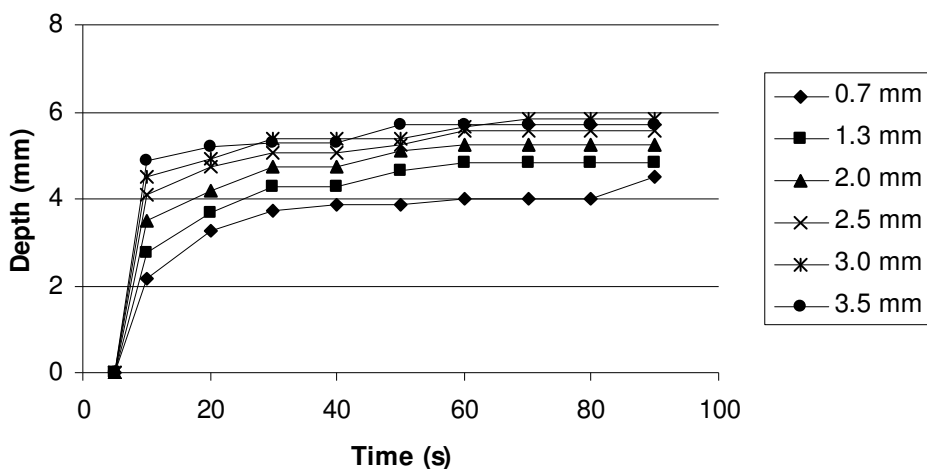
Fig. 2. Simulation of time response for depth for different insertion depths for high blood flow targeted at 50 °C
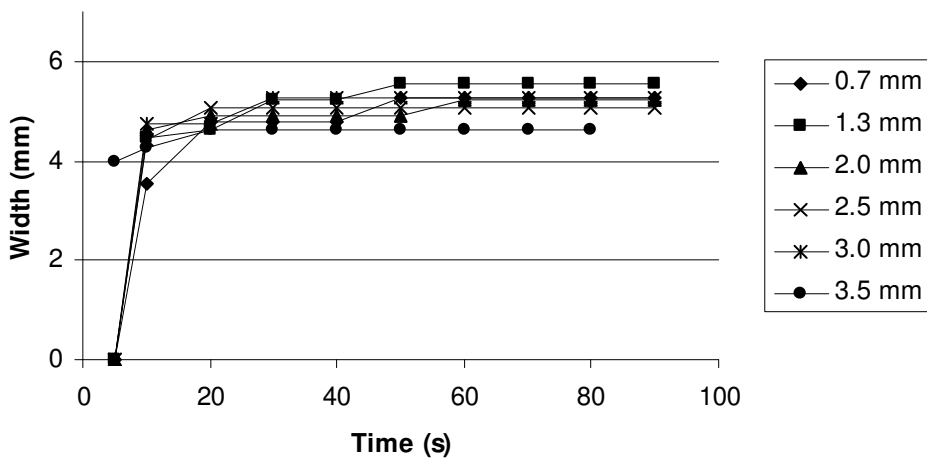
Fig. 3. Simulation of time response for width for different insertion depths for low blood flow targeted at 50 °C
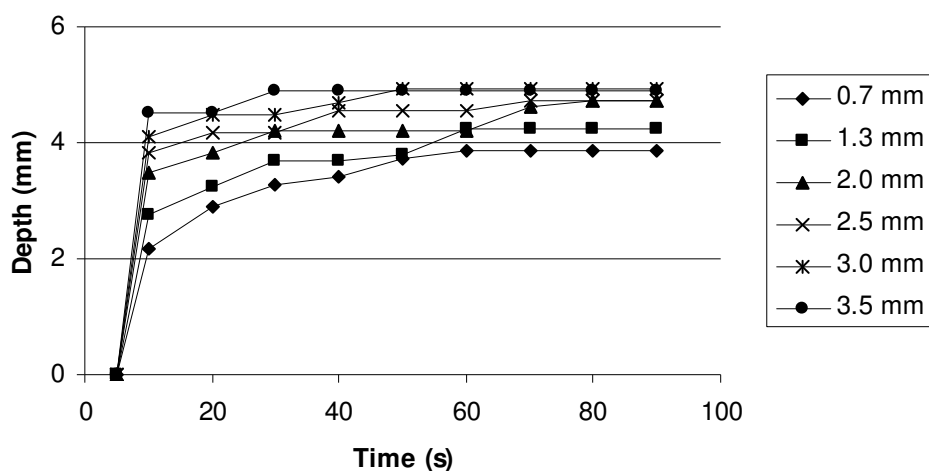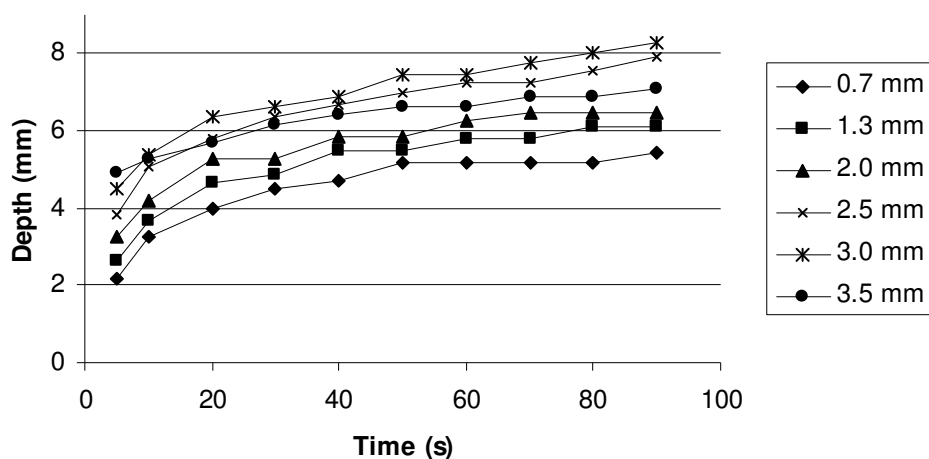
Fig. 4. Simulation of time response for depth for different insertion depths for low blood flow targeted at 50 °C
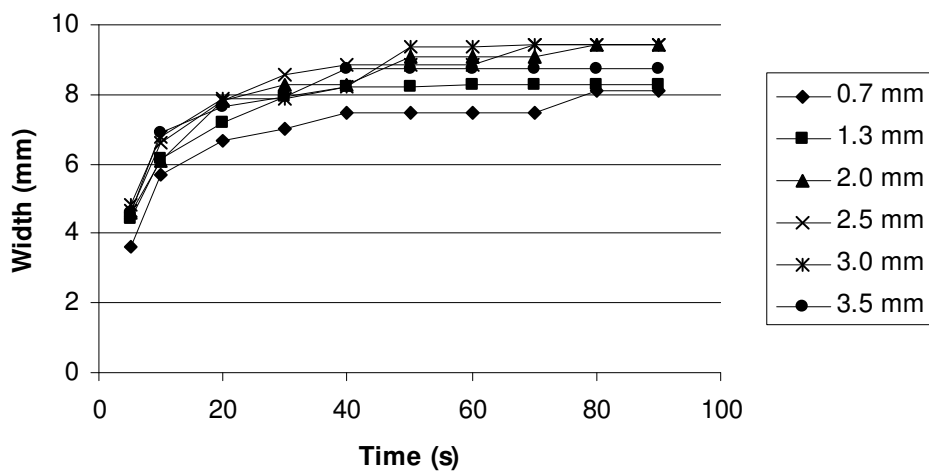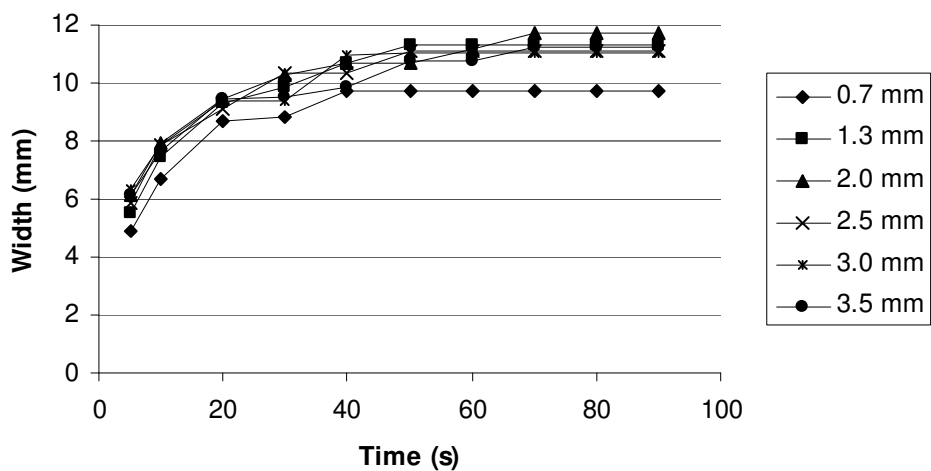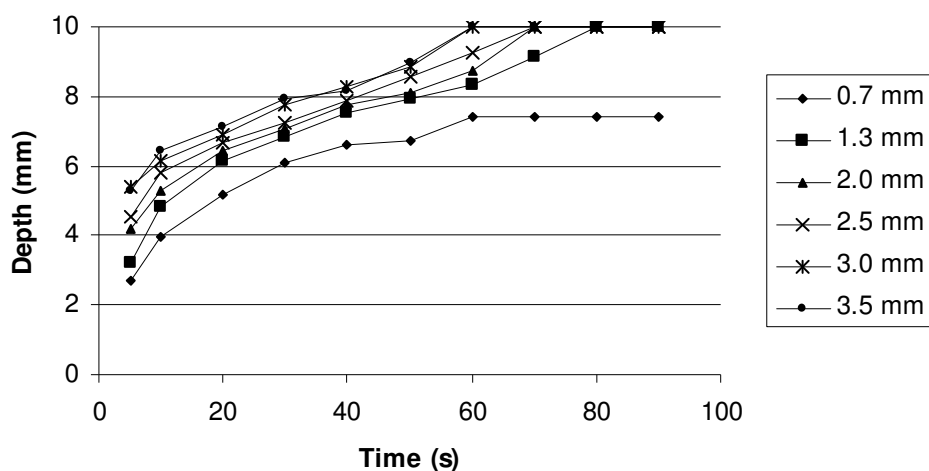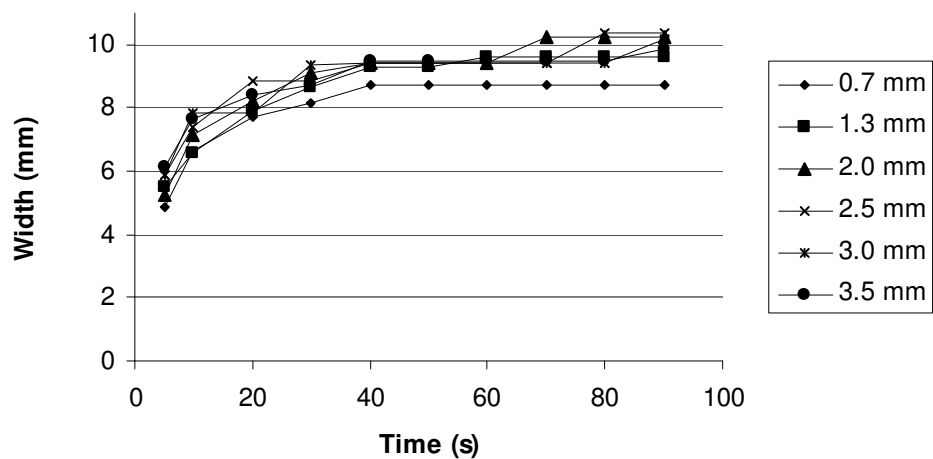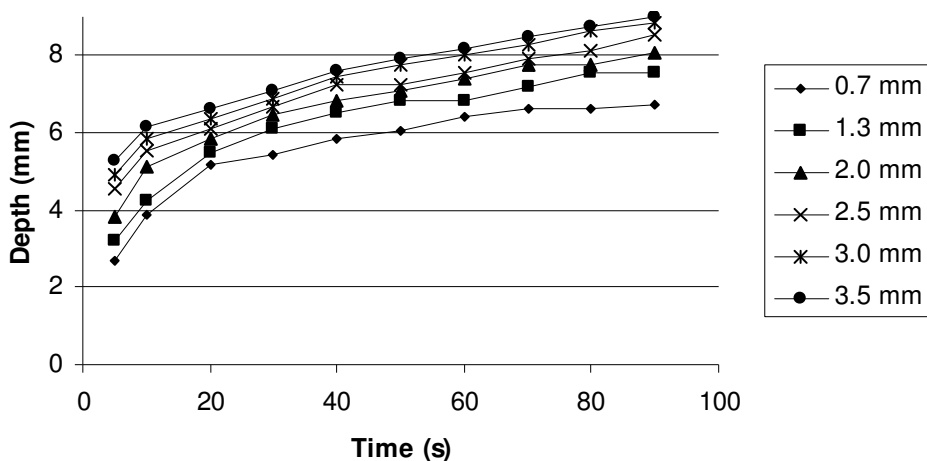

Fig. 5. Simulation of time response for width for different insertion depths for high blood flow targeted at 60 °C
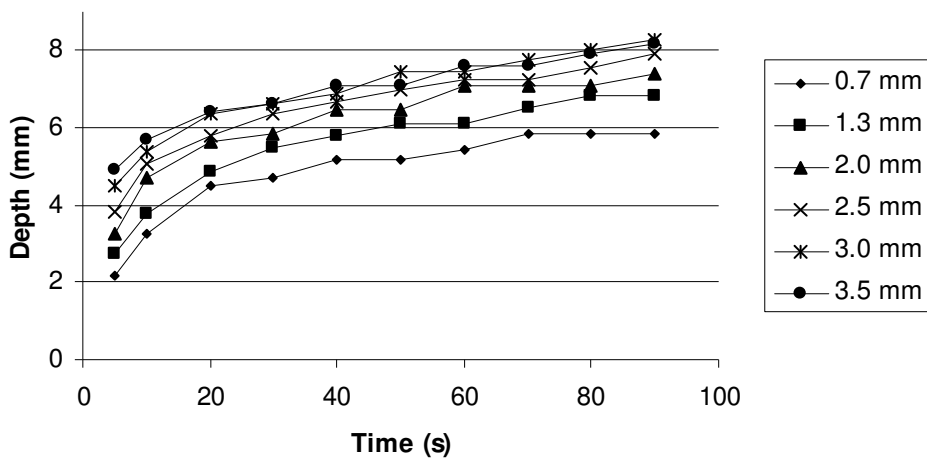
Fig. 6. Simulation of time response for depth for different insertion depths for high blood flow targeted at 60 °C
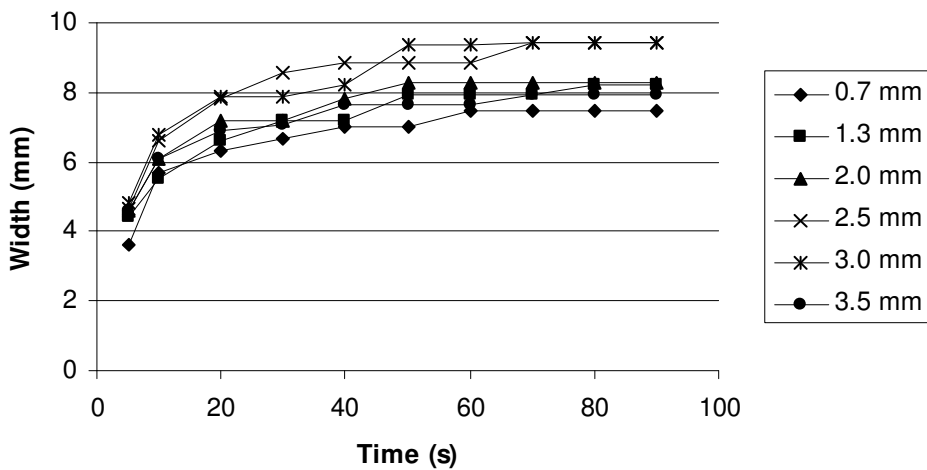
Fig. 7. Simulation of time response for width for different insertion depths for low blood flow targeted at 60 °C

Fig. 8. Simulation of time response for depth for different insertion depths for low blood flow targeted at 60 °C
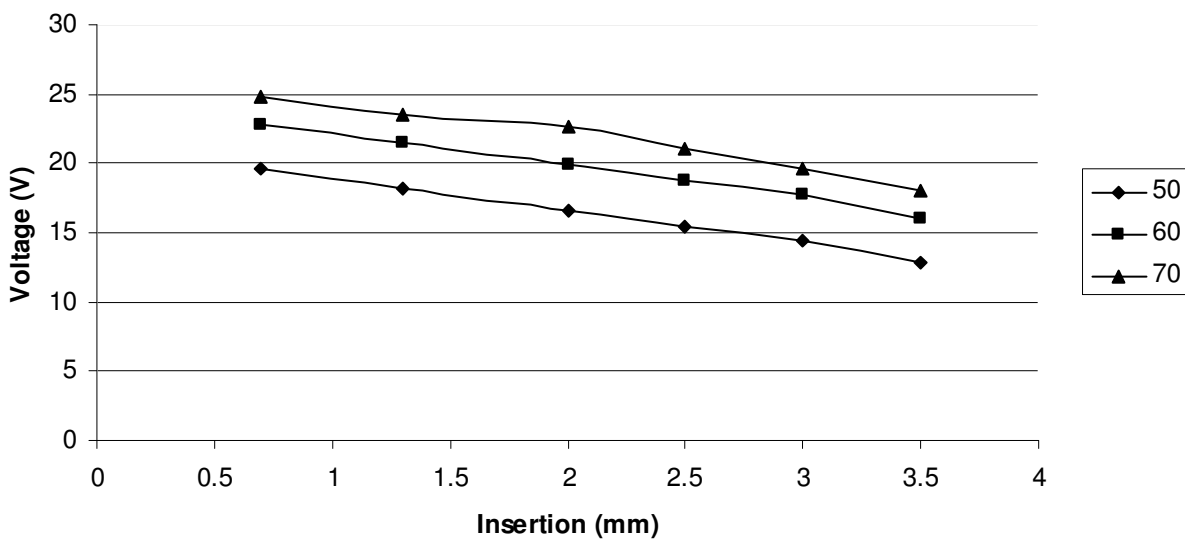

Fig. 9. Simulation of time response for width for different insertion depths for high blood flow targeted at 70 °C

Fig. 10. Simulation of time response for depth for different insertion depths for high blood flow targeted at 70 °C

Fig. 11. Simulation of time response for width for different insertion depths for low blood flow targeted at 70 °C

Fig. 12. Simulation of time response for depth for different insertion depths for low blood flow targeted at 70 °C

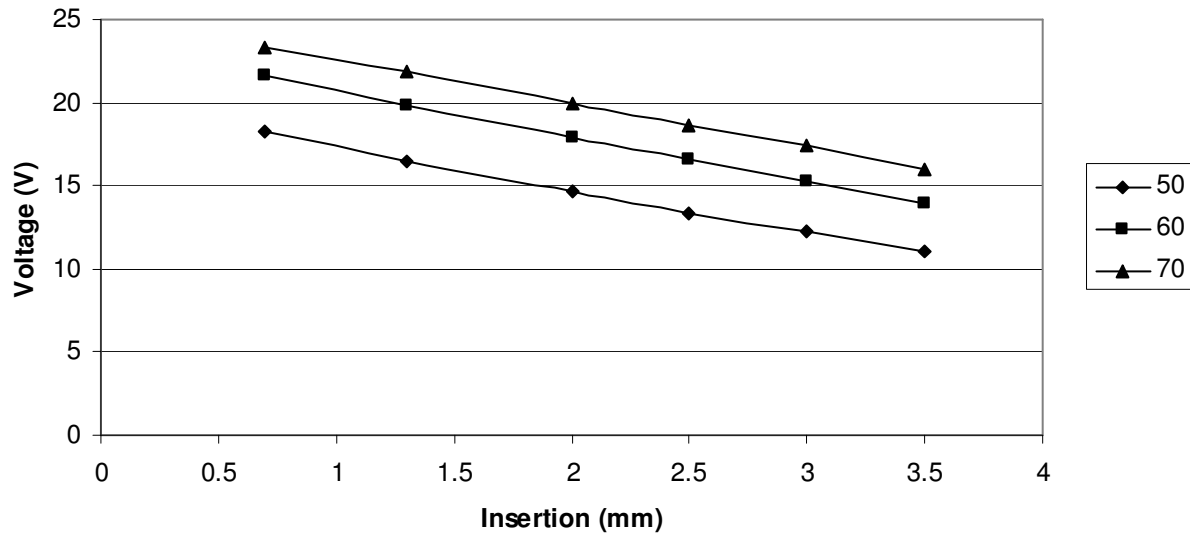**Fig. 13.** The applied voltage at 90 s for different insertion depths for high blood flow rate for different target tip temperatures.

Fig. 14. The applied voltage at 90 s for different insertion depths for low blood flow rate for different target tip temperatures.

APPENDIX D

SUPPORT MATERIAL FOR CHAPTER 6

Ch. 6 shows the time responses of the lesion width and lesion depth for different insertion angles

for high blood flow targeted at 60 °C and the lesion shapes for different insertion angles at 90 s

after starting the ablation targeted at 60 °C for high blood flow to illustrate the relationship

between insertion angle and lesion formation. Below are additional collected time responses for

different insertion angles targeted at 60 °C for low blood flow states. Figs. 1 and 2 in this

appendix represent the results of different insertion angles targeted at 60 °C for low blood flow

rate. Fig. 3 shows the lesion shapes for different insertion angles at 90 s after starting the ablation

targeted at 60 °C for low blood flow. Fig. 4 shows the power applied to the electrode at 90 s for

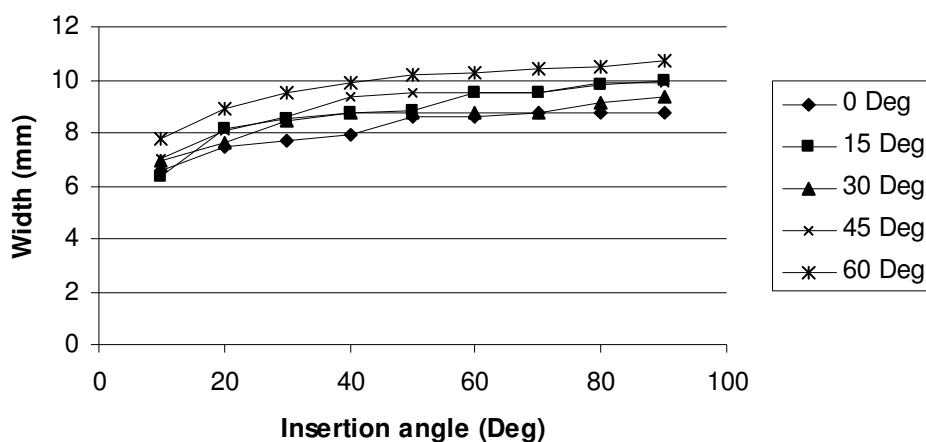different insertion depths for low blood flow.

Fig. 1. Lesion width increases with ablation time for low flow for different insertion angles at target tip temperature 60 °C.
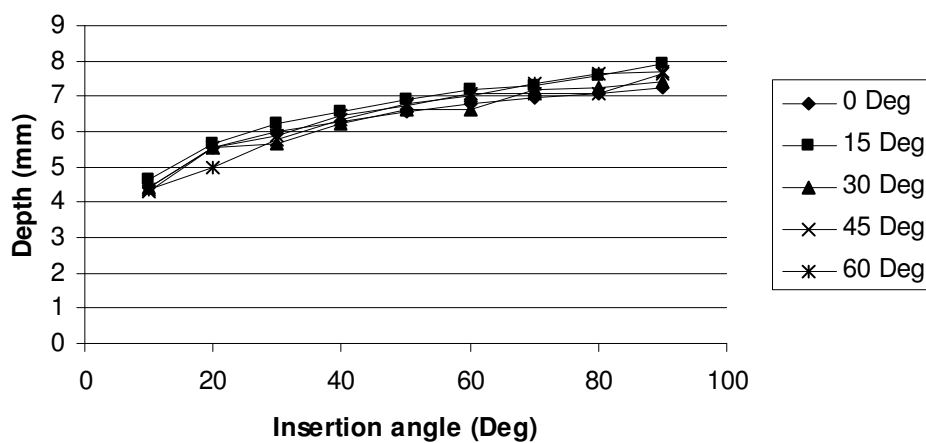

Fig. 2. Lesion depth increases with ablation time for low flow for different insertion angles at target tip temperature 60 °C.
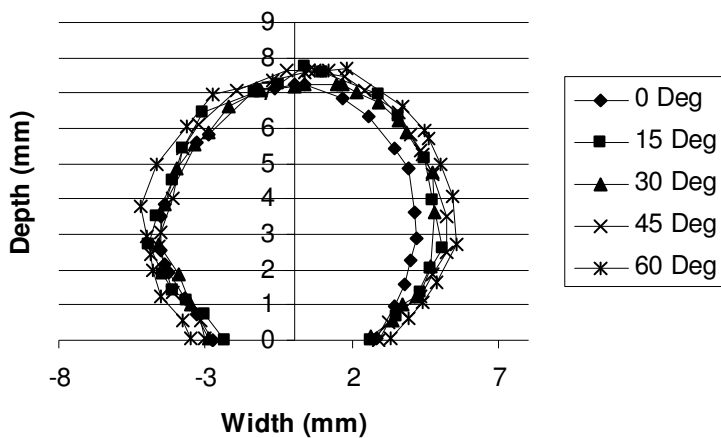
Fig. 3. The lesion shape along the catheter central axis at 90 s at high flow for different insertion angles at target tip temperature 60 °C.
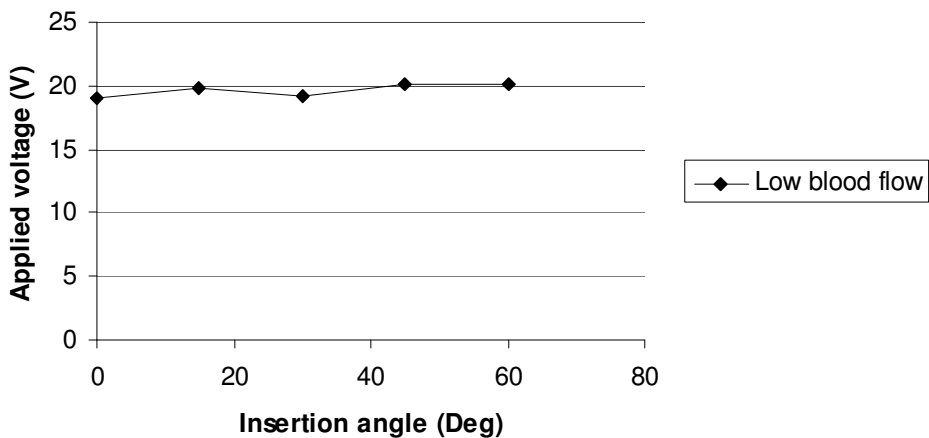

Fig. 4. The applied voltage at 90 s for different insertion angles for low blood flow rate at target tip temperature 60 °C.